Alma Mater Studiorum
Università di Bologna

SCHOOL OF ENGINEERING AND ARCHITECTURE
Forlí campus

Master's degree in

MECHANICAL ENGINEERING
class LM-33

GRADUATION THESIS
in Advanced Thermofluidodynamics and Thermal Control

STEADY-STATE MODELLING OF A VAPOR COMPRESSION REFRIGERATION CYCLE

Candidate
Giovanni Roberti

Supervisor
Prof. Marco Lorenzini

Co-supervisor
Dr. Michael Lucchi

Academic Year 2018/2019

To my second mum, Teresa:
the strength you had will always be
the light that illuminates my dark moments.

Contents

List of Figures ix
List of Tables xiii
List of Codes xv
List of Symbols xvii
Abstract xxi
Introduction xxiii

1 Chapter 1
Vapor compression refrigerating system: an overview

1.1 The thermodynamic cycle of a VCRS 1
1.2 Basic components of a VCRS 5
1.2.1 Heat exchangers *5*
1.2.2 Compressors *8*
1.2.3 Expansion devices *12*
1.3 The refrigeration machine studied 14
1.3.1 Condenser *15*
1.3.2 Evaporator *18*
1.3.3 Compressor *18*
1.3.4 Expansion valves *20*
1.3.5 Refrigerant *20*

23 Chapter 2
The physical model

2.1 Experimental data acquisition 23
2.2 Model equations 25
2.2.1 Condenser *25*

2.2.2 Evaporator *29*
2.2.3 Compressor *31*
2.2.4 Expansion valves *32*
2.3 Heat transfer correlations for BPHEs 34
2.3.1 Single-phase correlations *35*
2.3.2 Condensation correlations *43*
2.3.3 Evaporation correlations *43*
2.4 Pressure drop correlation for a BPHE 46
2.5 Effectiveness NTU relations for a BPHE 48
53 Chapter 3
Model implementation
3.1 Components algorithms 53
3.1.1 Compressor *54*
3.1.2 Condenser *60*
3.1.3 Evaporator *68*
3.2 Machine algorithm 70
3.3 Refrigerant and water properties 77
81 Chapter 4
Results and validation
4.1 Component validation 81
4.1.1 Compressor *81*
4.1.2 Condenser *85*
4.1.3 Evaporator *91*
4.2 Machine validation 94
4.3 Application of the models 97
4.4 Conclusions 104
4.5 Future developments 104
107 Appendix A
Zeotropic mixtures

111 Appendix B
The effectiveness NTU method

113 Appendix C
Condensation and boiling: an overview

Bibliography 117
Acknowledgements 123

List of Figures

Figure		Page
1.1	Input and output energy for a VCRS	2
1.2	$\log p - h$ qualitative diagram of a VCRS ideal cycle	3
1.3	A $\log p - h$ qualitative diagram of a VCRS real cycle	4
1.4	Major components of a VCRS	6
1.5	Shell and tube heat exchanger	8
1.6	Tube-fin heat exchanger: forms of finned tubes	8
1.7	Plate heat exchanger	9
1.8	Reciprocating compressor	10
1.9	Sliding vane compressor	10
1.10	Scroll compressors	11
1.11	Screw compressor	11
1.12	Centrifugal compressor	12
1.13	Range of capacity covered by various compressor types	12
1.14	Thermostatic expansion valve	13
1.15	Electronic expansion valve	14
1.16	Scheme of the studied refrigeration plant	15
1.17	Plate geometry	16
1.18	Phase and β effect on the channels	17
1.19	The plant condenser	19
1.20	The plant evaporator	19
1.21	Plant compressor	20
1.22	Plant EEVs	20
1.23	Condensation: R134a	21
1.24	Condensation: R450a	22
1.25	Glide temperature as function of the condensation pressure: R450a	22

FIGURE *Page*

2.1 Example of acquired data 24
2.2 Condenser regions 26
2.3 Qualitative $T - Q$ diagram for the condenser 27
2.4 Evaporator regions 29
2.5 Qualitative $T - Q$ diagram for the evaporator 30
2.6 Qualitative $T - Q$ diagram for the evaporator with pressure drop 31
2.7 Flow characteristic of the EEV 33
2.8 Nu comparison single phase correlations 39
2.9 Nu comparison single phase correlations: zoom 40
2.10 Nu comparison single phase correlations with Martin 41
2.11 Nu percent comparison single phase correlations with Martin . . 42
2.12 Nu comparison in boiling heat transfer correlations 46
2.13 Nu comparison in boiling heat transfer correlations: a zoom zoom 47
2.14 *Percentage incidence of the pressure drop in the heat exchangers.* In the evaporator the pressure drop has a certain relevance. . . . 48
2.15 f comparison in boiling pressure drop correlations 49
2.16 An example of multipass $X_1 = 3,\ X_2 = 2$ flow arrangement . . . 49
2.17 $\varepsilon - NTU$ relation comparison for zeotropic mixtures: low γ. . . 51
2.18 $\varepsilon - NTU$ relation comparison for zeotropic mixtures: high γ. . . 51

3.1 Inputs and outputs of the compressor model 55
3.2 Compressor m_r as a function of ΔT_{sh} varying one between $T_{sat,e}$ and $T_{sat,c}$ 57
3.3 Compressor T_{out} as a function of ΔT_{sh} varying eithero $T_{sat,e}$ or $T_{sat,c}$ 58
3.4 Compressor outputs as a function of $T_{sat,e}$ and $T_{sat,c}$ 59
3.5 Inputs and outputs of the condenser model 61
3.6 Computation time comparison: symbolic vs iterative model . . . 64
3.7 Execution time comparison: iterative models 65
3.8 Fixed step vs variable step in the condenser model 66
3.9 Execution time comparison: condenser iterative model fixed vs variable step 67

3.10 Inputs and outputs of the evaporator model 69
3.11 Fixed step vs variable step in the evaporator model 71
3.12 Inputs and outputs of the complete model 72
3.13 Linear polynomial fitting of the experimental data for ΔT_{sc} . . . 73
3.14 Schematic representation of the thermodynamic cycle in the first block on a $\log p - h$ diagram 74
3.15 Schematic representation of the thermodynamic cycle in the first block on a $\log p - h$ diagram 75
3.16 Execution time of the machine iteration cycle 75
3.17 Step control based on the gradient 76
3.18 Computation time comparison: refprop vs structure 80
3.19 Computation time comparison: refprop vs coolprop 80

4.1 Validation of the compressor model: m_r 82
4.2 Validation of the compressor model: T_{out} 83
4.3 Validation of the compressor model: P_{el} 83
4.4 Validation of the compressor model: P_{el} with corrective coefficient 84
4.5 Validation of the symbolic condenser model 88
4.6 Validation of the first iterative condenser model 88
4.7 Validation of the second iterative condenser model 89
4.8 Validation of the symbolic optimized condenser model 89
4.9 Validation of the first iterative condenser model optimized through the symbolic one 90
4.10 Validation of the optimized first iterative condenser model optimized 90
4.11 Validation of the symbolic evaporator model 91
4.12 Validation of the iterative evaporator model 92
4.13 Validation of the optimized symbolic evaporator model 92
4.14 Validation of the iterative evaporator model with pressure drop 93
4.15 Validation of the optimized iterative evaporator model with pressure drop 93

4.16 Validation of the first iterative block of the global model of the machine: p 94
4.17 Validation of global model of the machine: T 95
4.18 Validation of global model of the machine: p 95
4.19 Validation of global model of the machine: ΔT 96
4.20 Validation of global model of the machine: m 96
4.21 Global model of the machine: condenser $T - Q$ diagram 97
4.22 Global model of the machine: evaporator $T - Q$ diagram 98
4.23 Global model of the machine: $\log p - h$ diagram 98
4.24 Global model of the machine: Q balance 99
4.25 Global model of the machine: COP 99
4.26 Global model of the machine: η_{ex} in the components 99
4.27 Global model of the machine: η_{ex} in the machine 99
4.28 $T - \zeta_i$ diagram for the condenser 100
4.29 $T - \zeta_i$ diagram for the condenser 101
4.30 $T - \zeta_i$ diagram for the evaporator 102
4.31 Efficiency analysis: part one 103

A.1 R134a vs R450a: $\log p - h$ diagram 109

C.1 Evolution of the heat transfer rate as a function of T_{ecc} for the water at ambient pressure 115

List of Tables

Table		Page
1.1	Categorization of heat exchangers	7
1.2	BPHE geometric parameters	18
1.3	Condenser geometrical data	19
1.4	Evaporator geometrical data	19
1.5	Compressor technical data	20
2.1	Non-dimensional groups of heat and mass transfer	34
2.2	Non-dimensional groups of heat and mass transfer for two phase fluids	44
A.1	R134a vs R450a: properties comparison	108

List of Codes

Code		Page
2.1	The structure for the acquired data	24
3.1	Call to the model function in Matlab	54
3.2	Compressor model: determination of m_r	56
3.3	Part of the symbolic model of the condenser	61
3.4	Control of ε_{sh} for the condenser iterative model	63
3.5	Loop on ζ_{sh} for the condenser iterative model	63
3.6	Part of the symbolic model of the evaporator	68
3.7	Example of thermodynamics properties investigation using RefProp and CoolProp	77
3.8	The data structure for the refrigerant properties and an example of its use	78
4.1	The construction of the array of coefficient through the permutation of an array of values	86

List of Symbols

Greek letters

α	convection heat transfer coefficient	$W\ m^{-2}\ K^{-1}$
β	chevron angle	deg
ΔJ_{lv}	latent heat of vaporization	$J\ kg^{-1}$
ΔT	temperature difference	K, C
δ	thermal diffusivity	$m^2\ s^{-1}$
η_{ex}	exergetic efficiency	–
κ	thermal conductivity	$W\ m^{-1}\ K^{-1}$
μ	viscosity	$kg\ s^{-1}\ m^{-1}$
Φ	function	
ϕ	area enlargement factor	–
ρ	mass density	$kg\ m^{-3}$
σ	surface tension	$N\ m^{-1}$
τ_i	tolerance respect i	UoM of i
ε	heat exchanger effectiveness	–

Roman letters

A	area	m^2
B	plate width	m
b	plate offset	m
Bd	Bond number , page xv	–
Bo	boiling number	–
C	heat capacity rate	$W\ K^{-1}$
c_p	specific heat at constat pressure	$J\ kg^{-1}\ K^{-1}$

COP	coefficient of performance	$-$
D_h	hydraulic diameter	m
Ex	exergy rate	W
F	electrical frequency	Hz
f	friction factor	$-$
G	mass flux or mass velocity	$kg\ m^{-2}\ s^{-1}$
g	gravitational acceleration	$m\ s^{-2}$
h	specific enthaply	$J\ kg^{-1}$
L	plate length	m
m	mass flow rate	$kg\ s^{-1}$
n_{ch}	number of channels	$-$
Nu	Nusselt number	$-$
P	power	W
p	pressure	Pa
Pr	Prandtl number	$-$
Q	heat transfer rate	W
R_a	roughness	μm
Re	Reynolds number	$-$
Re_{eq}	equivalent Reynolds number	$-$
T	temperature	K, $^\circ C$
v	velocity	$m\ s^{-1}$
x	vapor quality	$-$

Subscripts

acce	acceleration
c	condenser
cb	convective boiling
cr	critical
e	evaporator
elev	elevation
eq	equivalent

$frict$	frictional
$meas$	measured
nb	nucleate boiling
$proj$	projected
ref	refrigerant

Abbreviations

BPHE	brazed plate heat exchanger
EEV	electronic expansion valve
GWP	global warming potential
HC	hydrocarbons
HFC	hydrofluorocarbons
HTC	heat transfer coefficient
PHE	plate heat exchanger
TEV	thermostatic expansion valve
UoM	unit of measurement
VCRS	vapor compression refrigeration system

Abstract

In this work a steady-state model of a simple vapor compression refrigeration cycle is presented. All the fundamental components of this system are modeled separately in order to consider them as black boxes that take inputs and convert them into output variables. The heat exchangers are treated as a set of multiple zones, identified by the refrigerant's state, connected in series, in which the heat transfer coefficient (HTC) is constant. A non-linear system of equations is obtained applying the energy balances and the $\varepsilon - NTU$ method for each zone in the heat exchangers. A study on the HTC correlations used to connect the length of the zones with the value of the respective HTC is developed. The compressor is modeled using a polynomial function. Some iterative methods for the resolution in MATLAB of the models of the components and the machine are presented, focusing on the strategy to decrease the execution time and to increase the accuracy of the results. Finally, all the models are validated through a set of experimental data and the global model is used to make some considerations about the efficiency and the exergy destruction in the plant.

Introduction

Refrigeration technology has had a significant impact on the culture and habits of the people. Diet, buildings, agricultures, industries, are some examples of things that have changed with the development of the refrigeration cycles. The first vapor compression refrigeration system (VCRS) using a closed cycle process was patented in 1834 by Jacob Perkins (1766-1849). In the 20^{th} century the global diffusion of the refrigeration, including the VCRS, cycles occurs [1].

In the last decades, the continuous progress in computers has led to remarkable improvements in the mathematical modeling, computational algorithms and data computing. As expressed in [2], computer modeling and simulation helps to explore natural events and engineered systems, which are too complex for the analysis with the traditional methods. Modelling and simulation improve predictions and optimized solutions which ensure performances and efficiency, minimizing costs and time.

For this reason, in the last years, modeling and simulation has involved the refrigeration cycles too. In literature a lot of dynamic models [3–6] and steady state ones [7, 8] of VCRS systems and their elements, based on different kinds of components and refrigerants, are proposed.

In this work a steady-state model of a vapor compression refrigeration cycle formed by the four fundamental components, an evaporator, a condenser, a compressor and an expansion-device, is developed. These components are treated separately in order to have a model of the machine flexible and reusable, which can be modified replacing the single models of the components. Before developing the model of the machine, for every component a model which replicates the behavior of this particular component is found. For this

reason the dissertation in the various chapter is often divided by the components: in particular, the work is focused on the modeling of the heat exchangers and the machine, while the expansion device and the compressor are modeled too, but in a very simple way. Anyway, the model is built in order to simulate the behavior of a real plant that is made of two brazed plate heat exchangers (condenser and evaporator) and a reciprocating compressor, where the refrigerant fluid is the R450a, which is a zeotropic mixture. Thanks to the experimental data acquired from this plant, the model can be validated.

In the first chapter, the thermodynamic transformations, the principal physical quantities and the most common kind of components of a vapor compression refrigeration systems are introduced. Next, the studied refrigeration plant is presented and its components are described in terms of geometry and other properties which are useful for their next modelling.

In the second chapter the physical principles that govern a VCRS cycle in steady state conditions are introduced, the hypothesis of the model are formulated and the solving equations are written. A short description of the experimental data (that will be used in the next chapters) processing is presented. Besides, a study about the empirical correlations for the determination of the heat transfer convective coefficients is proposed.

In the third chapter the problem of the implementation in the calculator is treated. All the iterative methods for the resolution of the non-linear system of equations for the heat exchangers are listed and some considerations about the criteria of convergence and the execution time are showed.

In the fourth chapter either the model of the components and the model of the machine are validated with the experimental data. Then, the model is used to analyse the exergy destruction in the components and the plant efficiency. At last, some possible future developments are proposed.

Chapter 1

Vapor compression refrigerating system: an overview

Refrigeration systems remove heat from a system at low temperature and discharge it into an ambient at a higher temperature, operating on a series of consecutive thermodynamic processes which return the working fluid to its initial state, completing a cycle [9]. These systems are classified according to the thermodynamic transformations to which is subject the working fluid.

This chapter presents an overview on the vapor compression refrigerating system (VCRS): the thermodynamic cycle (Section 1.1) and a short description of the fundamentals components (Section 1.2) are introduced. Detailed information about these topics is available in the scientific literature [1, 10–15] used as reference for this chapter. In the end the refrigeration plant considered for the development of the model is presented (Section 1.3).

Section 1.1

The thermodynamic cycle of a VCRS

Considering VCRS as a closed box which interacts with and separates two rooms at different temperatures, the heat transfer rate Q_1 (cooling effect) is removed cyclically from the room at a lower temperature T_1 while another heat transfer rate Q_2 is discharged into the room at a higher temperature T_2. According to the second law of thermodynamics, an external energy source P (work input) is needed: for a VCRS this part is supplied by a mechanical

compressor (Figure 1.1).

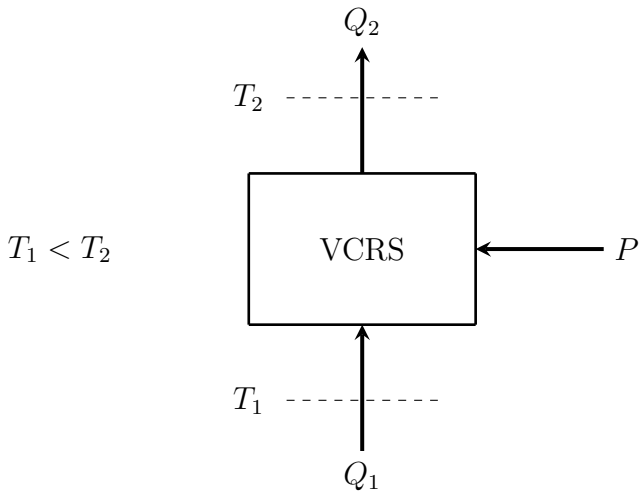

Figure 1.1
Input and output energy for a VCRS.

A simple energy balance is written respecting the first law of thermodynamics[1] (1.1).

$$Q_1 + P = Q_2 \tag{1.1}$$

The basic vapor compression cycle makes use of the boiling, in an evaporator, and condensation, in a condenser, of a working fluid, called refrigerant, at different pressures, to transfer heat. The thermodynamic cycle is usually represented on a $\log p - h$ diagram (Figure 1.2).

Ideal cycle

1 →2 reversible adiabatic compression: the compressor increases the pressure of the superheated vapor refrigerant from state 1 (output of evaporator) to state 2 (input of condenser);

2 →3 reversible heat rejection at constant pressure: the refrigerant flows along the condenser and discharges heat. The fluid leaves the heat exchanger as subcooled liquid in state 3;

3 →4 irreversible expansion at constant enthalpy: the refrigerant passes through an expansion device and its pressure is reduced to state 4. At the evaporator inlet, the working fluid is a saturated vapor;

[1] All possible irreversibilities are neglected.

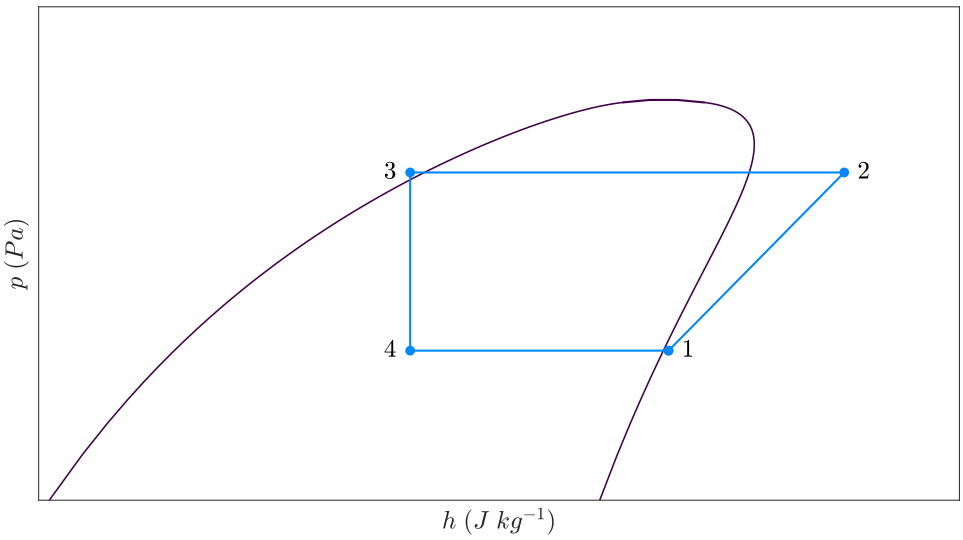

Figure 1.2
$\log p - h$ *qualitative diagram of a VCRS ideal cycle.*

$4 \rightarrow 1$ reversible heat addition at constant pressure: the refrigerant in the evaporator increases its enthalpy thanks to the heat received and becomes a superheated vapor [10].

An ideal VCRS operates essentially on a reversed Rankine cycle [1].

Real cycle

In a real refrigeration machine, there are some differences due to the practical realization of the cycle (Figure 1.3):

- the refrigerant pressure in the heat exchangers decreases because of friction losses. So $2 \rightarrow 3$ and $4 \rightarrow 1$ are no isobaric processes, and the compressor has to supply a higher pressure increase $1 \rightarrow 2$;
- to have heat exchangers with a finite area, a temperature drop is necessary between the refrigerant and the secondary fluid. For example, if the condenser of the refrigeration plant exchanges thermal energy with air at ambient condition, the maximal temperature of the working fluid in the heat exchanger has to be higher than ambient temperature;
- the compressor causes some irreversibilities which lead it to work following a polytropic transformation $1 \rightarrow 2$;
- usually, the expansion device cannot ensure that transformation $3 \rightarrow 4$ is adiabatic and isenthalpic;

- the refrigerant pressure decrease in the tubes between the components because of friction [10].

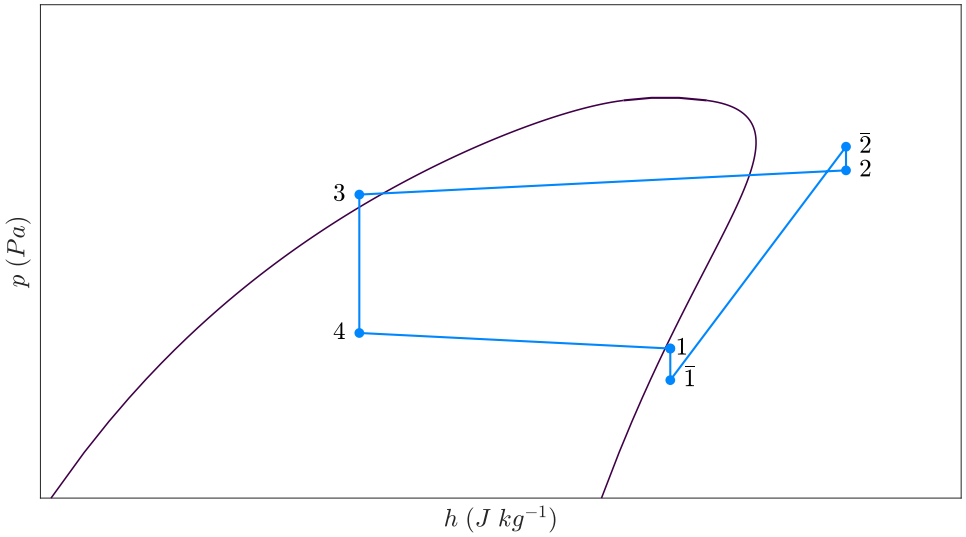

Figure 1.3
A $\log p - h$ *qualitative diagram of a VCRS real cycle.*
The pressure drops due to the friction factor along the tubes and the concentrate ones are taken into account in $1 \rightarrow \bar{1}$, $\bar{2} \rightarrow 2$. In the heat exchangers, the transformations are not isobaric. In this example, $3 \rightarrow 4$ is still isenthalpic.

COP

The efficiency of a power generation cycle is defined as the ratio between the energy output to the energy input. This definition would be ambiguous for a refrigeration cycle: it is more correct defining the efficiency as the desired quantity (the cooling effect) divided by what must be paid to achieve the desired quantity (the net work) [15]. This value can exceed the unit, so the term efficiency is not often used with this technology: in a refrigeration system, the term efficiency is replaced by the term coefficient of performance (COP), which is expressed as a pure number, usually between one and ten [1].

$$COP = \frac{Q_1}{P} \tag{1.2}$$

The COP of a Carnot cycle[2] depends on the boiling and condensation temper-

[2]The Carnot cycle consists of an expansion and a compression at constant entropy and two transformation at constant pressure.

atures T_1, T_2 (1.3) and its value is an upper limit.

$$COP_{Carnot} = \frac{T_1}{T_2 - T_1} \tag{1.3}$$

This limitation is a direct effect of the nature of heat as kind of energy. It's the sum of two different types of energy: the exergy, a form of energy which can be converted into other forms, and the anergy, a form of energy which cannot be converted into exergy. In a real cycle the COP is equal to the COP_{Carnot} only when all the exergy in input is transferred to the output. Examination of (1.3) shows that to obtain a maximum COP it's necessary to keep condensation temperature as low as possible and the evaporating temperature as high as possible. Yet, the selection of these two values is limited: in fact, T_1 must be lower than the cold room temperature and T_2 must be higher than the discharge room temperature, to transfer heat in a real system with heat exchangers of a finite area. So it seems clear that the practical realization of a refrigeration cycle causes a penalization of the COP [15].

Section 1.2

Basic components of a VCRS

There are several mechanical components required in a refrigeration system, but four of them are strictly necessary for the physical implementation of a VCRS: two heat exchangers, an expansion device and a compressor (Figure 1.4).

The selection of the components depends on some general factors like the refrigeration capacity, the type of refrigerant, the efficiency at the various working point, the system type and other considerations that are functions of the particular plant that has to be realized. [10].

1.2.1 | Heat exchangers

A heat exchanger is a device that promotes heat transfer from one medium to another. Usually, the mediums are fluids in gas or liquid phase: the heat coming from the cooling of the hotter fluid is used to warm the colder. In the

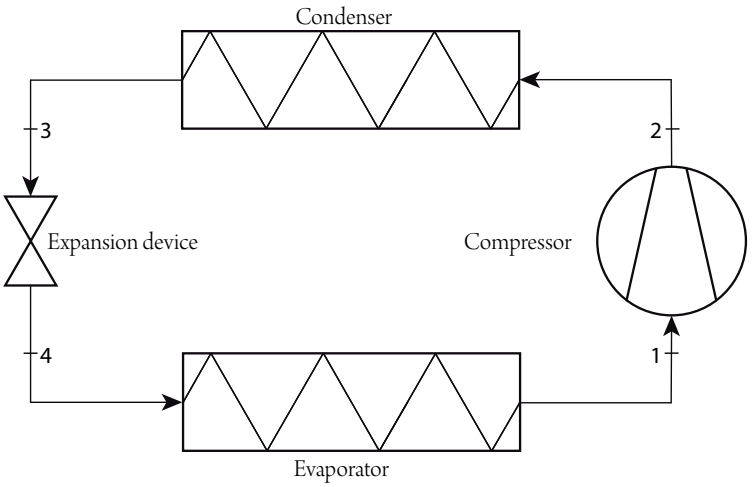

Figure 1.4
Major components of a VCRS.

VCRS one fluid is the refrigerant, the other is generally called secondary.

Condenser and evaporator

In a VCRS there are at least two heat exchangers: the evaporator and the condenser. The purpose of the evaporator is to receive cold, low pressure, saturated vapor from the expansion device and to bring it in contact with the thermal load to take its thermal energy, leaving the heat exchanger as superheated vapor. The purpose of the condenser is to take hot, high-pressure superheated vapor refrigerant from the compressor and cool it to the state of subcooled liquid [13].

Several types of heat exchangers are available on the market and only the most popular are mentioned in this short description. Still, there are some common properties that can be useful to categorize and illustrate them as shown in the Table 1.1.

For the correct choice of a heat exchanger, the designer has to consider a lot of factors, including the material of construction, the operating pressure and temperatures, flow rates, thermal effectiveness, pressure drops, type and phase of fluids, overall economy. The most common types of heat exchangers in the VCRS are now reviewed briefly, but for a wider point of view the book of Thulukkanam [12] which is used as a reference in this section is recommended.

Table 1.1
Categorization of heat exchangers [16].

Property	*Possibilities and description*
Transfer phenomena	direct contact: hot and cold flows can mix; indirect contact: hot and cold flows remain separate.
Surface compatibility	compact: the surface area to volume ratio is less then 700 $\frac{m^2}{m^3}$; non compact: the surface area to volume ratio exceeds 700 $\frac{m^2}{m^3}$.
Arrangement	parallel flow: hot and cold flows move in the same direction; counter flow: hot and cold flows move in the opposite direction; cross flow: one flow moves across the other at a certain angle.
Configuration	shell and tube heat exchanger; plate heat exchanger; tubular heat exchanger; spiral heat exchanger.
Transfer mechanism	single-phase convection on both sides; single-phase convection on one side and two-phase on the other; two-phase convection on both side.
Transfer surface	primary surfaces: the main surfaces separating the hot and cold flows; secondary surfaces: surfaces mounted on the primary surfaces to increase heat transfer area.

Shell and tube heat exchangers

The shell and tube heat exchangers (Figure 1.5) are normally employed in the condensation of the refrigerant for large thermal loads when the secondary fluid is a liquid to restrict the dimension of the component. The configuration and the design of tubes and shell define the layout of the heat exchanger.

Finned heat exchangers

Finned heat exchangers, plate-fin or tube-fin (Figure 1.6), are employed when there is a significant difference between the heat transfer coefficients of the two fluids. The fins increase the area available for heat transfer, decreasing the thermal global resistance, under the same occupied space. For this reason, the finned heat exchangers are ideal when the secondary fluid is a gas, e.g. ambient air. Tube-fin heat exchangers are extensively used as condensers and evaporators in refrigeration systems.

Plate heat exchangers

Plate heat exchangers (Figure 1.7) are used as condensers and evaporators in small- and medium-sized refrigeration applications. They offer some benefits like high heat transfer performance, small temperature difference between the two fluids in a generic section, very well defined counterflow, easy maintenance,

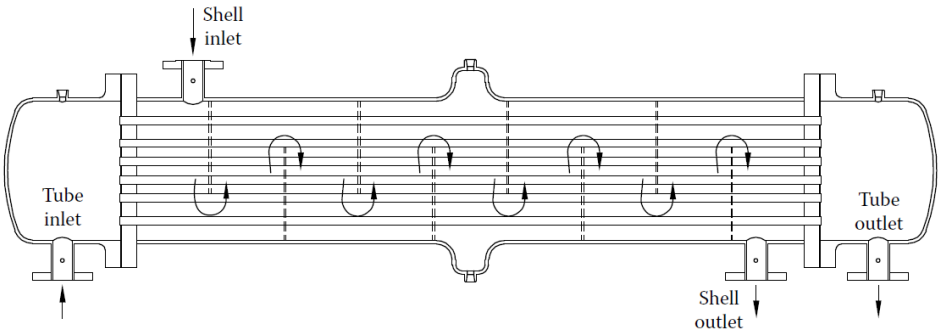

Figure 1.5
Shell and tube heat exchanger [12].
They consist of a series of tubes in which the secondary fluid in liquid phase flows. These pipes are contained in a closed space called shell where the refrigerant is.

Figure 1.6
Tube-fin heat exchanger: forms of finned tubes [12].
The fins are employed either on the outside or inside or both sides of the tubes, depending upon the applications.

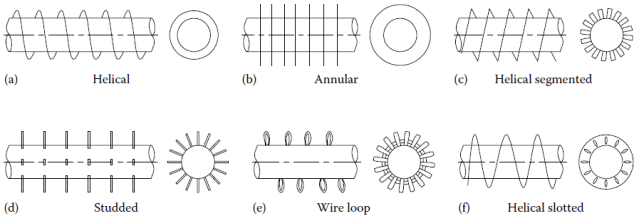

lower cost, lightweight and high viscosity fluid applications. Many construction technologies can be employed to realize a plate heat exchangers to increase performance and efficiency.

1.2.2 | Compressors

The purpose of the compressors in a VCRS is to compress the superheated vapor refrigerant from the evaporator's low-pressure to the condenser's high-pressure. Compressors may be divided into positive displacement, where the gas is compressed by the physical reduction of a volume, and dynamics, where, according to the energy conservation, a reduction of the velocity of the refrigerant causes a pressure increase [14]. Even if refrigeration takes place at the evaporator, the compressor is characterized as having refrigeration capacity, because it's capable of pumping the flow rate of refrigerant that will provide the stated refrigeration capacity at the evaporator [15].

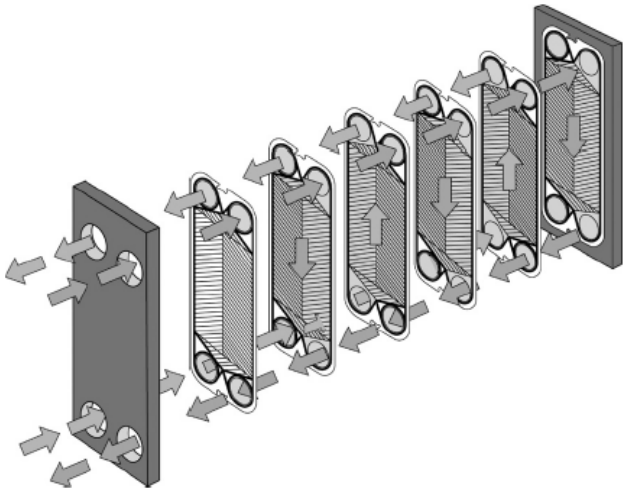

Figure 1.7
Plate heat exchanger [14].
A stack of metal plates are in mutual contact, forming a series of channels where the two fluids can flow alternately while exchanging heat. Each plate has four apertures serving as inlet and outlet ports for the fluids.

The main types of compressors used in VCRS are reciprocating, rotary vane, scroll, screw and centrifugal, which are now introduced. More details are available in the literature [10, 11, 13–15].

The superheated degree

First of all, it's necessary to underline a common property of all the compressors previously listed (except scroll). To safeguard the health of a compressor a superheated vapor is recommended at the inlet: the liquid drops in saturated vapor damage the machine's components, compromising its life and efficiency. For this reason at the evaporator outlet, the refrigerant is at the state of superheated vapor.

Reciprocating compressors

The reciprocating compressors (Figure 1.8) may be single or multi-cylinder (in V, W, radial or linear form), single-action or double-action compressor, single-stage (for few bars) or multi-stage with cooling between stages (for high pressure drops, up to around 50 bar), hermetic or semi-hermetic or open (according to the connection between the crankshaft and the electromotor). They are positive displacement machines and they are used for application with high refrigeration capacity or in low cooling capacities where a minimal cost is required.

Sliding and rotary vane compressors

Sliding (Figure 1.9) and rotary vane compressors are a subset of positive displacement machines. Their design varies widely and it is the main feature which distinguishes the different types of rotary vane compressors. Larger models do not require inlet or outlet valves and their best properties are a simple and compact design, a direct axial coupling to the motor, a low need

for maintenance and low cost. They are employed in domestic applications or in low capacity refrigeration.

Figure 1.8
Reciprocating compressor [14].
This type of compressor works like an internal combustion engine: thanks to the movement of a piston, the refrigerant is suctioned, compressed and discharged. The fluid enters and leaves the cylinder by lamellar valves that automatically open and close in accordance with the pressure drop between the cylinder and the suction and discharge ducts respectively.

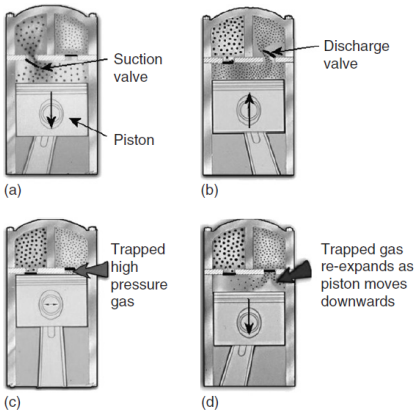

Figure 1.9
Sliding vane compressor [13].
The blades occupy their vanes and, during the rotation of an eccentric rotor, they slide outwards, creating some volumes which contain the refrigerant. The gas enters through the intake port where the section is large, is compressed and is discharged where the section is small.

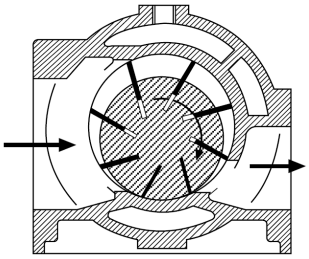

Scroll compressors

Scroll compressors (Figure 1.10), belonging to positive displacement machines, have a very important detail: they can suction some drops of liquid at the inlet without affecting their working life. Compression is a continuous process, so there are low noise and vibrations compared to other compression techniques. Scroll compressors are employed in medium refrigeration capacities, where the requirements are a very reliable component and high efficiency.

Screw compressors

The last positive displacement machine presented is the screw compressor (Figure 1.11). One of the most usual form of this machine has twin matching rotors on parallel shafts, one of them, the male, is driven by a motor, and the other, the female, is driven by the male. They are recommended in the applications were the refrigeration capacity is variable thanks to a sliding block, the working stroke can be varied, permitting a capacity reduction without compromising the efficiency.

Centrifugal compressor

Sometimes in VCRSs dynamic compressors are employed, like the centrifugal

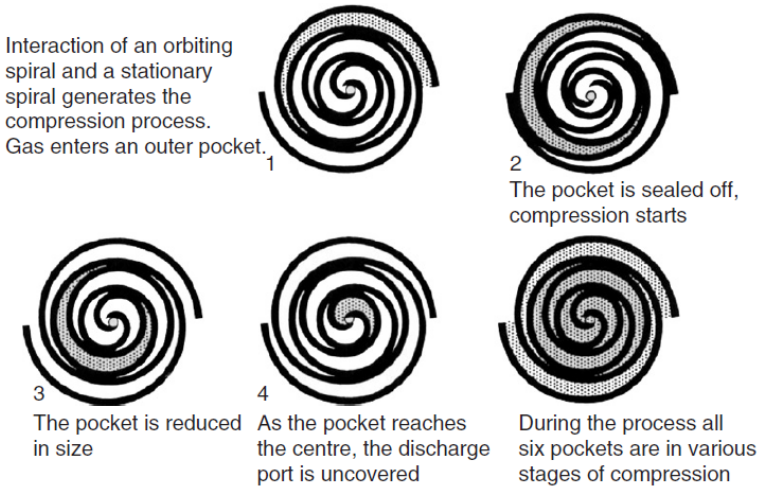

Figure 1.10
Scroll compressors [14].
The lower scroll, driven by an electric motor shaft, imparts an orbital motion to the driven scroll around the upper scroll which is stationary and contains the discharge port.

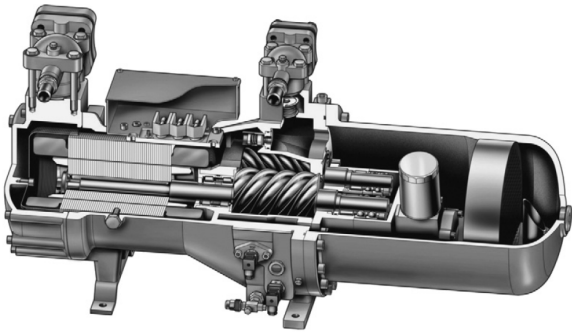

Figure 1.11
Screw compressor [14].
The gas is drawn into the volume identified by the male and the female rotors. Their motion forces the gas to move parallel to the rotor shaft, realizing the compression.

one (Figure 1.12): they are used for high refrigeration capacities where compression is usually divided over various steps, or for high-flow or low-pressure difference applications. This machine is very sensitive to the suction and discharge condition that have to be monitored to avoid failures of any kind.

Due to the presence of moving components, the designer must consider the correct management of the lubricating oil in many of the compressors previously described. Another interesting issue is the possibility of cooling the refrigerant during compression to reduce the specific volume of the gas, increasing the efficiency of the process. In conclusion there are a lot of factors that have to be considered for a correct choice of a compressor: but a very im-

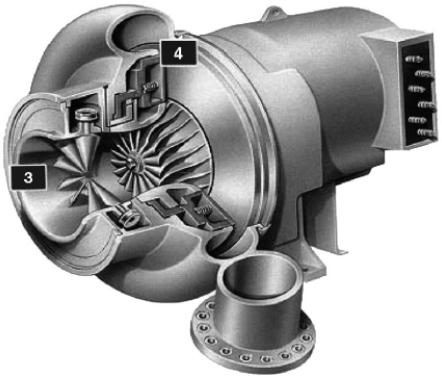

Figure 1.12
Centrifugal compressor [14].
First of all, a rotating impeller imparts velocity to the gas. Past the housing the gas flows out, converting a portion of the kinetic energy into static pressure.

portant driver in VCRS is the refrigeration capacity that a kind of compressor can assure, as shown in (Figure 1.13).

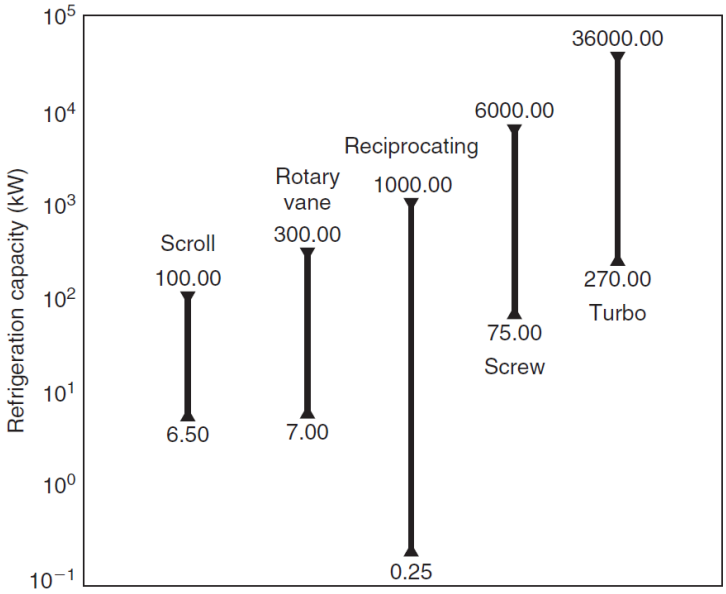

Figure 1.13
Range of capacity covered by various compressor types [14].

1.2.3 | Expansion devices

Reducing the refrigerant pressure from condensation to evaporation conditions by a throttling operation and controlling the refrigerant flow to match the load characteristics are the main purposes of an expansion device [10].

A simple way to realize an expansion device is to create a pressure reduction through a variable flow orifice. This happens inside the expansion valves which

Expansion valves

may be classified according to the method of control. Thermostatic expansion valves (TEV) (Figure 1.14) automatically control the refrigerant flow to the evaporator. Electronic expansion valves (EEV) (Figure 1.15) are recommended for a finer degree of control.

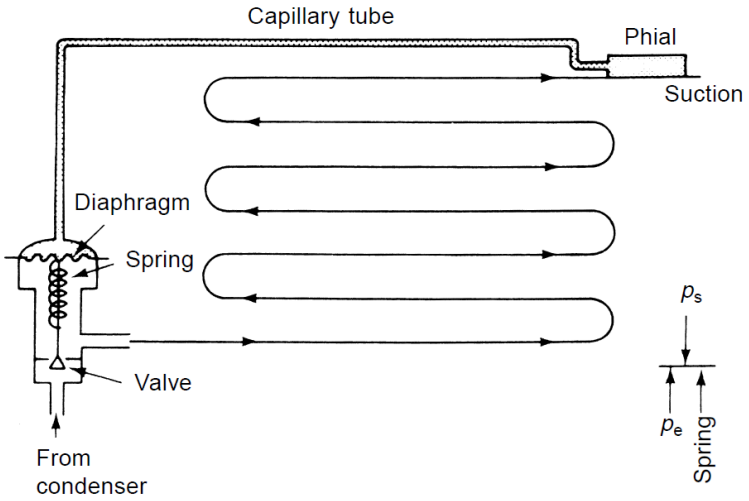

Figure 1.14
Thermostatic expansion valve [14].
A diaphragm and a spring define the position of the valve. The diaphragm is subject to the difference between the pressure generated in the phial by the superheated vapor (passing through the capillary tube) and the pressure at the inlet of the evaporator. At equilibrium, this force is balanced by the spring. When the evaporator load is modified, the suction temperature and the pressure into the capillary tube change. The force of the spring in the previous position of the valve is not balanced, so the valve moves to a new equilibrium position and the orifice changes its aperture.

Capillary tube

The capillary tube is a valid alternative to the expansion valves in small refrigeration capacity applications. Refrigerant mass flow is a function of the pressure drop and the subcooling degree at the inlet and cannot be manually controlled [13].

Energy recovery

The devices presented previously cannot recover the enthalpy difference. A turbine might be used to produce mechanical energy while the refrigerant passes from condenser to evaporator pressure. But this work will be very little and not large enough to justify the costs of a turbine.

Ejectors

For this reason ejectors are employed as recovery components. The inclusion of an ejector in VCRS results in a theoretical energy efficiency increase

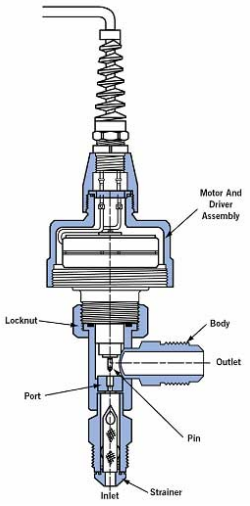

Figure 1.15
Electronic expansion valve [17].
An EEV offers some benefits over a TEV: precise flow control over a wide range of capacities, rapid response to load changes, better control at low superheats, greater flexibility in system layout, the possibility to close the valve when the system shuts down without other devices [14].

with the advantages of simplicity and economy in construction, installation and maintenance [18]. Sarkar [19] shows the energetic and exergetic performance improvement using ejectors and the possibility of adjusting the geometric parameters to maximize them. Kursad Ersoy and Bilir Sag [20] compare a traditional VCRS with one in which the expansion valve is substituted by an ejector. The studies underline that the work recovery in the ejector cycle is between 14% and 17%, depending on the operating conditions. There is also an improvement of the COP until 14.5%.

Section 1.3

The refrigeration machine studied

The machine studied for the development and the validation of the model (Figure 1.16) is owned by the Mechanical Department of the Politecnico di Milano. The refrigerant and secondary circuits possess some auxiliary components that are often used in the practical realization of a refrigeration cycle to improve the performance and the efficiency of the plant and the reliability of the mechanical parts. These components are not modelled because their contribution to the thermodynamic cycle is not relevant. Instead, the condenser, the evaporator, the compressor and the expansion valves must be carefully described. In this way, it is possible to understand the physical phenomena and the geometric parameterswhich must be taken into account for an appropriate

modelling of all the components. meted

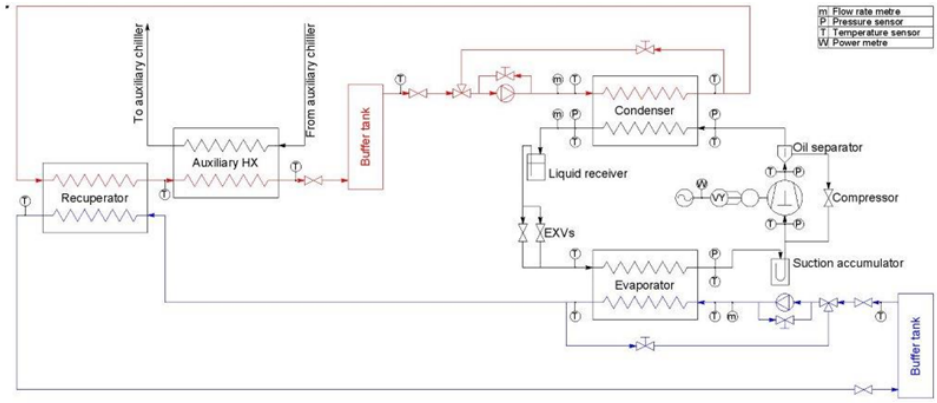

Figure 1.16
Scheme of the studied refrigeration plant

1.3.1 | Condenser

Brazed plate heat exchangers

The condenser is a brazed plate heat exchanger (BPHE), a particular kind of PHE. The plates are brazed together in a vacuum oven to form a unit, without gaskets, which can be used in high-pressure and high-temperature duties thanks to its robustness. The BPHE ensures a compact size and high thermal efficiency [12]. The working principle is the same as a PHE (Section 1.2), with the refrigerant and the secondary fluid which flow alternately in the channels between two adjacent plates. In the condenser (Figure 1.16), the refrigerant inlet is on the same side as the secondary fluid outlet and vice versa: so the condenser is a counter flow heat exchanger.

Chevron type BPHE

The chevron type BPHEs, like the condenser, are used in most industrial applications. Their design is responsible for the heat transfer performances. They are formed by a series of corrugated plates. In this way, two adjacent plates are in contact in some portions, while there is a gap in the other area: in these channels the fluid can flow. As a consequence, the route of the fluid is influenced by the geometry characteristic of the corrugated plate. Martin [21] states that the most important parameter for the fluid dynamic and heat transfer performance in a chevron type BPHE is the chevron angle β, which is the angle of the corrugation (Figure 1.17).

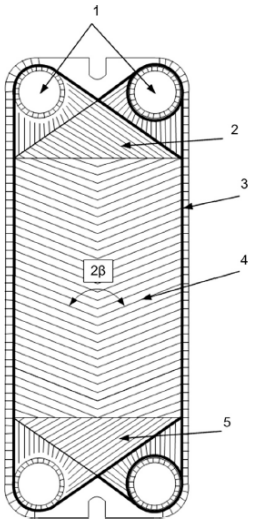

Figure 1.17
Plate geometry [22].
1: Inlet and outlet of the hot and cold fluids. 2,5: Portion of the plate where the fluids occupy, entering from the inlet, and exiting from the outlet, all the channels. 3: This isn't a BPHE (even if the plate geometry is the same), so there are the gaskets to avoid fluid leakage. 4: Useful area for the heat exchange. The fluids are in the channels and their hydrodynamic conditions are the best for optimal thermal performance.

The phase between two adjacent plates is also another important parameter. Considering two plates with the same β, if the plates are in phase there aren't point of contact, while if they are π out of phase, there are a lot of points of contact and the channel is very different (Figure 1.18).

β and the fluid hydrodynamic

There are several combinations of β and the phase which define the fluid hydrodynamic. For example, two plates with $\beta = 90$ and π out of phase restrict the fluid motion, which could not move from the first channel met. The friction factor becomes equal to infinity. In this way, the heat transfer is inhibited as well. So β and the phase are very important for a correct modeling of the heat exchanger. This is the reason why, a lot of studies, show the connection between β and the friction factor or the Nusselt number, like Martin [21]. This topic will be discussed in the next chapter.

The BPHE parameters

In Tab 1.2 the most important geometric parameters of a chevron type BPHE are listed.

Starting from the plate dimensions, the projected plate surface area A_{proj} (1.4) is defined.

$$A_{proj} = B\ L \tag{1.4}$$

In fact, due to the corrugation, the real plate surface area A_{plate} is higher than the simple product of B times L. For this reason, the constructors usually give

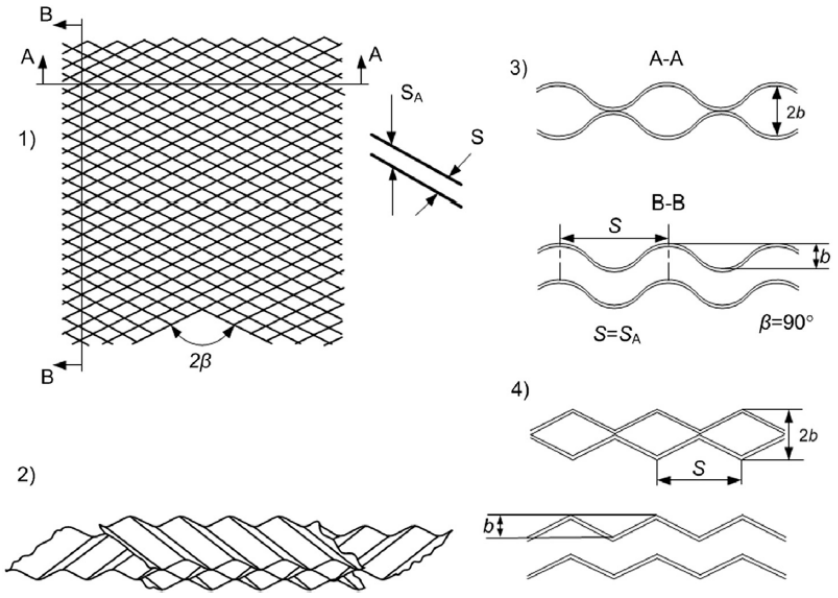

Figure 1.18
Phase and β effect on the channels [22].
1: The corrugation profiles of two adjacent plates. 2: The intersection of two adjacent plates. 3: The phase effect for a sinusoidal form of corrugation. 4: The phase effect for a triangular form of corrugation.

the value of ϕ: in this way, A_{plate} can be obtained from the A_{proj} (1.5).

$$A_{plate} = \phi \, A_{proj} \tag{1.5}$$

The total surface area of a BPHE can be obtained from n_{plates} (1.6).

$$A_{total} = A_{plate} \, n_{plates} \tag{1.6}$$

As shown in (Figure 1.17) there are some regions of the plates where the fluid dynamics isn't well defined (regions 2,5), and others like the inlet and outlets where the fluid is just introduced and evacuated (region 1). In these areas it's very hard to understand the heat transfer mechanism. For this reason, the estimation of A_{plate} is very difficult. According to literature, only the plate surface where the fluid dynamics is developed can be considered useful for the heat transfer. This surface is estimated inserting in the (1.5) correct quantities for L and B, defined as the semi-sum between the total length/width and the

Table 1.2
BPHE geometric parameters

Symbol	*Physical quantity*
B	Plate width
L	Plate length
b	Offset between two plates
ϕ	Plate area enlargement factor
β	Chevron angle
n_{plates}	Number of plates
$n_{ch,ref}$	Number of refrigerant channels

distance between two ducts along the length/width (1.7).

$$L = \frac{289 + 243}{2} = 266\ (mm) \qquad B = \frac{119 + 72}{2} = 95,5\ (mm) \tag{1.7}$$

To compute the total surface area of exchange it's important to take into account that the first and last plate aren't involved in the heat transfer process. So the (1.6), if n_{plates} considers the outside plates, has to be modified (1.8).

$$A_{total} = A_{plate}\ (n_{plates} - 2) \tag{1.8}$$

The condenser data (Table 1.3) can be found consulting the catalogue [23]. The scheme (Figure 1.19) is useful to characterize B and L.

1.3.2 | Evaporator

The evaporator (Figure 1.20) is a chevron type BPHE, so the considerations of the condenser are valid for this case too. The only differences concern the heat exchanger size. The values of the geometric parameters (Table 1.4) are deducted from the catalogue [24] and the same calculations seen previously.

1.3.3 | Compressor

A semi-hermetic reciprocating compressor is used in the circuit (Figure 1.21). This means that the motor and the compressor are within one casing which may be unbolted without refrigerant leakage [10]. Some properties, obtained

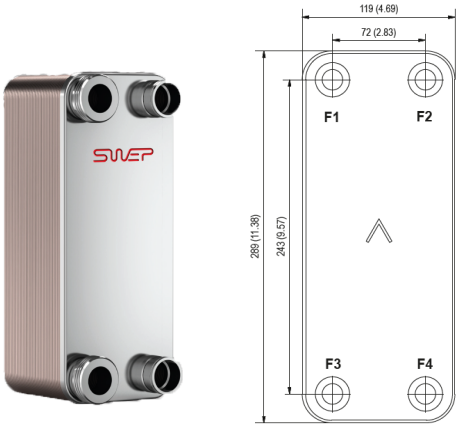

(a) *Photo* (b) *Plate dimension*

Figure 1.19
The plant condenser [23].

Symbol	*Value*	*UoM*
L	266	mm
B	$95,5$	mm
b	$2,4$	mm
β	50	deg
ϕ	$1,19$	–
$n_{ch,ref}$	20	–
$n_{ch,sec}$	20	–

Table 1.3
Condenser geometrical data [23].

(a) *Photo* (b) *Plate dimension*

Figure 1.20
The plant evaporator [24].

Symbol	*Value*	*UoM*
L	348	mm
B	91	mm
b	$2,6$	mm
β	60	deg
ϕ	$1,21$	–
$n_{ch,ref}$	15	–
$n_{ch,sec}$	15	–

Table 1.4
Evaporator geometrical data [24].

from catalogue [25], are shown in the Table 1.5.

Figure 1.21
Plant compressor [25].

Physical quantity	*UoM*	*Value*
Cylinders	–	2
Nominal motor power	kW	$2,2$
Max power consumption	kW	$4,8$
Head capacity control steps	%	$100-50$
Frequency min	Hz	30
Frequency max	Hz	87
Motor voltage at 50 Hz	V	$220-240$

Table 1.5
Compressor technical data [25].

1.3.4 | Expansion valves

In the plant there are two EEVs (Figure 1.22). They control the mass flow rate thanks to a nozzle coupled to a torpedo-shaped aperture over a wide operating range. More informations are available in the technical documentation [26]: the valve's code is E2V24.

Figure 1.22
Plant EEVs [26].
This type of valves ensure high precision control in all applications, even at low flow-rates and in both directions.

1.3.5 | Refrigerant

The refrigerant used in the plant is the R450a, a particular zeotropic mixture of two more common refrigerants, the R134a and the R1234ze.

Azeotropic and zeotropic mixtures

An azeotropic mixture, like the R134a, is formed by two or more fluids but it can be treated as a pure fluid: at constant pressure, it condenses or evaporates

at the same temperature (Figure 1.23) and it has the same composition both at liquid and vapor state. The temperature of a non-azeotropic or zeotropic

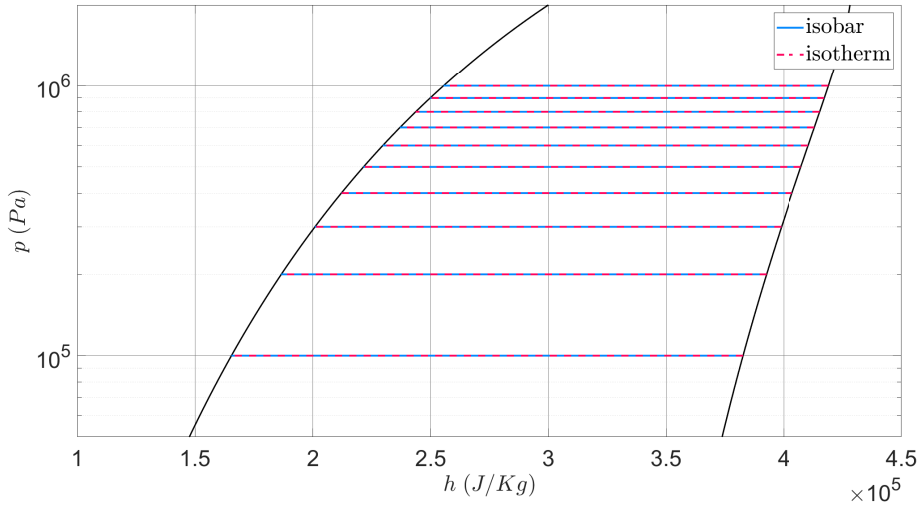

Figure 1.23
Condensation: R134a

mixture is not equal during the condensation or evaporation process at constant pressure (Figure 1.24). Considering a two-substance mixture, the concentration of the two substances in the vapor is different from that in the liquid at a given pressure and temperature [15]. For these kinds of blends the glide temperature, defined as the difference between the dry saturated vapor and temperature and the saturated liquid temperature at the same pressure, is introduced. The glide temperature is a function of the mixture considered and pressure, and, for the R450a, has a small value (1.25). More information about this refrigerant is available in Appendix A.

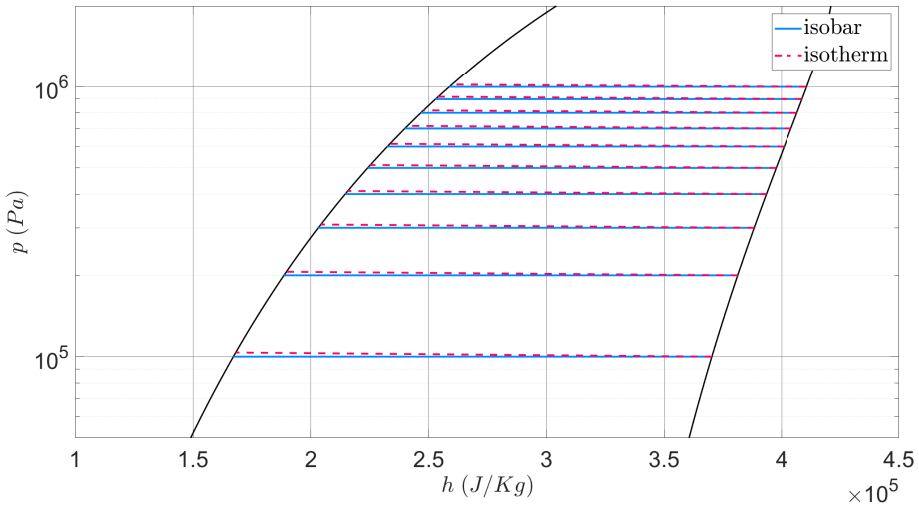

Figure 1.24
Condensation: R450a

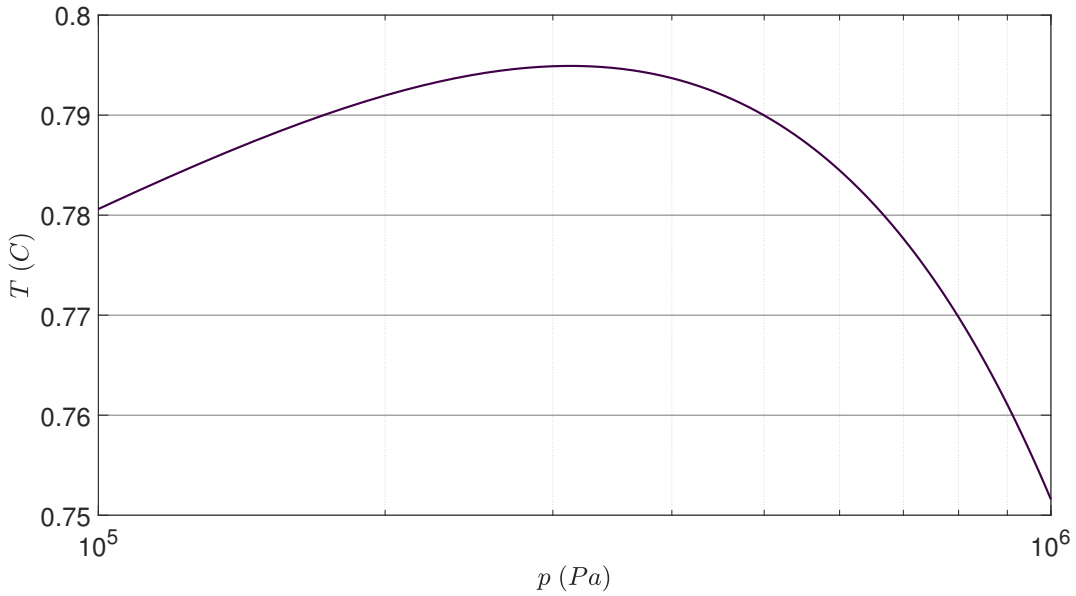

Figure 1.25
Glide temperature as function of the condensation pressure: R450a

Chapter 2

The physical model

The models are a description, a representation, a simplification of a real phenomenon. They can be considered as a box that converts inputs into outputs and they are used to explain and predict the behavior of real systems. In a physical model inputs (I) and outputs (O) are physical quantities connected through a set of equations ($\boldsymbol{M}$).

$$O = \boldsymbol{M} \cdot I$$

The modeler identifies the problem for which the model is necessary. Then, this is developed, implemented and is used to make predictions after validation.

In this chapter, the model structure is developed: the physical principles and the equations that govern a VCRS cycle in steady state conditions are introduced (Section 2.2), (Section 2.3), (Section 2.4). First of all, it is necessary to focus on the experimental data which are essential for the correct validation of the model before its use (Section 2.1).

Section 2.1

Experimental data acquisition

The experimental data are available from previous works on the same refrigerant plant focused on dynamic characterization. Only the stationary points of work are useful for the correct validation of the model, so pre-processing of this data is necessary. First of all, the data is filtered and smoothed. Next, the

time intervals where the refrigerant pressures and enthalpies are reasonably constant are found. For each interval the mean value of the signal considered (Figure 2.1) is evaluated. Finally, all the mean signals for the same time interval are saved as structure in Matlab (Code 2.1).

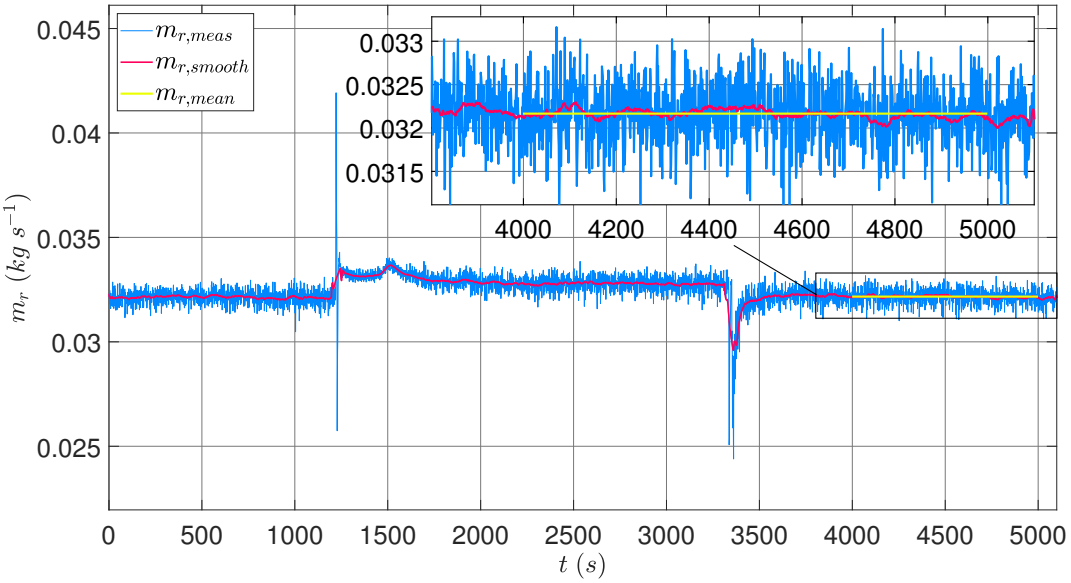

Figure 2.1

Example of acquired data.

In this example the signal processed is m_r. The acquired data is smoothed and next for the time interval from 4000 s to 5000 s the mean value is calculated.

Code 2.1

The structure for the acquired data.

In the structure are listed some physical quantities of interest including enthalpies, pressures, temperatures and mass flow rate of refrigerant and secondary fluids.

```
Dati_sperimentali =

  struct with fields:

    Ref: [1x1 struct]
    Sec: [1x1 struct]

Dati_sperimentali.Ref=

  struct with fields:

      m_r: 0.0321
     Cond: [1x1 struct]
     Evap: [1x1 struct]
     Comp: [1x1 struct]

Dati_sperimentali.Ref.Cond

  struct with fields:

      pc_in: 1.0554e+06
     pc_out: 1.0525e+06
```

```
      T_r_in: 74.8254
     T_r_out: 37.2292
       T_r_v: 44.0696
       T_r_l: 43.9635
     DT_sott: 6.7344
      h_r_in: 4.4442e+05
     h_r_out: 2.5170e+05

Dati_sperimentali.Sec.Evap

  struct with fields:

         m_f: 0.2789
      T_f_in: 8.5142
     T_f_out: 4.0482
```

Section 2.2

Model equations

As previously mentioned, the model uses a physical approach: so the governing equations of all the components, which are now introduced, are obtained from the application of physical laws, principles and observations and consulting similar works in literature. Bejarano, Rodríguez, Alfaya, Ortega, and Castaño [7] and Yang, Ordonez, and Vargas [8] suggest the physical quantities and some relations which could be useful for the correct mathematical approach to the model.

2.2.1 | Condenser

The condenser model is based on some hypothesis:

Hypothesis

- cross-section area constant in the heat exchanger;
- negligible pressure loss in the heat exchanger;
- negligible conductive thermal resistance of the plates;
- negligible axial conduction in fluids;
- the condenser always works with a degree of subcooling.

Under these assumptions, the heat transfer rate is calculated using the energy balance between the refrigerant and the secondary fluid (2.1) and the effectiveness NTU method (2.2) (Appendix B).

Global equations

$$m_r \left(h_{r,in} - h_{r,out}\right) = m_f \; c_{p,f} \left(T_{f,in} - T_{f,out}\right) \tag{2.1}$$

$$\varepsilon \; C_{min}(T_{r,in} - T_{f,in}) = m_r \left(h_{r,in} - h_{r,out}\right) \tag{2.2}$$

If the first relation (2.1) can be implemented even for the determination of the total heat flux exchanged, the second one (2.2) is not correct because the thermophysical properties of the fluids and the mechanism of the heat transfer change along the condenser: it is therefore impossible to find a correct expression for the effectiveness.

Condenser regions

As underlined by the experimental data, the refrigerant enters the condenser as superheated vapor and exits as subcooled liquid. So in the condenser, there are three regions, according to the refrigerant state (Figure 2.2):

- superheated region;
- two-phase region;
- subcooled region.

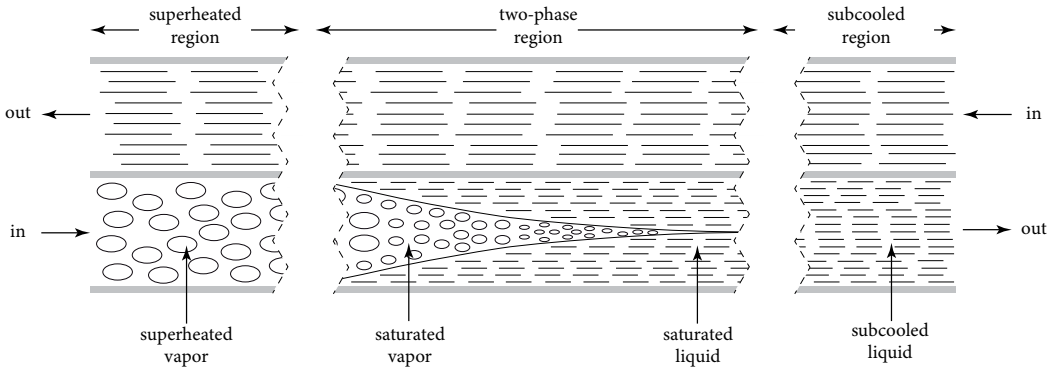

Figure 2.2
Condenser regions

Equations of the regions

Every zone has its balance and $\varepsilon - NTU$ equation. Thus, the condenser can be treated as a set of three different heat exchangers connected in series. Referring to the qualitative $T - Q$ diagram in Figure 2.3, for each zone the energy balance and the $\varepsilon - NTU$ method are written (2.3) (2.4) (2.5) (2.6) (2.7) (2.8).

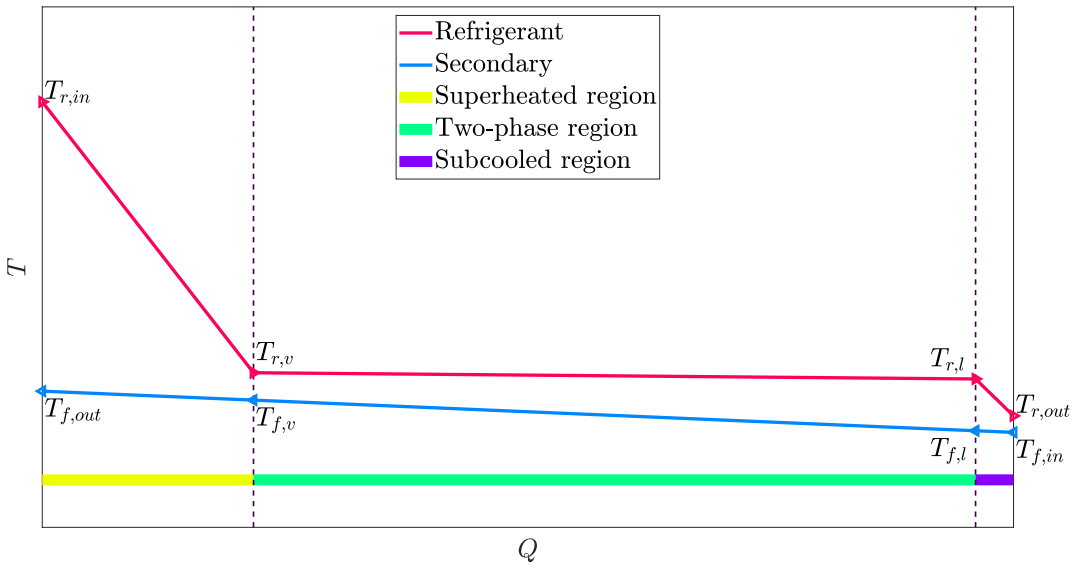

Figure 2.3
Qualitative $T-Q$ diagram for the condenser.

sh zone energy balance	$m_r\ (h_{r,in} - h_{r,v}) = m_f\ c_{p,f,sh}\ (T_{f,out} - T_{f,v})$	(2.3)
sh zone $\varepsilon - NTU$	$m_r\ (h_{r,in} - h_{r,v}) = \varepsilon_{sh}\ C_{min,sh}\ (T_{r,in} - T_{f,v})$	(2.4)
tp zone energy balance	$m_r\ (h_{r,v} - h_{r,l}) = m_f\ c_{p,f,tp}\ (T_{f,v} - T_{f,l})$	(2.5)
tp zone $\varepsilon - NTU$	$m_r\ (h_{r,v} - h_{r,l}) = \varepsilon_{tp}\ C_{min,tp}\ (T_{r,v} - T_{f,l})$	(2.6)
sc zone energy balance	$m_r\ (h_{r,l} - h_{r,out}) = m_f\ c_{p,f,sc}\ (T_{f,l} - T_{f,in})$	(2.7)
sc zone $\varepsilon - NTU$	$m_r\ (h_{r,l} - h_{r,out}) = \varepsilon_{sc}\ C_{min,sc}\ (T_{r,l} - T_{f,in})$	(2.8)

For each zone, the effectiveness ε_i $(i = sh,\ tp,\ sc)$ is a function of the number of transfer units NTU_i (2.10) and the heat capacity ratio γ_i (2.11).

$$\varepsilon_i = f\ (NTU_i,\ \gamma_i) \tag{2.9}$$

$$NTU_i = \frac{(UA)_i}{C_{min,i}} \tag{2.10}$$

$$\gamma_i = \frac{C_{min,i}}{C_{max,i}} \tag{2.11}$$

The form of these functions (2.9) is discussed later (Section 2.5). NTU_i is

The overall conductance

a non-dimensional number defined as the ratio of the product between the overall conductance times the heat transfer surface area of the i-th zone $(UA)_i$ to the minimum heat capacity ratio C_{min}. In general $(UA)_i$ depends on the convective heat transfer coefficients for the refrigerant $\alpha_{r,i}$ and the secondary fluid $\alpha_{f,i}$, the heat transfer surface area, refrigerant $A_{r,i}$ and secondary $A_{f,i}$ side respectively, and the convective thermal resistance of the plate $R_{th,plate}$ (2.12).

$$(UA)_i = \frac{1}{\frac{1}{\alpha_{r,i}A_{r,i}} + R_{th,plate} + \frac{1}{\alpha_{f,i}A_{f,i}}} \tag{2.12}$$

Under the assumptions previously listed, the (2.12) can be simplified (2.13), because $A_{f,i} = A_{r,i} = A_i$ and $R_{th,plate} \approx 0$.

$$(UA)_i = \frac{A_i}{\frac{1}{\alpha_{r,i}} + \frac{1}{\alpha_{f,i}}} \tag{2.13}$$

In short, in every i-th zone, a heat transfer surface area A_i and an overall heat transfer coefficient U_i^{-1} (2.14) are identified.

$$\frac{1}{U_i} = \frac{1}{\alpha_{r,i}} + \frac{1}{\alpha_{f,i}} \tag{2.14}$$

The determination of $\alpha_{r,i}$ and $\alpha_{f,i}$ is presented later (Section 2.3). A_i is a function of the total heat transfer surface area of the condenser A_{tot}. Obviously (2.15) must be verified.

$$A_{sh} + A_{tp} + A_{sc} = A_{tot} \tag{2.15}$$

Moving A_{tot} from the right to the left of the equation, (2.15) can be rewritten as (2.16) and (2.18), highlighting three non-dimensional quantities ζ_i (2.17).

$$\frac{A_{sh}}{A_{tot}} + \frac{A_{tp}}{A_{tot}} + \frac{A_{sc}}{A_{tot}} = 1 \tag{2.16}$$

$$\zeta_i = \frac{A_i}{A_{tot}} \tag{2.17}$$

$$\zeta_{sh} + \zeta_{tp} + \zeta_{sc} = 1 \tag{2.18}$$

Equation (2.18) is a sort of congruence law for the three zones of the condenser.

2.2.2 | Evaporator

The evaporator model is similar to the condenser: the nature of the equations is the same and, at first, the model is developed according to the same assumptions as for the condenser. The most relevant difference is about the regions into which the evaporator can be divided: in fact, the refrigerant enters as a liquid vapor mixture and exits as a superheated vapor. So in the evaporator, there are only two regions (Figure 2.4), according to the refrigerant state:

- two phase region;
- superheated region.

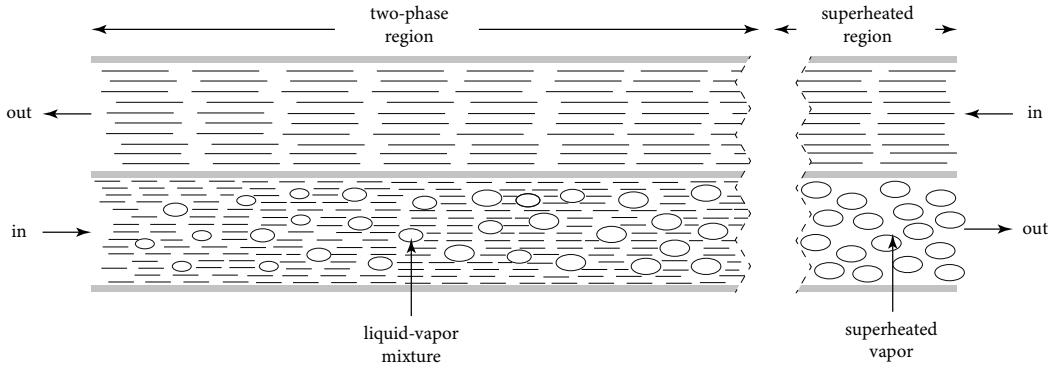

Figure 2.4
Evaporator regions

For each zone the energy balance and the $\varepsilon - NTU$ method are written (2.19) (2.20) (2.21) (2.22) (Figure 2.5).

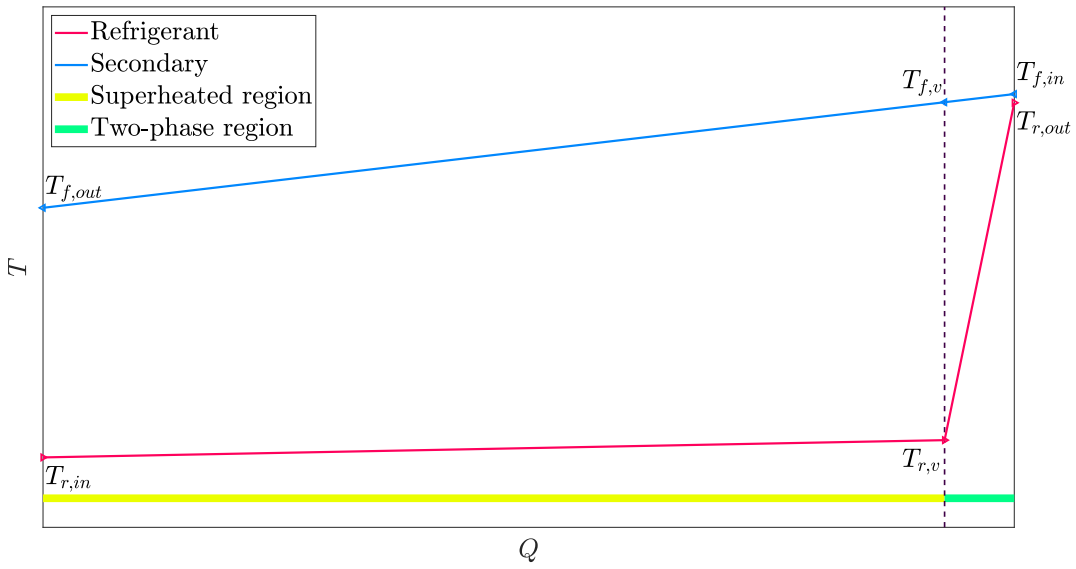

Figure 2.5
Qualitative $T-Q$ diagram for the evaporator.

$$\text{tp zone} \quad \text{energy balance} \qquad m_r\,(h_{r,v}-h_{r,in}) = m_f\,c_{p,f,tp}\,(T_{f,v}-T_{f,out}) \tag{2.19}$$

$$\text{tp zone} \quad \varepsilon - NTU \qquad m_r\,(h_{r,v}-h_{r,in}) = \varepsilon_{tp}\,C_{min,tp}\,(T_{f,v}-T_{r,in}) \tag{2.20}$$

$$\text{sh zone} \quad \text{energy balance} \qquad m_r\,(h_{r,out}-h_{r,v}) = m_f\,c_{p,f,sh}\,(T_{f,in}-T_{f,v}) \tag{2.21}$$

$$\text{sh zone} \quad \varepsilon - NTU \qquad m_r\,(h_{r,out}-h_{r,v}) = \varepsilon_{sh}\,C_{min,sh}\,(T_{f,in}-T_{r,v}) \tag{2.22}$$

Obviously, also for the evaporator, $\varepsilon_i \quad i = sh,\ tp$ is a function of the NTU_i, an overall HTC is identified and the condition on the total area must be obeyed (2.23).

$$\zeta_{sh} + \zeta_{tp} = 1 \tag{2.23}$$

Pressure drop

The condensation pressure is about 10 *bar* that of evaporation is about 2 *bar*. Therefore, the assumption of constant pressure along the heat exchangers, could not be acceptable for the evaporator where pressure drops are significant compared to working pressure. As new assumption, for the development of this model, all the pressure drop is concentrated in the two-phase region of the evaporator. So the superheated vapor and the saturated vapor are at the same pressure, whilst the inlet liquid vapor mixture is at a higher pressure. The

structure of the equation is the same of the model without the pressure drop even if the qualitative $T - Q$ diagram expected is different (Figure 2.6).

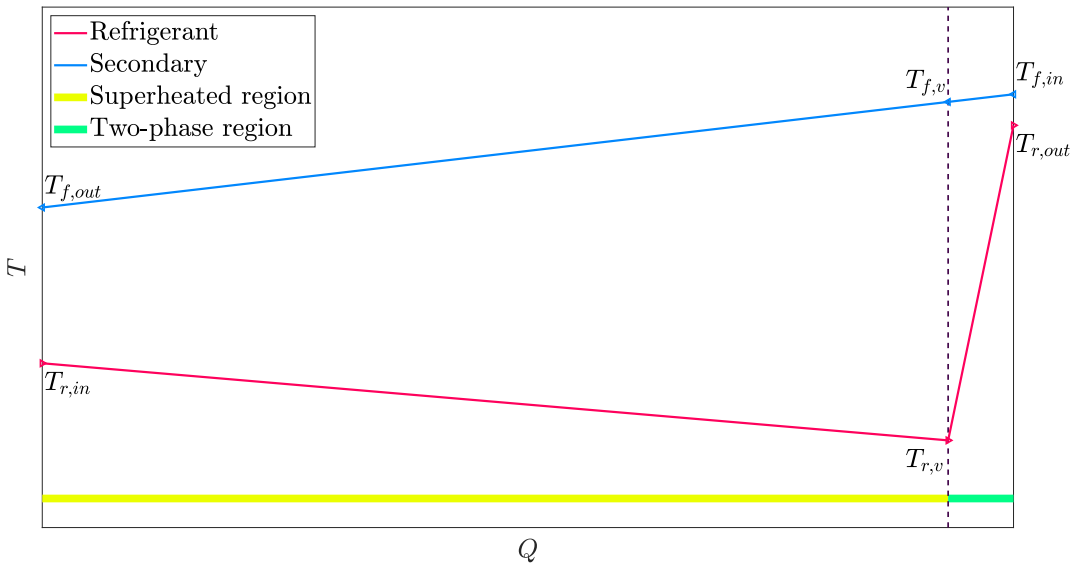

Figure 2.6
Qualitative $T - Q$ diagram for the evaporator with pressure drop.

2.2.3 | Compressor

A reciprocating compressor can be modeled in several ways: there are thermodynamic, dynamic, and global energy models, which can be more or less complex. But the purpose of this work is to model a refrigeration machine, not the compressor as a single component: many models are too detailed and useless for the main goal. A thermodynamic model is certainly very clear but might be difficult, heavy and onerous to implement as an element of a more general model and could use properties and quantities which are not important. In a refrigeration plant, the compressor is used to increase the pressure of the refrigerant mass flow rate, using work supplied by an electrical motor. So, the duct and suction pressure, the refrigerant mass flow rate, the power input, the enthalpy variations are examples of quantities useful for the model.

AHRI standard

For the refrigeration applications, the compressor's performances are regulated by some standards (AHRI 450 and UNI EN 12900). According to these specifications, the compressor's performances, as the mass flow rate m_r, the

power input W_k and the outlet temperature $T_{k,out}$ can be expressed as a third-degree equation of ten coefficients function of the dew point, evaporation $T_{sat,e}$ and condensation $T_{sat,c}$ temperatures (2.24).

$$X = a_1 + a_2 T_{sat,e} + a_3 T_{sat,c} + a_4 T_{sat,e}^2 + a_5 T_{sat,e} T_{sat,c} + a_6 T_{sat,c}^2 + \\ + a_7 T_{sat,e}^3 + a_8 T_{sat,e}^2 T_{sat,c} + a_9 T_{sat,e} T_{sat,c}^2 + a_{10} T_{sat,c}^3 \quad (2.24)$$

The generic performance $X = \{m_r,\ W_k,\ T_{k,out}\}$ depends on a series of coefficients $\boldsymbol{a_X} = [a_1, a_2, a_3, a_4, a_5, a_6, a_7, a_8, a_9, a_{10}]$: these are usually functions of other quantities and they are provided by the manufacturer or defined by an experimental campaign. This kind of model is very useful in refrigeration systems, thanks to its simplicity. For this work, $\boldsymbol{a_X}$ are available from previous analyses and they are a matrix of coefficients, mapped on the values of two inputs, the frequency of the electric motor F and the degree of superheat from the evaporator $\Delta T_{sh,e}$. In conclusion, m_r, W_k and $T_{k,out}$ are defined from knowledge of $T_{sat,e}$, $T_{sat,c}$, $\Delta T_{sh,e}$ and F. For the zeotropic blends, like the R450a, $T_{sat,e}$, $T_{sat,c}$ are the semi-sum of the liquid and vapor saturated temperatures at the same pressure (2.25).

$$T_{sat,c} = \frac{T_{r,v,c} + T_{r,l,c}}{2} \qquad T_{sat,e} = \frac{T_{r,in,e} + T_{r,v,e}}{2} \quad (2.25)$$

2.2.4 | Expansion valves

Considering a steady state model, the refrigerant mass flow rate is the same in all the positions of the circuit and is determined by the compressor. For this reason the expansion valves modeling is really simple. Under the hypothesis of adiabatic isoenthalpic transformation, the only equation that describes the behavior of the valves is an identity (2.26).

$$h_{r,in} = h_{r,out} \quad (2.26)$$

The flow characteristic of the valve is reported below,(2.27) (Figure 2.7)

$$m = \rho \frac{k_v \, (0.1)^{\frac{L-(X-10)}{L}} \sqrt{1000 \, \rho \Delta p}}{3600} \tag{2.27}$$

where:

ρ = refrigerant mass density at valve inlet ($kg \; m^{-3}$)
k_v = flow coefficient ($m^3 \; h^{-1}$)
L = valve total stroke (%)
Δp = pressure drop between the inlet and the outlet (bar)
m = mass flow rate ($kg \; h^{-1}$)
X = valve stroke (%)

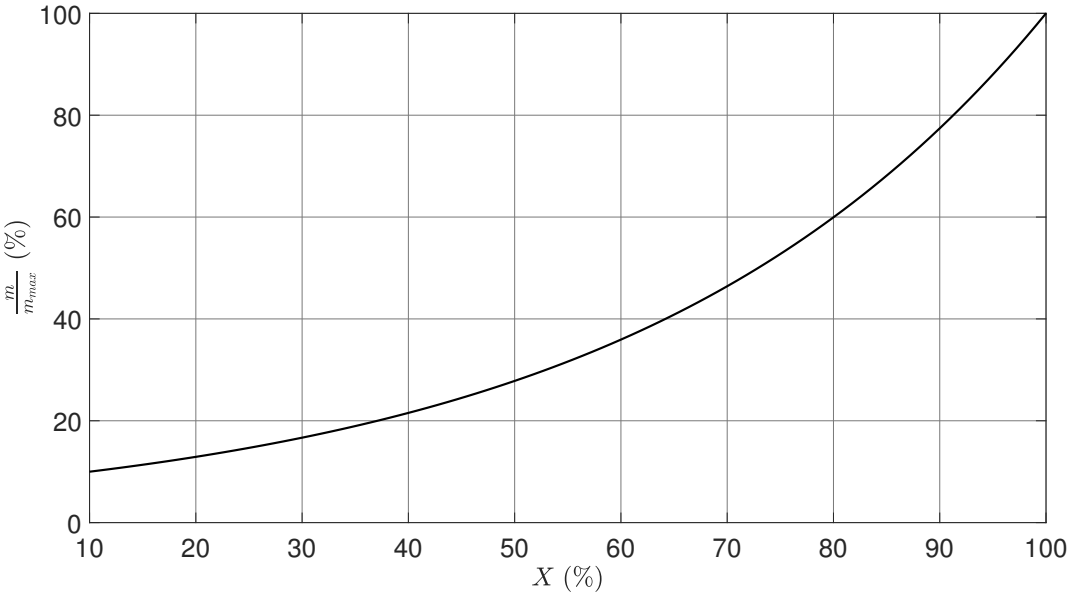

Figure 2.7
Flow characteristic of the EEV.
The valve follow an equal percentage characteristic, which guarantee a better control at low flow rate.

Section 2.3

Heat transfer correlations for BPHEs

The $\varepsilon - NTU$ method is built on the thermal properties of fluids flowing through the heat exchanger. For its application (Section 2.2), knowledge of the convective heat transfer coefficients (HTC) of both refrigerant and water is essential.

The problem of convection

The determination of the generic convective HTC is not a simple problem because it requires knowledge of the flow conditions of the thermophysical properties of the fluid of the heat-transfer surface geometry. For this reason, it is often called the fundamental problem of convection [27]. The convective HTC is strictly connected to the development of the boundary layer on the heat transfer surface. There are some very simple cases in which the solution of the problem can be found analytically, but, in practical applications, the mathematical approach cannot be applied very often. In these cases, mass and heat transfer correlations are very useful. This approach is not general, because every correlation is valid under specific operating conditions, but it allows to simplify the problem.

Dimensionless groups

Several non-dimensional groups of parameters, listed below, (Table 2.1), are used to free the problem from its dimensions and to relate it directly to the physical laws.

Table 2.1
Non-dimensional groups of heat and mass transfer [27].

Group	*Definition*	*Interpretation*
Reynolds number	$Re = \frac{\rho\, v\, y}{\mu}$	Ratio of the inertia to viscous forces.
Nusselt number	$Nu = \frac{\alpha\, y}{\kappa}$	Ratio of convection to pure conduction heat transfer.
Prandtl number	$Pr = \frac{\mu\, c_p}{\kappa}$	Ratio of momentum diffusivity to the thermal diffusivity.

Usually, in the correlations, Nu is obtained from Re, Pr and other quantities.

Nu yields the value of the convective HTC (2.28).

$$\alpha = \frac{Nu\ \kappa}{y} \tag{2.28}$$

In this work, the correlations are used to determine the convective HTC for the R450a and the water in the BPHE. To this aim, the velocity v can be obtained from the mass flow rate through the plates of the generic fluid considered (2.29) and the characteristic length y can be associated to the hydraulic diameter D_h, which for the BPHE is defined by the plate offset (2.30).

$$v = \frac{m}{\rho\ B\ b\ n_{ch}} \tag{2.29}$$

$$y = D_h = 2\ b \tag{2.30}$$

In literature several correlations are available which can be used to obtain Nu for a fluid in a PHE. The correlations can be divided into:

- single-phase flow: for the refrigerant as superheated vapor or subcooled liquid and the water in all the BPHE regions;
- boiling process: for the refrigerant as saturated vapor in the evaporator;
- condensation process: for the refrigerant as saturated vapor in the condenser.

2.3.1 | Single-phase correlations

Martin [21] studies the influence of the BPHE geometry on the heat transfer and the pressure drop. The friction factor f is a function of β and some constants (2.32), which are the specific values of the friction factor for a particular geometry: when $\beta = 0°$, the friction factor is f_0, when $\beta = 90°$, the friction

Martin

factor is f_1 (2.31).

$$\begin{cases} Re < 2000 \implies \begin{cases} f_0 = 64\ Re^{-1} \\ f_1 = 597\ Re^{-1} + 3.85 \end{cases} \\ Re \geq 2000 \implies \begin{cases} f_0 = (1.8\ \log_{10} Re - 1.5)^{-2} \\ f_1 = 39\ Re^{-0.289} \end{cases} \end{cases} \tag{2.31}$$

$$\frac{1}{\sqrt{f}} = \frac{\cos\beta}{(0.18\ \tan\beta + 0.36\ \sin\beta + f_0 \cos\beta)^{-1})^{1/2}} + \frac{1-\cos\beta}{\sqrt{3.8\ f_1}} \tag{2.32}$$

The geometry of the BPHE (β,f), the thermophysical properties (Pr,μ,μ_w) and the dynamic (Re) of the fluid affect Nu (2.33).

$$Nu = 0.122\ Pr^{1/3} \left(\frac{\mu}{\mu_w}\right)^{1/6} \left(f Re^2 \sin 2\beta\right)^{0.374} \tag{2.33}$$

Kim

The Kim correlation [28] is obtained from the experimental data of water to water PHE. Nu is a function of Re, Pr and β (2.34).

$$Nu = 0.295\ Re^{0.64}\ Pr^{0.32} \left(\frac{\pi}{2} - \beta\frac{\pi}{180}\right)^{0.09} \tag{2.34}$$

Wanniarachchi

Wanniarachchi, Ratnam, Tilton, and Dutta-Roy [29] found two values of the Colburn factor which can be associated to a laminar ($j_{Nu,l}$) and a turbulent ($j_{Nu,t}$) flow (2.35) respectively. For a generic flow, which can have both laminar and turbulent regions, a third quantity (j_{Nu}) is obtained as a function of the previous two, to account for the effects of the turbulent and laminar regions, (2.36).

$$\begin{cases} j_{Nu,lam} = 3.65\ (90-\beta)^{-0.445}\ Re^{0.339} \\ j_{Nu,tur} = 12.6\ (90-\beta)^{-1.142}\ Re^{[0.646+0.00111(90-\beta)]} \end{cases} \tag{2.35}$$

$$j_{Nu} = \sqrt[3]{j_{Nu,lam}^3 + j_{Nu,tur}^3} \tag{2.36}$$

Nu depends on the fluid thermophysical properties (Pr, μ, μ_p) and the dy-

namical characteristics (j_{Nu}) (2.37).

$$Nu = j_{Nu}\ Pr^{1/3}\ \left(\frac{\mu}{\mu_p}\right)^{0.17} \tag{2.37}$$

Bogaert and Böles [30] suggest an exponential correlation of the type Re^k Boagert Bölcs (2.38). B_1 and B_2 are function of Re (2.39).

$$Nu = B_1\ Re^{B_2}\ Pr^{\frac{1}{3}e^{\left(\frac{6.4}{Pr+30}\right)}}\ \left(\frac{\mu}{\mu_p}\right)^{\frac{0.3}{(Re+6)^{0.125}}} \tag{2.38}$$

$$\begin{cases} 0 \leq Re < 20 & \Rightarrow & B_1 = 0.4621, & B_2 = 0.4621 \\ Re = 20 & \Rightarrow & B_1 = 1.730, & B_2 = 0 \\ 20 < Re < 50 & \Rightarrow & B_1 = 0.0875, & B_2 = 1 \\ Re = 50 & \Rightarrow & B_1 = 4.4, & B_2 = 0 \\ 50 < Re < 80 & \Rightarrow & B_1 = 0.4223, & B_2 = 0.6012 \\ Re = 80 & \Rightarrow & B_1 = 5.95, & B_2 = 0 \\ 80 < Re & \Rightarrow & B_1 = 0.26347, & B_2 = 0.7152 \end{cases} \tag{2.39}$$

Muley and Manglik [31] show the effects of β and ϕ . Increasing β, Nu can Muley be five times higher with respect to the same PHE with $\beta = 0$. A similar consideration is valid at the small scale for ϕ. The correlations are functions of Re, β and some fluid thermophysical properties (Pr, μ, μ_p), while for a turbulent flow, Nu depends on ϕ too (2.40, 2.41). For $400 < Re < 1000$ no correlations are suggested, but the experience recommands the second of those below.

$$Nu = 0.44\ \left(\frac{6\beta}{180}\right)^{0.38} Re^{0.5}\ Pr^{1/3}\ \left(\frac{\mu}{\mu_p}\right)^{0.14} \tag{2.40}$$

$$\begin{aligned} Nu = &\left(0.2668 - 0.0006967\ \beta + 7.244 \cdot 10^{-5}\ \beta^2\right) \cdot \\ &\cdot \left(20.7803 - 50.9372\ \phi + 41.1585\ \phi^2 - 10.1507\ \phi^3\right) \cdot \\ &\cdot \left(Re^{\left[0.728 + 0.0543 \sin\left(\frac{4\beta\pi}{180} + 3.7\right)\right]}\ Pr^{1/3}\ \left(\frac{\mu}{\mu_p}\right)^{0.14}\right) \end{aligned} \tag{2.41}$$

Chisholm Wanniarachchi

The Chisholm-Wanniarachchi correlation ([28]) expresses Nu, as a function of Pr, Re and β (2.42).

$$Nu = 0.724 \left(\frac{6\beta}{\pi}\right)^{0.646} Re^{0.583} Pr^{1/3} \tag{2.42}$$

The Martin correlation is chosen for the convective HTC determination of the refrigerant in single-phase and the water in the condenser and evaporator. A comparison is now presented between the various correlations in a non-dimensional diagram (2.8), focusing on the Reynolds values compatible with the operating points of the plant (2.9). The difference between all the correlations and that of Martin is plotted in absolute (2.10) and percent terms (2.11).

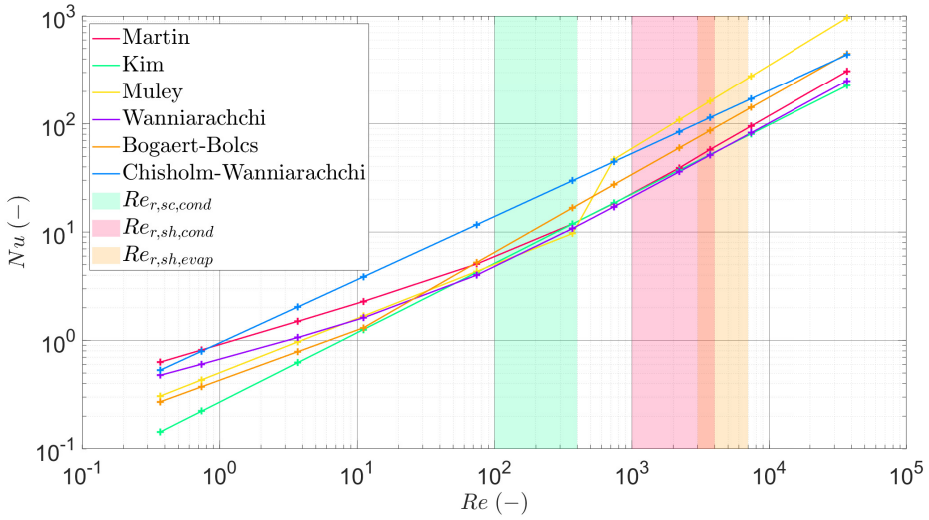

(a) *Refrigerant*

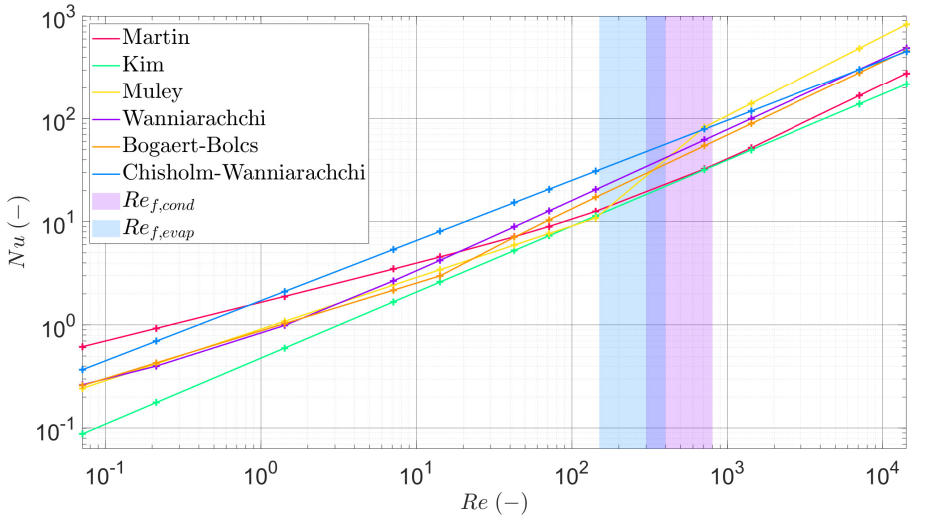

(b) *Water*

Figure 2.8

Nu comparison single phase correlations.
A view of the correlations in a wide range of *Re*.

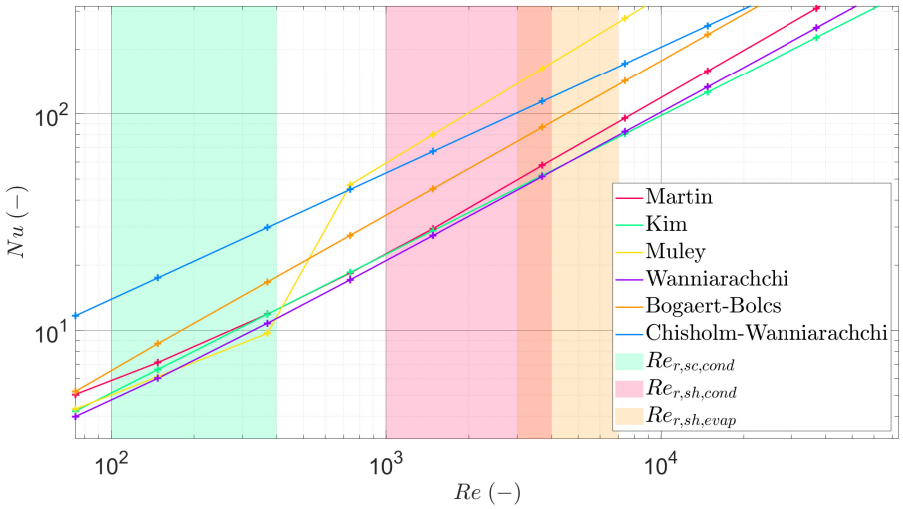

(a) *Refrigerant*

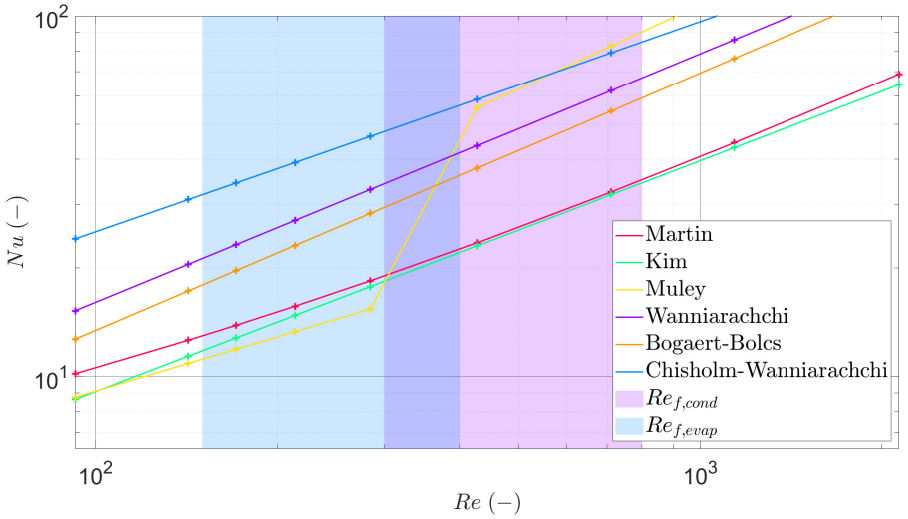

(b) *Water*

Figure 2.9

Nu comparison single phase correlations: zoom.

More in detail the Martin correlation is sufficiently conservative, especially for the refrigerant at superheated vapor state and for water. Chisholm-Wanniarachchi gives the highest mean value of Nu. Wanniarachchi, Martin and Kim are very similar for the refrigerant, whereas for water Wanniarachchi is higher. The transition zone for the Muley correlation is evident.

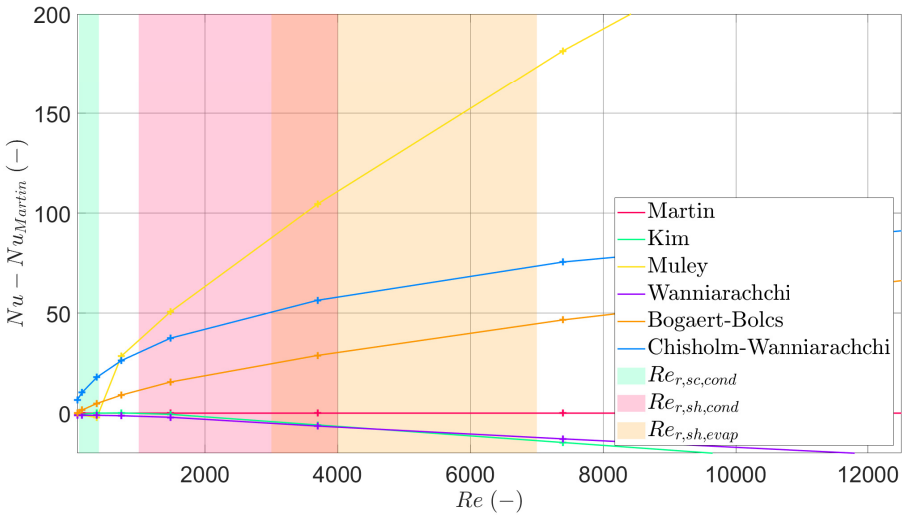

(a) *Refrigerant*

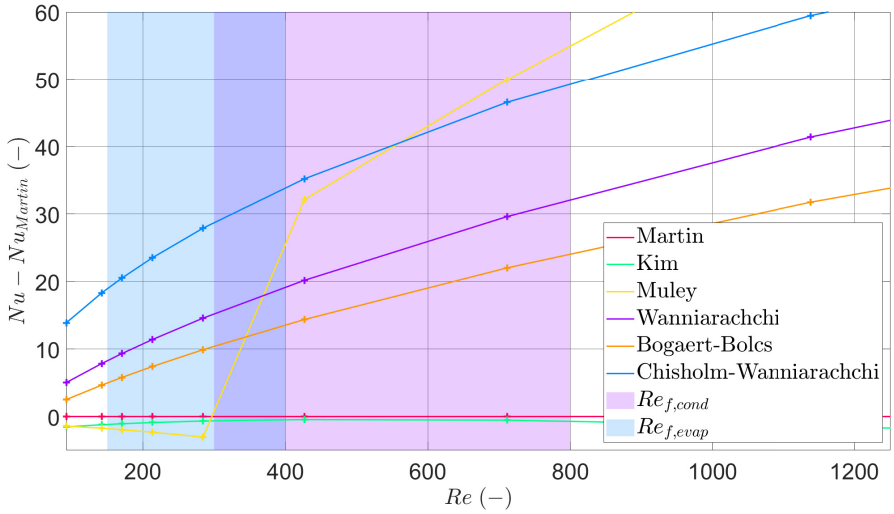

(b) *Water*

Figure 2.10

Nu comparison single phase correlations with Martin.

In a non-logarithmic scaled plot, the differences between the correlations are more evident. For the refrigerant at subcooled liquid state, the differences are very small. Instead, for the refrigerant at higher Reynolds number the Chisholm, Chisholm-Wanniarachchi and Bogaert-Bölcs correlations return a Nu number very different from Martin. For water, the differences in absolute terms are less important.

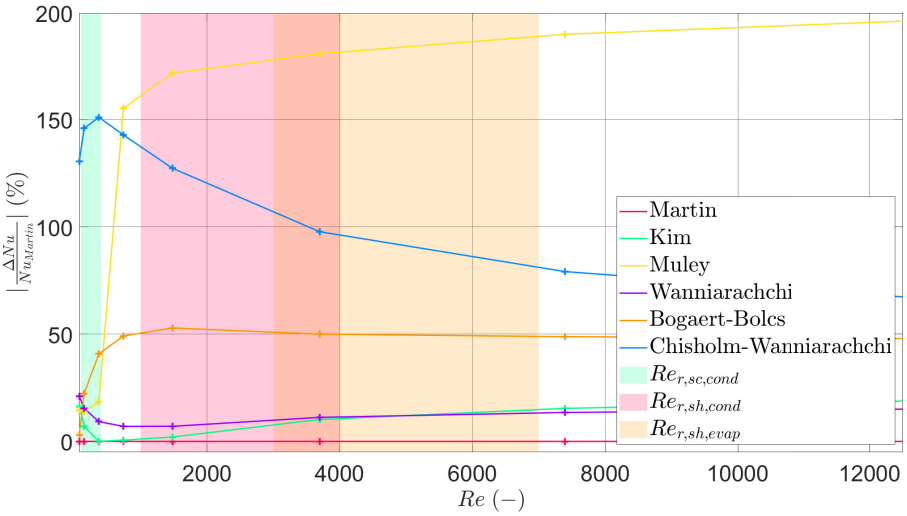

(a) *Refrigerant*

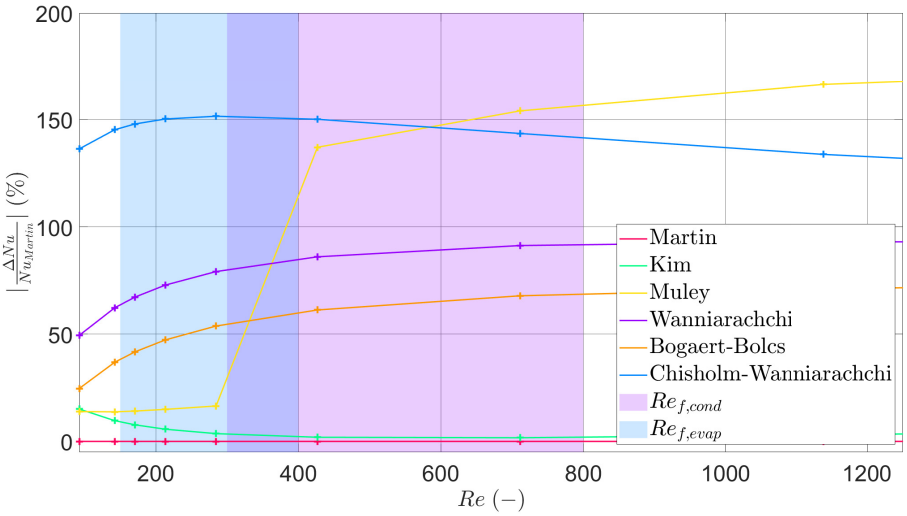

(b) *Water*

Figure 2.11

Nu percent comparison single phase correlations with Martin.

Evaluating the difference relative in percent terms respect to Martin correlations, it is interesting to note that both refrigerant and water have higher values inte 150-180% range. As general trend, Muley and Chisholm-Wanniarachchi are high, Bogaert-Bölcs is on intermediate values, Martin and Kim are low. Wanniarachchi is low for refrigerant and intermediate for water.

2.3.2 | Condensation correlations

In literature some correlations are available for condensation heat transfer and pressure drop in PHE as Eldeeb, Aute, and Radermacher [32] show in their review work. After comparison, the correlation recommended by Longo is deemed the most suitable for the model and the characteristics of the refrigeration plant studied. The condensation process inside the BPHE can be gravity controlled or convective (Appendix C). Longo, Righetti, and Zilio [33] found two correlations which determine the convective HTC for the gravity controlled condensation ($Re < 1600$) and for the convective condensation ($Re > 1600$). Longo

Two important parameters used in the two-phase correlations are the mass flux G (2.43) and the equivalent Reynolds number Re_{eq} (2.44).

$$G = \frac{m}{n_{ch}\, W\, b} \tag{2.43}$$

$$Re_{eq} = G \left[(1 - x) + x \left(\frac{\rho_l}{\rho_v} \right)^{\frac{1}{2}} \right] \frac{D_h}{\mu_l} \tag{2.44}$$

For $Re < 1600$ the convective HTC is independent of G (2.45) and is obtained from a model based on the Nusselt study of the vertical plate film condensation [34].

$$\alpha_{grav} = 0.943\ \phi\ \left(\frac{\kappa_l^3\ \rho_l^2\ g\ \Delta J_{lv}}{\mu_l\ \Delta T\ L} \right)^{\frac{1}{4}} \tag{2.45}$$

On the contrary, when $Re > 1600$, there is a dependence on G (2.46).

$$\alpha_{fc} = 1.875\ \phi\ \frac{\kappa_l}{D_h}\ Re^{0.445}\ Pr^{\frac{1}{3}} \tag{2.46}$$

2.3.3 | Evaporation correlations

The evaporation correlations often use the non-dimensional groups presented in the Table 2.2.

Eldeeb, Aute, and Radermacher [32] offer a review of the boiling heat transfer and pressure drop correlations in a PHE evaporator, too. From the list, only three are considered suitable for this work.

Table 2.2
Non-dimensional groups of heat and mass transfer for two phase fluids [27].

Group	*Definition*	*Interpretation*
Bond number	$Bd = \frac{g\,(\rho_l - \rho_v)\,y^2}{\sigma}$	Ratio of gravitational and surface tension forces.
Boiling number	$Bo = \frac{q}{G\,\gamma}$	Ratio of mass of vapor generated per unit heat transfer area to the mass flow rate per unit cross sectional area.

Longo Mancin

Longo, Mancin, Righetti, and Zilio [35] present a model for refrigerant boiling inside BPHE based on a set of experimental data. This model includes specific equations for pressure drop and heat transfer coefficient for nucleate and convective boiling (Appendix C). For convective boiling, the HTC is a simple function of Re_{eq} (2.47).

$$\alpha_{cb} = 0.122\ \phi\ \frac{\kappa_l}{D_h}\ Re_{eq}^{0.8}\ Pr^{\frac{1}{3}} \tag{2.47}$$

The correlations are more complex in case of nucleate boiling (2.48), where $q_0 = 20000$ and $n = 0.467$.

$$\alpha_{nb} = 0,58\ \phi\ \alpha_{nb,0}\ C_{Ra}\ F(\hat{p})\ \left(\frac{q}{q^0}\right)^n \tag{2.48}$$

These correlations take into account the effects of the plate roughness R_a (2.49) and the ratio of work to critical pressure $\hat{p}$ (2.51), with the factor $F(\hat{p})$ (2.50).

$$C_{Ra} = \left(\frac{R_a}{0.4}\right)^{0.1333} \tag{2.49}$$

$$F(\hat{p}) = 1,2\ \hat{p}^{0,27} + \left(2,5 + \frac{1}{1-\hat{p}}\right)\ \hat{p} \tag{2.50}$$

$$\hat{p} = \frac{p}{p_{cr}} \tag{2.51}$$

Finally, the HTC is the maximum value of the nucleate and convective boiling

heat transfer coefficient (2.52).

$$h_b = \max\left(h_{cb}, h_{nb}\right) \tag{2.52}$$

Huang, Sheer, and Bailey-McEwan [36] propose two-phase heat transfer and pressure drop characteristics for PHE, without considering the boiling mechanism. The convective HTC is function of a series of factors (2.53) including the liquid thermal diffusivity δ_l (2.54) and a parameter d_0 depending on some thermophysical properties of the refrigerant (2.55). Huang

$$\alpha = 1.87 \cdot 10^{-3} \left(\frac{\kappa_l}{D_h}\right) \left(\frac{q\ d_0}{\kappa_l\ T_{sat}}\right)^{0.56} \left(\frac{\gamma\ d_0}{\delta_l^2}\right)^{0.31} Pr^{0.33} \tag{2.53}$$

$$\delta = \frac{\kappa}{\rho\ c_p} \tag{2.54}$$

$$d_0 = 0.0146 \cdot 35 \left[\frac{2\ \sigma}{g\ (\rho_l - \rho_v)}\right]^{0.5} \tag{2.55}$$

Amalfi, Vakili-Farahani, and Thome [37] develop another predictive model of convective HTC in PHE evaporator. Two correlations are available according the value of Bond number Bd (2.56). Amalfi

$$Bd = \frac{(\rho_l - \rho_v)\ g\ D_h^2}{\sigma} \tag{2.56}$$

For $Bd < 4$, HTC is not function of Bd (2.57).

$$\alpha = 982 \left(\frac{\kappa_l}{D_h}\right) \left(\frac{\beta}{\beta_{max}}\right)^{1.101} \left(\frac{G^2\ D_h}{\rho_m\ \sigma}\right)^{0.315} \left(\frac{\rho_l}{\rho_v}\right)^{-0.224} Bo^{0.32} \tag{2.57}$$

For $Bd \geq 4$, HTC depends on Bd (2.58)

$$\alpha = 18.495 \left(\frac{\kappa_l}{D_h}\right) \left(\frac{\beta}{\beta_{max}}\right)^{0.248} \left(\frac{x\ G\ D_h}{\mu_v}\right)^{0.135} \cdot \left(\frac{G\ D_h}{\mu_l}\right)^{0.351} \left(\frac{\rho_l}{\rho_v}\right)^{0.223} Bd^{\,0.235}\ Bo^{0.198} \tag{2.58}$$

The correlations are compared as a function of Re and q[1] (Figure 2.12, Figure 2.13).

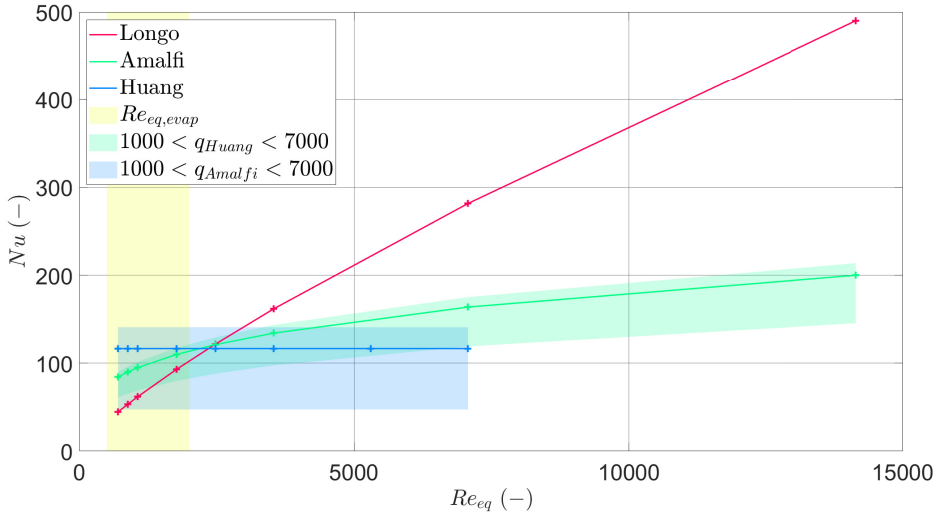

Figure 2.12
Nu comparison in boiling heat transfer correlations.
The Longo's correlation is the most conservative, particularly at low Re_{eq}.

Section 2.4

Pressure drop correlation for a BPHE

All the heat exchanger models are based on the hypothesis that the pressure of the working fluid is constant along them, but looking at the experimental data if this hypothesis can be true for the condenser, it does not hold for the evaporator.

For this reason, two correlations for the pressure drop in a BPHE for a boiling refrigerant[2] are now presented. The correlations give the value of the Darcy factor f. Amalfi, Vakili-Farahani, and Thome [37] suggest to employ the (2.59).

$$f = 4\,C \cdot 15.698 \left(\frac{G^2\,d_h}{\rho_m\,\sigma}\right)^{-0.475} \left(\frac{(\rho_l - \rho_v)\,g\,d_h^2}{\sigma}\right)^{0.255} \left(\frac{\rho_l}{\rho_v}\right)^{-0.571} \tag{2.59}$$

[1] The Longo correlation does not depend on q
[2] These correlations are not considered into the evaporator model in the first items, but they are employed in successive models.

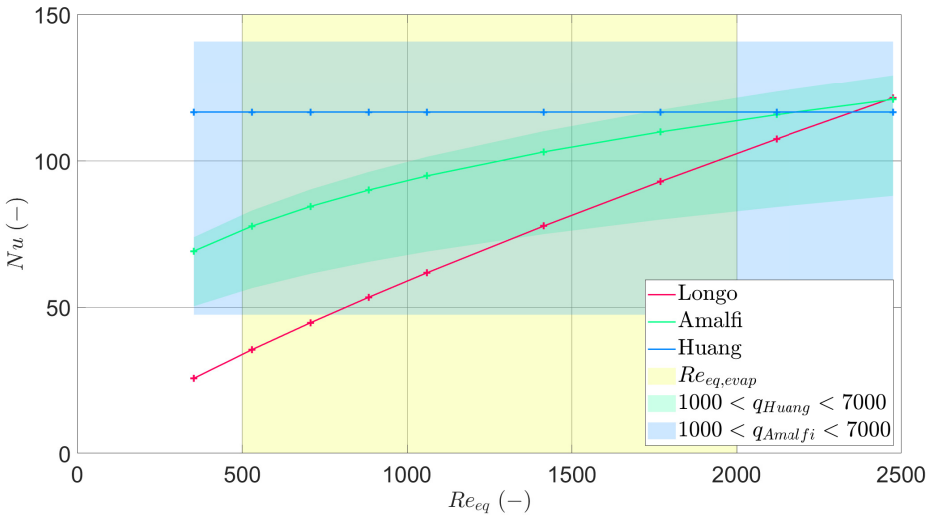

Figure 2.13
Nu comparison in boiling heat transfer correlations: a zoom.

$$C = 2.125 \left(\frac{\beta}{\beta_{max}}\right)^{9.993} + 0.955 \tag{2.60}$$

According to Huang, Sheer, and Bailey-McEwan [36], the Darcy factor has another expression, shown in (2.61).

$$f = \frac{3.81\ 10^4\ F_{R,f}}{Re_{tp}^{0.9} \left(\frac{\rho_l}{\rho_v}\right)^{0.16}} \tag{2.61}$$

$$Re_{tp} = \frac{G\ d_h}{\mu_{tp}} \tag{2.62}$$

$$\mu_{tp} = \rho_m \left[\frac{x_m\ \mu_v}{\rho_v} + (1 - x_m)\ \frac{\mu_l}{\rho_l}\right] \tag{2.63}$$

$$\rho_m = \left[\frac{x_m}{\rho_v} + \frac{1 - x_m}{\rho_l}\right]^{-1} \tag{2.64}$$

$$F_{R,f} = 0.183\ R^2 - 0.275\ R + 1.10 \qquad R = \frac{\beta}{30°} \tag{2.65}$$

Knowing f, the pressure drop is computed as a function of the geometry of the

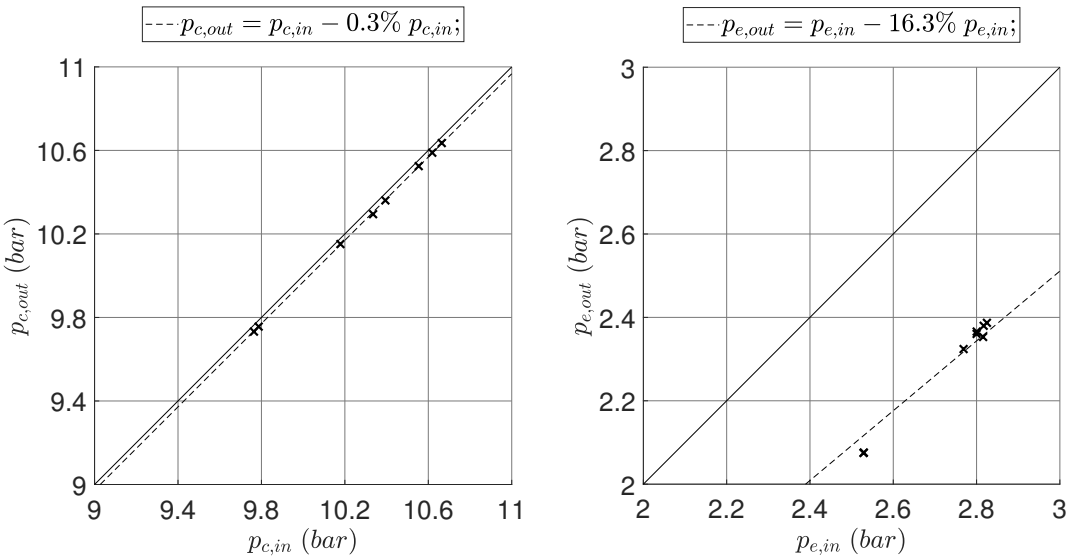

Figure 2.14
Percentage incidence of the pressure drop in the heat exchangers. In the evaporator the pressure drop has a certain relevance.

heat exchanger and of the flow characteristics (2.66).

$$\Delta p = \frac{f\ G^2}{2\ \rho_m\ d_h\ L} \tag{2.66}$$

As highlighted by Huang, Sheer, and Bailey-McEwan [36], the total pressure drop measured in a heat exchanger consists of a series of contributions (2.67). The frictional term is the most relevant, but there is also the effect of pressure drop at the inlet and outlet ports and that of the acceleration and elevation. All these parts summed gives the pressure drop measured.

$$\Delta p_{meas} = \Delta p_{port} + \Delta p_{acce} + \Delta p_{elev} + \Delta p_{frict} \tag{2.67}$$

The pressure drop correlations are compared (Figure 2.15).

Section 2.5

Effectiveness NTU relations for a BPHE

For the development of the model, the (2.9) has to be identified for every zone of the heat exchangers. As shown in (Appendix B) for a counter-flow

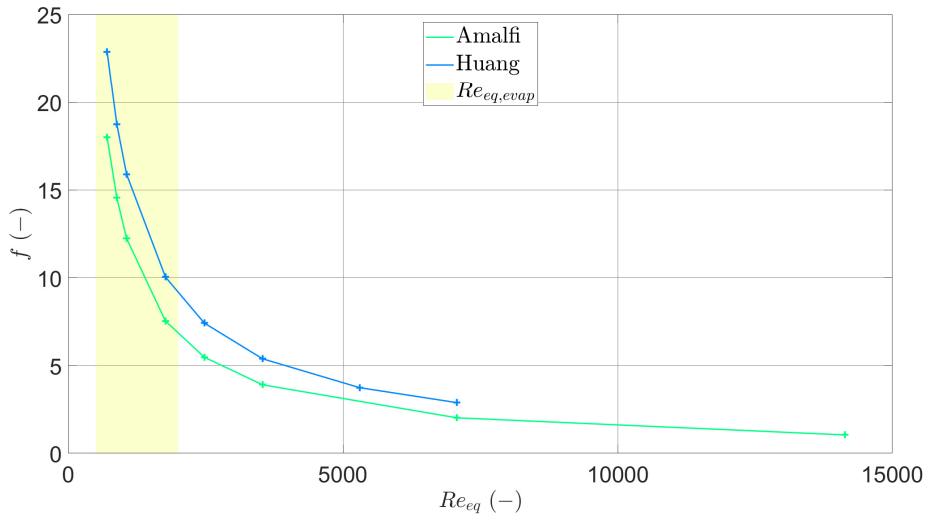

Figure 2.15
f comparison in boiling pressure drop correlations.

heat exchanger and when at least one fluid is two-phase the (B.7) and the (B.8) respectively are valid.

PHE flow arrangement

In general, the flow arrangement of a PHE can be more complex than the simple counter-flow or parallel-flow arrangement. In a counter-flow PHE, in every couple of channels, the refrigerant and the secondary fluid are in counter-flow. There are some particular configurations, called multi-pass PHE design, in which the plates can be separated into several parallel blocks. In each block, conditions are the same for all the couples of channels: so a block can be in counter-flow or parallel-flow design. The general X_1-X_2 multi pass PHE is a particular PHE in which X_1 and X_2 are the pass numbers of hot and cold fluid respectively (Figure 2.16) [38].

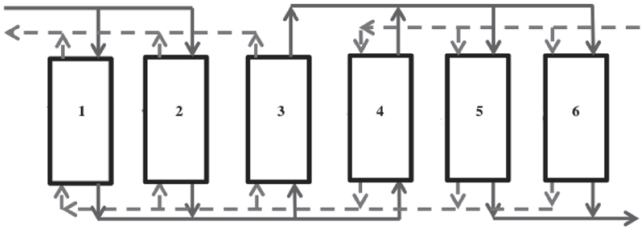

Figure 2.16
An example of multipass $X_1 = 3$, $X_1 = 2$ flow arrangement.
In this configuration, there are three blocks either in counter-flow and parallel-flow [38].

The $\varepsilon - NTU$ relation for one-phase zones

As shown in the works of Kandlikar and Shah [39, 40] the effectiveness of

a PHE with a finite number of plates is affected by the flow and pass arrangements. More recently, Fernández-Torrijos, Almendros-Ibáñez, Sobrino, and Santana [41] obtained a general algebraic expression of the effectiveness of PHEs in the $X_1 - 1$ pass configuration as a function of γ and NTU. The condenser and the evaporator studied are $1-1$ pass configuration, so either are in the total counter-flow arrangement. In this case, in the single-phase zones, the literature suggest to employ the general analytic relation (B.7) as shown in (2.68), (2.69) and (2.70).

$$\text{condenser sh zone} \qquad \varepsilon_{sh} = \frac{1 - e^{-NTU_{sh}(1-\gamma_{sh})}}{1 - \gamma_{sh}\, e^{-NTU_{sh}(1-\gamma_{sh})}} \tag{2.68}$$

$$\text{condenser sc zone} \qquad \varepsilon_{sc} = \frac{1 - e^{-NTU_{sc}(1-\gamma_{sc})}}{1 - \gamma_{sc}\, e^{-NTU_{sc}(1-\gamma_{sc})}} \tag{2.69}$$

$$\text{evaporator sh zone} \qquad \varepsilon_{sh} = \frac{1 - e^{-NTU_{sh}(1-\gamma_{sh})}}{1 - \gamma_{sh}\, e^{-NTU_{sh}(1-\gamma_{sh})}} \tag{2.70}$$

The $\varepsilon - NTU$ relation for two-phase zones

For the two-phase zone, there is a complication. As mentioned, for an azeotropic blend the temperature does not change during the process of boiling or condensation at constant pressure. It means that $C_{min} = 0$ and in this case the relation used is the (B.8). A zeotropic mixture varies its temperature under the same operating conditions: still, the glide temperature of R450a is very small. A comparative study between the effectiveness calculated with (B.7) and (B.8) show how in the operating condition of the plant the two correlations are very similar, due to the small value of γ. If γ was higher, the difference would be relevant.

The condenser (2.71) and evaporator (2.72) effectiveness is modelled using the equation (B.8) which has a simple structure without loss of precision.

$$\text{condenser tp zone} \qquad \varepsilon_{tp} = 1 - e^{-NTU_{tp}} \tag{2.71}$$

$$\text{evaporator tp zone} \qquad \varepsilon_{tp} = 1 - e^{-NTU_{tp}} \tag{2.72}$$

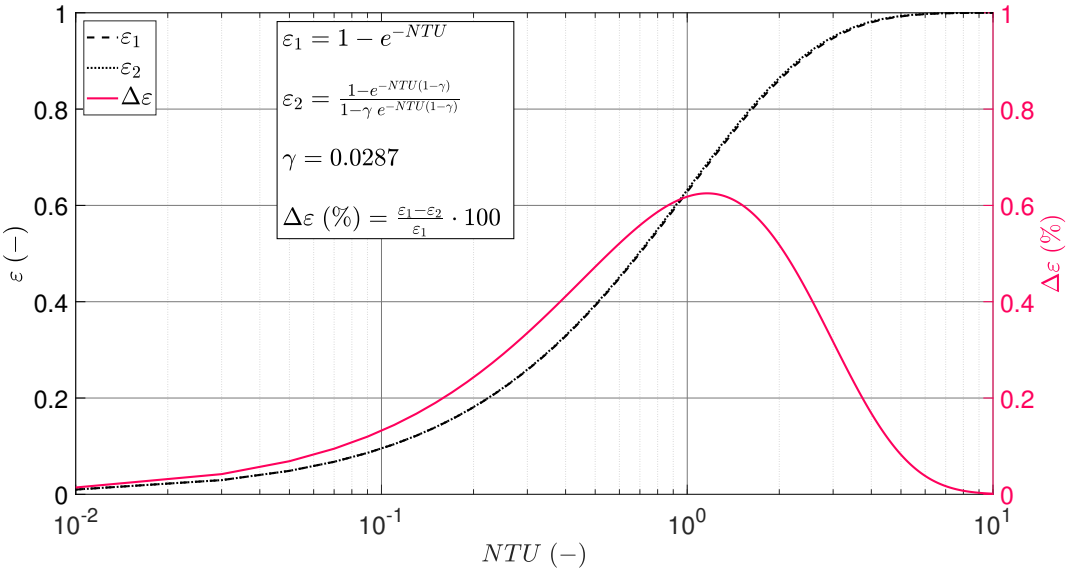

Figure 2.17
$\varepsilon - NTU$ relation comparison for zeotropic mixtures: small γ.

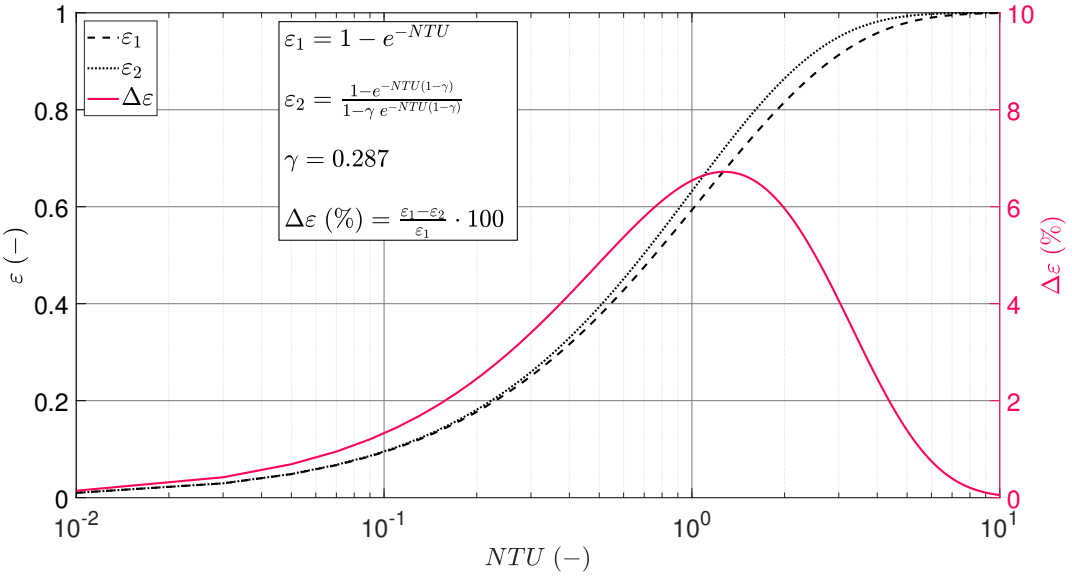

Figure 2.18
$\varepsilon - NTU$ relation comparison for zeotropic mixtures: high γ.

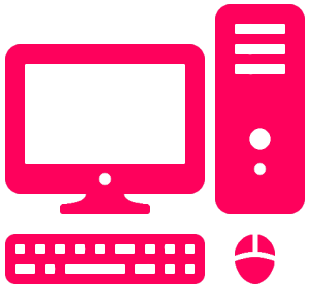

Chapter 3

Model implementation

Implementation is the second important step of the modelling process. After the development of the physical laws which govern a VCRS cycle in steady state conditions, a non-linear algebraic system of equations has been found. For this problem, it is not possible to determine an analytical solution, so the implementation in a solver is the only way to obtain some results.

In this chapter some methods for the resolution in Matlab of the models of the components (Section 3.1) and the model of the VCRS (Section 3.2) are proposed. In the end, some considerations about the determination of the thermophysical properties (Section 3.3) are discussed.

Section 3.1

Components algorithms

According to Winkler, Aute, and Radermacher [42], there are two approaches which can be used to solve the variables of the models of the components a VCRS cycle:

- a non-simultaneus successive approach, where a variable is solved to convergence before moving to the next unknown variable;
- a multi-variable non-linear equation solver which solves all the variables simultaneously.

A priori, these two possibilities are taken both into account in this work,

because there is another significant issue which guides the implementation: to have a model which adapts to the change of configuration of the plant or to the substitution of a component, every element is modeled like a black box which takes some inputs and returns some outputs. In this way, every component has its own model. The model of the complete plant consists of the assembly of the models of the components that are connected to each other through the input and the output quantities.

The resolution algorithm for the generic component is developed as a Matlab function: this function can be called in a Matlab script, where the inputs are assigned and the outputs are calculated after the script execution.

Code 3.1
Call to the model function in Matlab.
In this code the function condensator is called, which takes the inputs specified in parentheses and gives the outputs in brackets.

```
1 [h_r_out_c,DT_sc_calc]=condensator(p_c,h_r_in_c,m_r,T_f_in_c,m_f_c);
```

The expansion valves, as introduced previously, are not treated because their model consist of an identity, so use of a function would be pointless.

3.1.1 | Compressor

The compressor implementation is very simple because the model consists of three polynomial functions depending on ten coefficients and the evaporation $T_{sat,e}$ and condensation $T_{sat,c}$ temperatures at saturated states. The coefficients change as a function of the frequency F and the degree of superheat of the refrigerant at the evaporator outlet ΔT_{sh}. Schematically, the compressor model, knowing the polynomial function, takes four inputs and gives three outputs (Figure 3.1).

More in detail, F and ΔT_{sh} are used to determinate the correct values of the coefficients for every function. For every pair $(\Delta T_{sh},\ F)$ an array of ten coefficient $\boldsymbol{a_X}$ for the generic performance X (3.1) is identified.

$$\boldsymbol{a_X} = \{a_{X,i}\} = \Phi\left(\Delta T_{sh},\ F\right) \quad i = 1, \ldots, 10 \quad \forall\ X = \{m_r; P_{el}; T_{out}\} \tag{3.1}$$

Thanks to an experimental campaign based on a grid of data points $(\Delta T_{sh},\ F)$

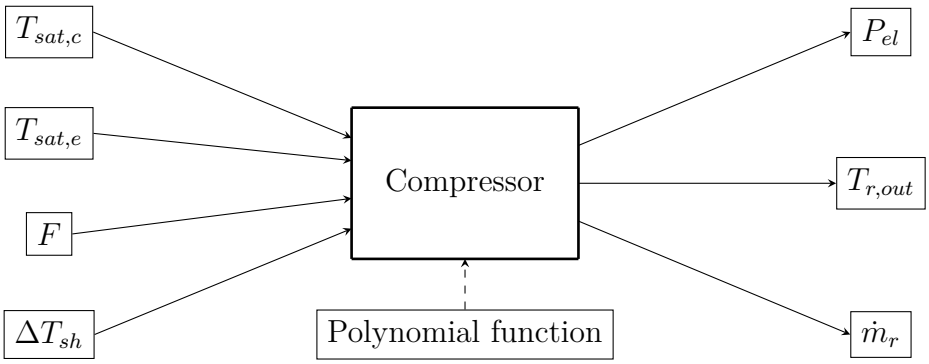

Figure 3.1
Inputs and outputs of the compressor model.

(26×11 data points, respectively), every $a_{X,i}$ is mapped as a matrix: the rows are obtained varying T_{sh} and maintaining F constant, the columns vice versa. In this way, for the generic performance X a tensor $\boldsymbol{A_X}$ is obtained as a set of ten matrices $A_{X,i}$: $A_{P_{el}}$ is an exception, because every coefficient is function only of F: so $A_{P_{el}}$ is a matrix which derives from ten array.

$$\begin{cases} \boldsymbol{A_{m_r}} = \{A_{m_r,i}\} \\ A_{m_r,i} = \left\{(a_{m_r,i})_{s,t}\right\} \end{cases} \tag{3.2}$$

$$\begin{cases} \boldsymbol{A_{T_{out}}} = \{A_{T_{out},i}\} \\ A_{T_{out},i} = \left\{(a_{T_{out},i})_{s,t}\right\} \end{cases} \tag{3.3}$$

$$\begin{cases} A_{P_{el}} = \{\boldsymbol{a_{P_{el},i}}\} \\ \boldsymbol{a_{P_{el},i}} = \left\{(a_{P_{el},i})_{s}\right\} \end{cases} \tag{3.4}$$

where:

$i = 1, \ldots, 10$; is the number of coefficients of the polynomial functions;
$s = 1, \ldots, 11$; is the number of experimental values of F;
$t = 1, \ldots, 26$; is the number of experimental values of ΔT_{sh}.

$\boldsymbol{A_{m_r}}$, $\boldsymbol{A_{T_{out}}}$, $A_{P_{el}}$ are saved in a MATLAB structure. When a pair (T_{sh}, F) is chosen, using the structure it is possible to define every coefficient of the three functions through a simple linear interpolation, bi-dimensional for A_{m_r} and

$A_{T_{out}}$ and mono-dimensional for $\boldsymbol{a_{P_{el}}}$. In summary, the outputs of the model are evaluated as a function of the inputs as shown in (3.5), (3.6) and (3.7).

$$m_r = \Phi\left(T_{e,sat},\ T_{c,sat},\ \Delta T_{sh},\ F\right) \tag{3.5}$$

$$T_{out} = \Phi\left(T_{e,sat},\ T_{c,sat},\ \Delta T_{sh},\ F\right) \tag{3.6}$$

$$P_{el} = \Phi\left(T_{e,sat},\ T_{c,sat},\ F\right) \tag{3.7}$$

Code 3.2
Compressor model: determination of m_r.
Every $a_{m_r,i}$ coefficient is calculated as function of ΔT_{sh} and F by bidimensional linear interpolation. There is a built in Matlab function, interp2 which can be used for the interpolation, but in order to increase the velocity of the process, the simpler and faster function quick_interp2 has been created.

```
m=(quick_interp2(F_array,DT_sh_array,coeff_m_r(:,:,1)',F,DT_sh)+...
quick_interp2(F_array,DT_sh_array,coeff_m_r(:,:,2)',F,DT_sh).*Te+...
quick_interp2(F_array,DT_sh_array,coeff_m_r(:,:,3)',F,DT_sh).*Tc+...
quick_interp2(F_array,DT_sh_array,coeff_m_r(:,:,4)',F,DT_sh).*Te.^2+...
quick_interp2(F_array,DT_sh_array,coeff_m_r(:,:,5)',F,DT_sh).*Te.*Tc+...
quick_interp2(F_array,DT_sh_array,coeff_m_r(:,:,6)',F,DT_sh).*Tc.^2+...
quick_interp2(F_array,DT_sh_array,coeff_m_r(:,:,7)',F,DT_sh).*Te.^3+...
quick_interp2(F_array,DT_sh_array,coeff_m_r(:,:,8)',F,DT_sh).*Te.^2.*Tc+...
quick_interp2(F_array,DT_sh_array,coeff_m_r(:,:,9)',F,DT_sh).*Te.*Tc.^2+...
quick_interp2(F_array,DT_sh_array,coeff_m_r(:,:,10)',F,DT_sh).*Tc.^3)/3600;
```

The model of this component, as first purpose, can be used to explore how the outputs are affected by the inputs (Figure 3.3, Figure 3.3 and Figure 3.4).

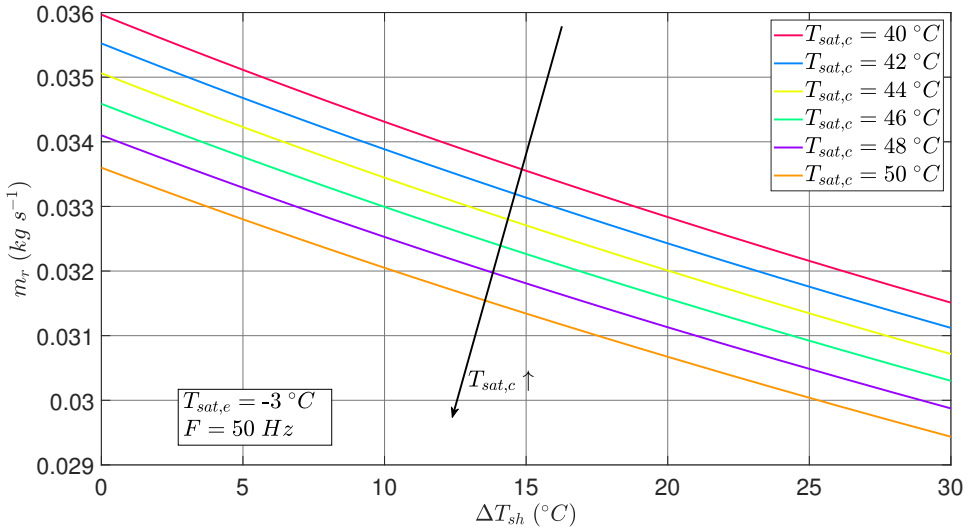

(a) $T_{sat,e}$ *constant*

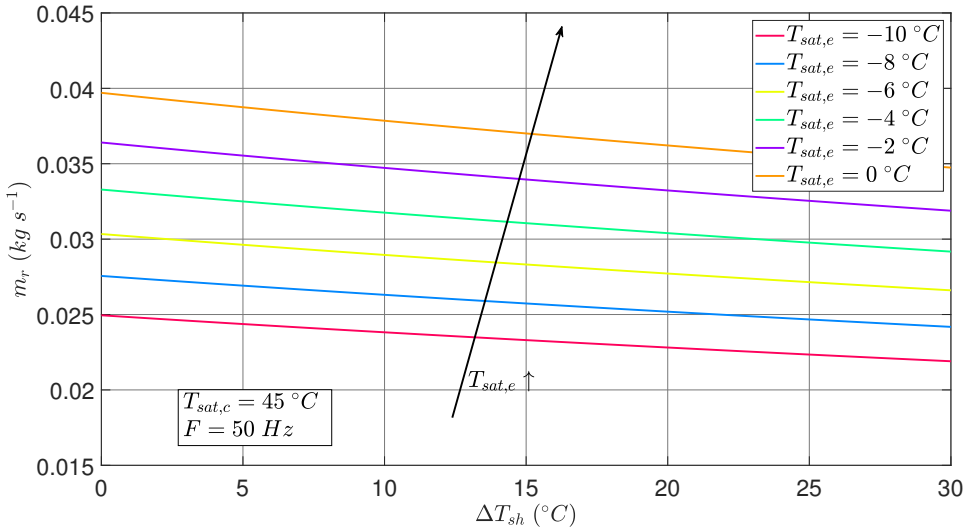

(b) $T_{sat,c}$ *constant*

Figure 3.2

Compressor m_r as a function of ΔT_{sh} varying one of $T_{sat,e}$ and $T_{sat,c}$.
When ΔT_{sh} increases, m_r decreases because the vapor density of the refrigerant decreases too. For a fixed degree of superheat m_r is higher when $T_{sat,e}$ increases and $T_{sat,c}$ decreases: the temperature drop corresponds to that related to pressure, so when the former is small, the latter is small too and the compressor can operate a larger mass flowrate m_r

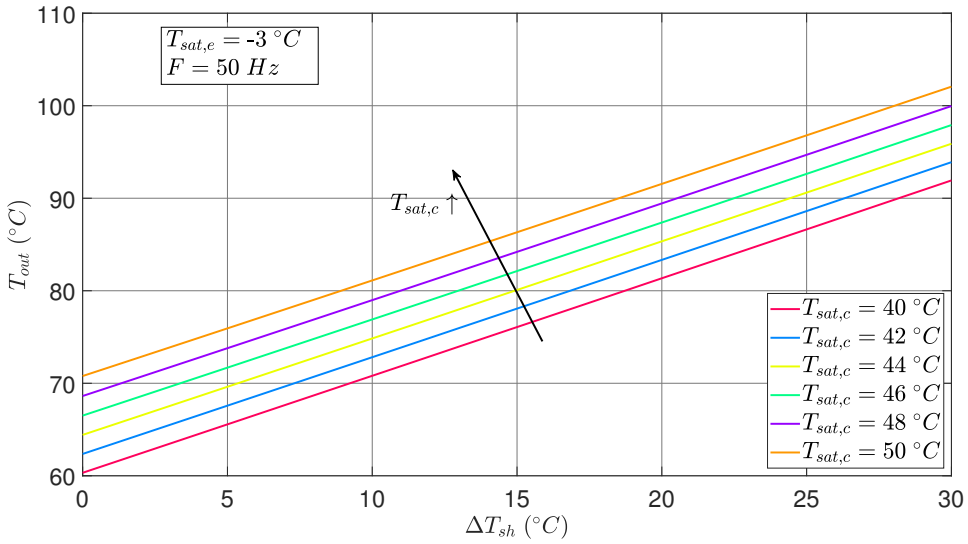

(a) $T_{sat,e}$ *constant*

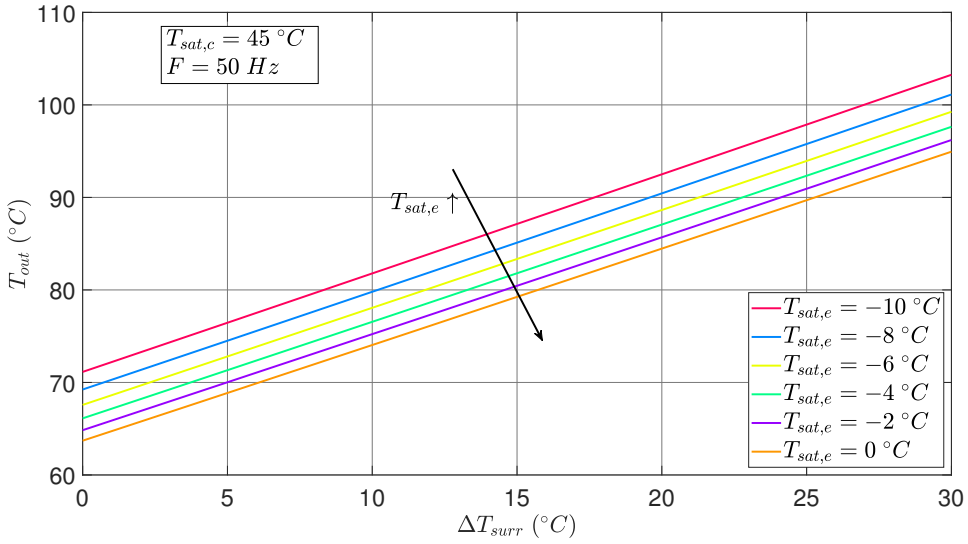

(b) $T_{sat,c}$ *constant*

Figure 3.3

Compressor T_{out} as a function of ΔT_{sh} varying one of $T_{sat,e}$ and $T_{sat,c}$.
T_{out} increase with ΔT_{sh} because the vapor at the compressor inlet is more superheated. Under the same ΔT_{sh}, the refrigerant at compressor outlet is hotter when $T_{sat,e}$ decreases and $T_{sat,c}$ increases: it is a consequence of the reduction in m_r which occurs when these two conditions are verified.

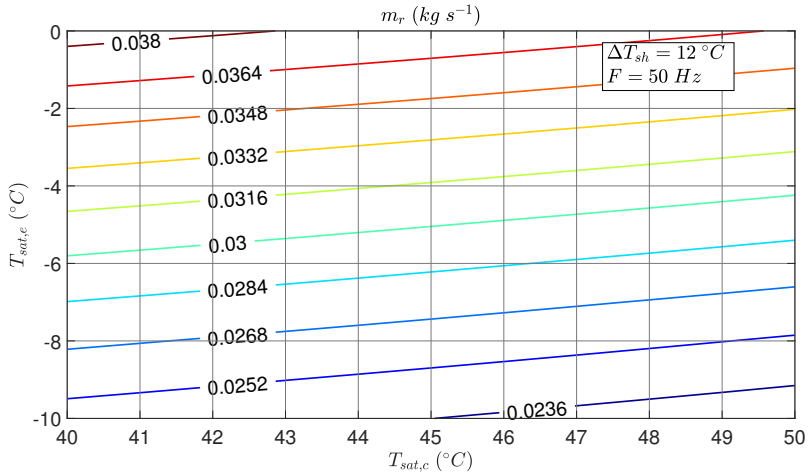

(a) m_r

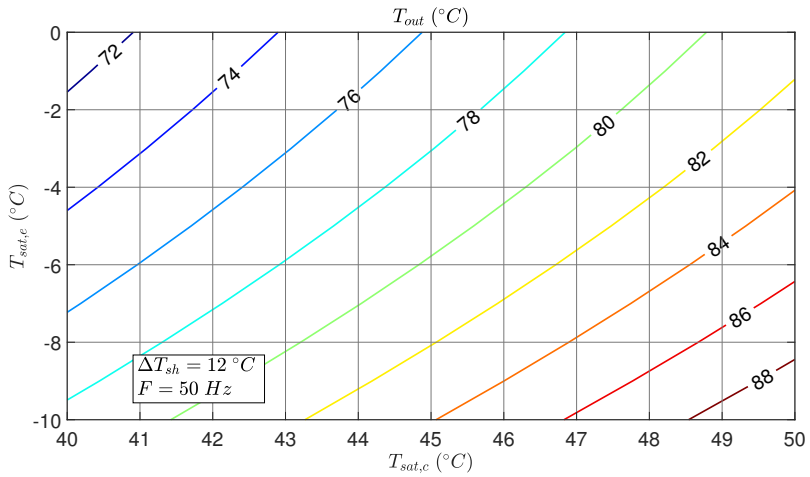

(b) T_{out}

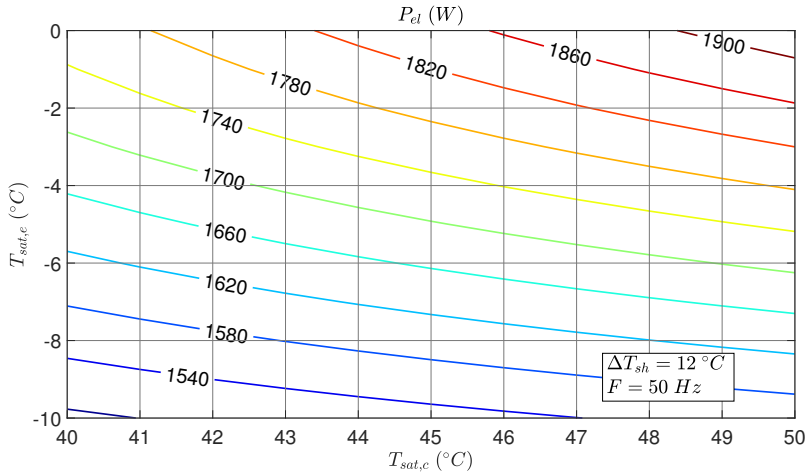

(c) P_{el}

Figure 3.4
Compressor outputs as a function of $T_{sat,e}$ and $T_{sat,c}$.

3.1.2 | Condenser

Summarising what has been developed in the previous chapter, the condenser model is based on ten algebraic equations. The heat exchanger geometry and the thermodynamic properties of the refrigerant and secondary fluid are the first inputs of the model. Focusing on the physical sense of the model and studying similar problems in literature, p, $h_{r,in}$, $T_{f,in}$, m_f and m_r are considered as inputs. Fixed the condensation pressure p, the enthalpies of the saturated states $h_{r,v}$ and $h_{r,l}$ are known and an algebraic system of ten equations in ten variables is obtained (3.8).

$$\begin{cases} m_r\ (h_{r,in} - h_{r,v}) = m_f\ c_{p,f,sh}\ (T_{f,out} - T_{f,v}) \\ m_r\ (h_{r,in} - h_{r,v}) = \varepsilon_{sh}\ C_{min,sh}\ (T_{r,in} - T_{f,v}) \\ m_r\ (h_{r,v} - h_{r,l}) = m_f\ c_{p,f,tp}\ (T_{f,v} - T_{f,l}) \\ m_r\ (h_{r,v} - h_{r,l}) = \varepsilon_{tp}\ C_{min,tp}\ (T_{r,v} - T_{f,l}) \\ m_r\ (h_{r,l} - h_{r,out}) = m_f\ c_{p,f,sc}\ (T_{f,l} - T_{f,in}) \\ m_r\ (h_{r,l} - h_{r,out}) = \varepsilon_{sc}\ C_{min,sc}\ (T_{r,l} - T_{f,in}) \\ \zeta_{sc} + \zeta_{tp} + \zeta_{sh} = 1 \\ \varepsilon_{sc} = \Phi\ (\zeta_{sc}) \\ \varepsilon_{tp} = \Phi\ (\zeta_{tp}) \\ \varepsilon_{sh} = \Phi\ (\zeta_{sh}) \end{cases} \tag{3.8}$$

$$\{h_{r,out},\ T_{f,out},\ T_{f,v},\ T_{f,l},\ \zeta_{sh},\ \zeta_{tp},\ \zeta_{sc},\ \varepsilon_{sh},\ \varepsilon_{tp},\ \varepsilon_{sc}\} = \\ = \Phi\ (p,\ h_{r,in},\ T_{f,in},\ m_r,\ m_f) \tag{3.9}$$

Schematically the model is represented in Figure 3.5, where only four outputs are highlighted. The subcooled degree ΔT_{sc} (3.10) and the heat transfer rate Q_r (3.11) are not directly given by the system, but they are known from the variables of the model.

$$\Delta T_{sc} = T_{r,l} - T_{r,out} \tag{3.10}$$

$$Q_r = m_r\ (h_{r,in} - h_{r,out}) \tag{3.11}$$

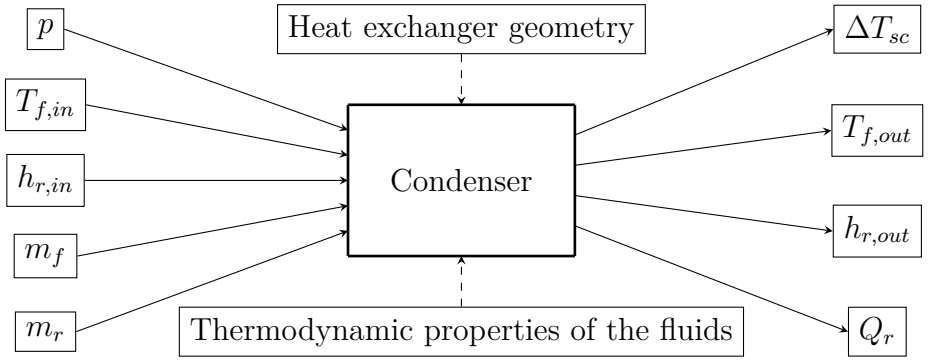

Figure 3.5
Inputs and outputs of the condenser model.

Due to its non-linearity, it is impossible to transport the system in a matrix form equation $Ax = b$ where x is the variable vector. Two possible resolution methods for the non-linear systems are considered:

- use of symbolic variables;
- development of a numeric iterative cycle for resolution.

Symbolic model

The use of the symbolic variables is the easiest one method but has some drawbacks. First, a non-linear system with a number of variables equal to the number of equations does not imply that a unique solution exists: the numerical solver of Matlab finds the solutions of the non-linear system, without considering the physics of the problem. This fact could lead to the determination of unwanted solutions resulting in a waste of computational time. Moreover, the use of symbolic variables in Matlab is very heavy in terms of computational time and resources employed[1].

Still, a symbolic model (Code 3.3) of the condenser is implemented in a Matlab script in order to experiment the validity of the resolution method and to test the computational cost.

Code 3.3
Part of the symbolic model of the condenser.

```
1 syms zeta_sc zeta_sh zeta_tp T_f_out T_f_l T_f_v h_r_out epsilon_sh ...
```

[1]This fact will be hightlighted in the next pages.

```
    epsilon_sc epsilon_tp NTU_sh NTU_sc NTU_tp positive
eqn_bil_sc=m_f*(T_f_l-T_f_in)*cp_f==m_r*(h_r_l-h_r_out);
eqn_bil_tp=m_f*(T_f_v-T_f_l)*cp_f==m_r*(h_r_v-h_r_l);
eqn_bil_sh=m_f*(T_f_out-T_f_v)*cp_f==m_r*(h_r_in-h_r_v);
eqn_eps_ntu_sh=m_r*(h_r_in-h_r_v)==epsilon_sh*C_min_sh*(T_r_in-T_f_v);
eqn_eps_ntu_sc=m_r*(h_r_l-h_r_out)==epsilon_sc*C_min_sc*(T_r_l-T_f_in);
eqn_eps_ntu_tp=m_r*(h_r_v-h_r_l)==epsilon_tp*cp_f*m_f*(T_r_l-T_f_in);
eqn_efficacia_sc=epsilon_sc==(1-exp(-NTU_sc*(1-rho_c_sc)))/...
    (1-rho_c_sc*exp(-NTU_sc*(1-rho_c_sc)));
eqn_efficacia_sh=epsilon_sc==(1-exp(-NTU_sh*(1-rho_c_sh)))/...
    (1-rho_c_sh*exp(-NTU_sh*(1-rho_c_sh)));
eqn_efficacia_tp=epsilon_tp==1-exp(-NTU_tp);
eqn_ntu_sh=NTU_sh==1/(1/(total_area*alpha_r_sh*zeta_sh)+...
    1/(total_area*alpha_f*zeta_sh))*1/C_min_sh;
eqn_ntu_sc=NTU_sc==1/(1/(total_area*alpha_r_sc*zeta_sc)+...
    1/(total_area*alpha_f*zeta_sc))*1/C_min_sc;
eqn_ntu_tp=NTU_tp==1/(1/(total_area*alpha_r_tp*zeta_tp)+...
    1/(total_area*alpha_f*zeta_tp))*1/(cp_f*m_f);
eqn_sum=zeta_sc+zeta_sh+zeta_tp==1;
```

First iterative model

Some iterative methods are also implemented to solve the (3.8). The first one is an algorithm based on the maximum heat transfer rate of the condenser: in this case $T_{r,out} = T_{f,in}$. From this point, where theoretically the heat transfer surface area might have an infinite extension, the $T_{r,out}$ is increased until (3.8) is verified.

0. the variables are initialized, $T_{r,out} = T_{f,in}$;
1. the iterative cycle starts and $T_{r,out} = T_{r,out} + \Delta T$;
2. knowing $h_{r,out}$, from (2.7), (2.5) and (2.3) $T_{f,l}$, $T_{f,v}$ and $T_{f,out}$ respectively are evaluated;
3. ε_{sh} is obtained from (2.4). If $\varepsilon_{sh} > 1 \vee \varepsilon_{sh} < 0$ the cycle restarts from point 1 (Code 3.4);
4. ε_{tp} is calculated from (2.6). If $\varepsilon_{tp} > 1 \vee \varepsilon_{tp} < 0$ the cycle restarts from point 1;
5. ε_{sc} is computed from (2.8). If $\varepsilon_{sc} > 1 \vee \varepsilon_{sc} < 0$ the cycle restarts from point 1;
6. through the inversion of (2.71) ζ_{tp} is calculated. If $\zeta_{tp} > 1 \vee \zeta_{tp} < 0$ the cycle restarts from point 1;
7. the (2.8) cannot be written isolating ζ_{sc}. In order to evaluate ζ_{sc} without employing the symbolic variables an iterative cycle is necessary. While $\varepsilon_{sc} = \Phi(\zeta_{sc})$, determined by (2.8), is out of a certain tolerance near the value of ε_{sc} evaluated at point 5,ζ_{sc} is increased $\zeta_{sc} = \zeta_{sc} + \Delta\zeta$ and the (2.8) is evaluated anew. If the iteration oversteps the upper limit $\zeta_{sc} > 1$, the total cycle restarts from

point 1;

8. the value of ζ_{sh} is evaluated using (2.4) in the same way as ζ_{sc} at point 7 (Code 3.5);
9. the cycle is terminated if (2.18) is verified: when $|\zeta_{sc} + \zeta_{tp} + \zeta_{sh} - 1| < \tau_\zeta$, the variables calculated are saved and the loop is exited. If the (2.18) is not verified the cycle restarts from point 1.

Code 3.4
Control of ε_{sh} for the condenser iterative model.

```
%Determination of the minimum heat capacity rate
if m_r*cp_r_surr>m_f*cp_f_surr
    rho_c_surr=m_f*cp_f_surr/(m_r*cp_r_surr);
    C_min_surr=m_f*cp_f_surr;
else
    rho_c_surr=m_r*cp_r_surr/(m_f*cp_f_surr);
    C_min_surr=m_r*cp_r_surr;
end

efficacia_surr=m_r*(h_r_in-h_r_v)/(C_min_surr*(T_r_in-T_f_v));

%Control on epsilon
if efficacia_surr>1 || efficacia_surr<0
    continue
end
```

Code 3.5
Loop on ζ_{sh} for the condenser iterative model.

```
while abs(epsilon_surr-efficacia_surr)>eps_efficacia
    %Increase of zeta
    zita_surr=zita_surr+delta_zita;

    %Criteria for the exit from the loop
    if zita_surr>1
        break
    end

UA_surr=1/(1/(total_area*alpha_r_surr*zita_surr)+1/...
    (total_area*alpha_f_surr*zita_surr));

NTU_surr=UA_surr/C_min_surr;

epsilon_surr=(1-exp(-NTU_surr*(1-rho_c_surr)))/...
    (1-rho_c_surr*exp(-NTU_surr*(1-rho_c_surr)));
end
```

Execution time symbolic model

An important driver for the choice of the model is how fast the symbolic

and iterative ones work. For this reason, the computation time for the determination of different operating points is evaluated and compared. In order to take into account the variance due to the execution of other processes in background, the script repeats the operations a certain number of times and at different operating conditions (Figure 3.6).

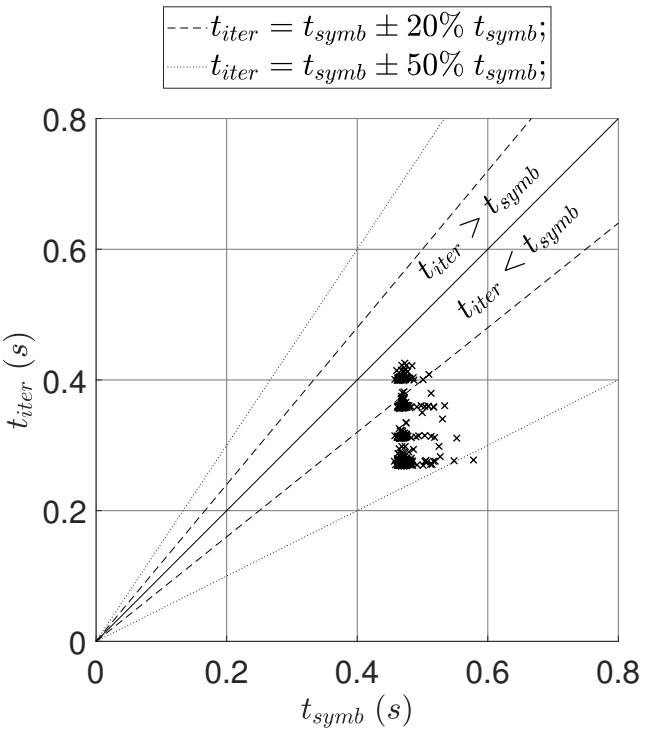

Figure 3.6
Execution time comparison: symbolic vs iterative model. The iterative method is about 1.4 times faster than the symbolic one. Note that the computational cost of the symbolic model is quite constant independently of the operating conditions. The iterative model computation time is longer for the points where $T_{r,out} - T_{f,in}$ is higher because ΔT is constant.

The iterative model ensures a smaller computational cost and a major and more physical control of the numerical resolution process. These two advantages suggest to employ the iterative approach for the development of the heat exchanger models.

Second iterative model

A second iterative model is developed to reduce the number of iterations.

0. the variables are initialized: $T_{r,out} = \frac{T_{r,l}+T_{f,in}}{2}$;
1. the iterative cycle starts with the actual value of $T_{r,out}$;
2. determination of $T_{f,l}$ and ε_{sc} from (2.7) and (2.8) respectively;
3. the (2.8) cannot be written isolating ζ_{sc}. In order to evaluate ζ_{sc} without employing the symbolic variables an iterative cycle is necessary. While $\varepsilon_{sc} = \Phi(\zeta_{sc})$, determined by (2.8), falls outside a certain tolerance near the value of ε_{sc} evaluated at point 2, $\zeta_{sc} = \zeta_{sc} + \Delta\zeta$ and the (2.8) is

re-evaluated;

4. determination of ε_{tp} and ζ_{tp} from (2.6) and (2.71) respectively;
5. ζ_{sh} is noted from (2.18) knowing ζ_{sc} and ζ_{tp};
6. determination of ε_{sh} as function of ζ_{sh} (2.70);
7. a value of the inlet temperature $T_{r,in,calc}$ can now be determined using (2.4);
8. if $h_{r,in,calc} > h_{r,in}$, the distance between the refrigerant and the secondary fluid temperature is too high at the inlet region of the condenser. This difference can be reduced decreasing the temperature differnce at the refrigerant outlet $T_{r,out} = T_{r,out} - \Delta T$. When $h_{r,in,calc} > h_{r,in}$, the behaviour is symmetric, so $T_{r,out} = T_{r,out} + \Delta T$: Δ T is reduced and the cycle restart from 1;
9. the cycle ends when $|T_{r,in,calc} - T_{r,in}|$ is within a certain tolerance.

This second iterative model is often faster than the first one (Figure 3.7), because there is one iterative loop less, but in this case the computation time depends on the working point.

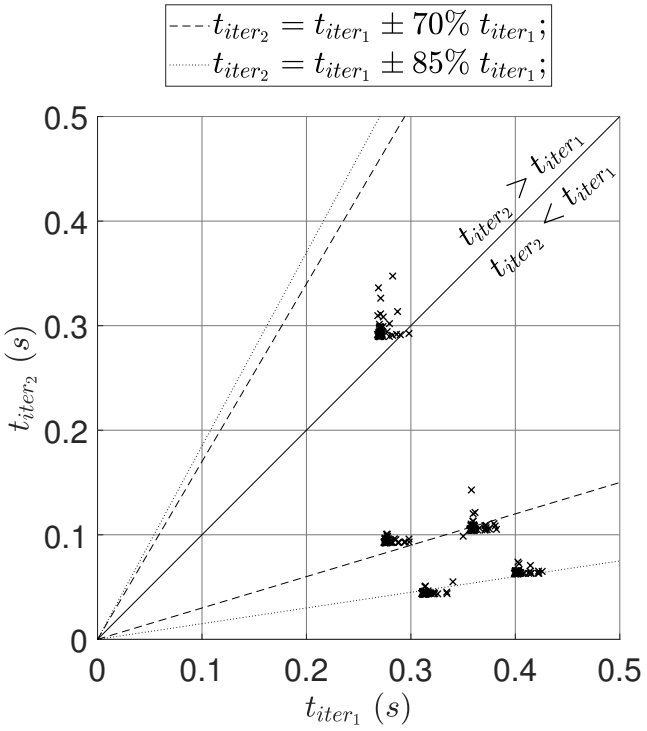

Figure 3.7
Execution time comparison: iterative models.
The iterative method is about 4 times faster than the symbolic one (except for one working point).

The iteration step

There is an important difference between these two models: in the first one the iteration step is given by a ΔT which is constant; in the second one the iteration step is still given by a ΔT, but in this case, it decreases while the cycle

is running: this reduction is necessary to prevente the cycle from oscillating between two temperatures.

This step plays a key role in the iterative cycle: it affects the accuracy, the number of cycles and the computational cost. If the step is small, a little tolerance can be set as termination criterion for the cycle and the model accuracy increases and vice versa. A good compromise could be a variable step which is bigger or smaller when the error computed by the model is high or low respectively.

This effect is tested in the first iterative model. A first simulation is run with a fixed step, a second one with a step which varies according to the error computed (Figure 3.8). With a variable step the computational cost of the function is about eight times smaller than the function with a fixed step (Figure 3.9).

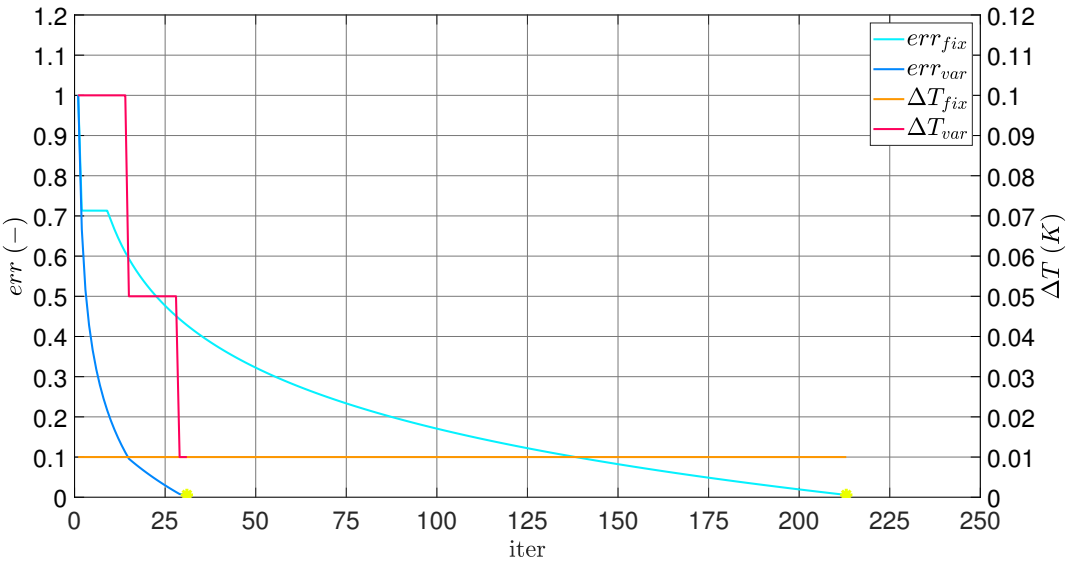

Figure 3.8

Fixed step vs variable step in the condenser model.
Employing a variable step, the number of iterations and the computation time (fixed an equal error tolerance as termination criteria) is reduced. The number of iteration required for the convergence is about eight times smaller with a variable step.

Reducing the computational cost of the single heat exchanger model of only few tenths of second when it operates at a single point of work has a great relevance when these models are employed as part of the model of the whole

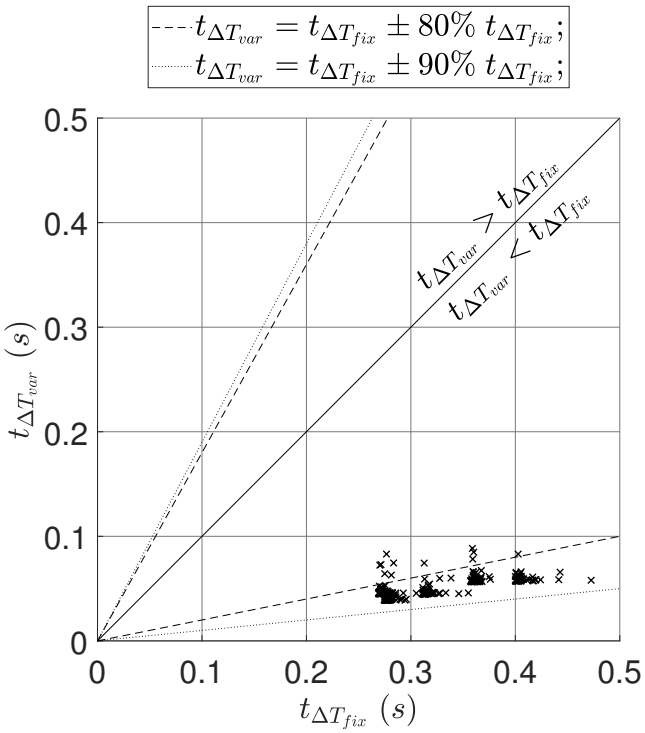

Figure 3.9
Execution time comparison: condenser iterative model fixed vs variable step.
With a variable step the computation time is quite constant varying the working point, because the step follows the error trend. The computational cost of the first iterative model with variable step is about eight time smaller than the same model with fixed step.

plant, which is based on other iterative cycles, as presented in (Section 3.2). The symbolic model[2] and the two iterative ones will be validated in the next chapter.

[2]The symbolic model will not be considered for the implementation in the model of the VCRS, but is used in the next chapter as reference for a comparison in terms of accuracy of the variables solved.

3.1.3 | Evaporator

What has been done for the condenser is repeated for the evaporator. p, $h_{r,in}$, $T_{f,in}$, m_f and m_r are considered as inputs. Once the evaporation pressure p is set, the enthalpy of the saturated vapor $h_{r,v}$ is known and an algebraic system of seven equations is obtained (3.12).

$$\begin{cases} m_r\ (h_{r,v} - h_{r,in}) = m_f\ c_{p,f,tp}\ (T_{f,v} - T_{f,out}) \\ m_r\ (h_{r,v} - h_{r,in}) = \varepsilon_{tp}\ C_{min,tp}\ (T_{f,v} - T_{r,in}) \\ m_r\ (h_{r,out} - h_{r,v}) = m_f\ c_{p,f,sh}\ (T_{f,in} - T_{f,v}) \\ m_r\ (h_{r,out} - h_{r,v}) = \varepsilon_{sh}\ C_{min,sh}\ (T_{f,in} - T_{r,v}) \\ \zeta_{tp} + \zeta_{sh} = 1 \\ \varepsilon_{tp} = \Phi\,(\zeta_{tp}) \\ \varepsilon_{sh} = \Phi\,(\zeta_{sh}) \end{cases} \tag{3.12}$$

$$\{h_{r,out},\ T_{f,out},\ T_{f,v},\ \zeta_{sh},\ \zeta_{tp},\ \varepsilon_{sh},\ \varepsilon_{tp}\} = \Phi\,(p,\ h_{r,in},\ T_{f,in},\ m_r,\ m_f) \tag{3.13}$$

The model is represented schematically in (Figure 3.10). The degree of superheat ΔT_{sh} (3.14) and the heat transfer rate Q_r (3.15) are not directly given by the system but are simple function of some variables.

$$\Delta T_{sh} = T_{r,out} - T_{r,v} \tag{3.14}$$

$$Q_r = m_r\ (h_{r,out} - h_{r,in}) \tag{3.15}$$

Also for the evaporator a symbolic model (Code 3.6) and an iterative one has been developed.

Code 3.6
Part of the symbolic model of the evaporator.

```
syms zeta_surr zeta_tp T_f_out T_f_v h_r_out epsilon_surr epsilon_tp...
    NTU_surr NTU_tp positive
eqn_bil_tp=m_f*(T_f_v-T_f_out)*cp_f==m_r*(h_r_v-h_r_in);
eqn_bil_surr=m_f*(T_f_in-T_f_v)*cp_f==m_r*(h_r_out-h_r_v);
eqn_eps_ntu_surr=m_r*(h_r_out-h_r_v)==epsilon_surr*C_min_surr*...
    (T_f_in-T_r_v);
eqn_eps_ntu_tp=m_r*(h_r_v-h_r_in)==epsilon_tp*cp_f*m_f*(T_f_v-T_r_in);
```

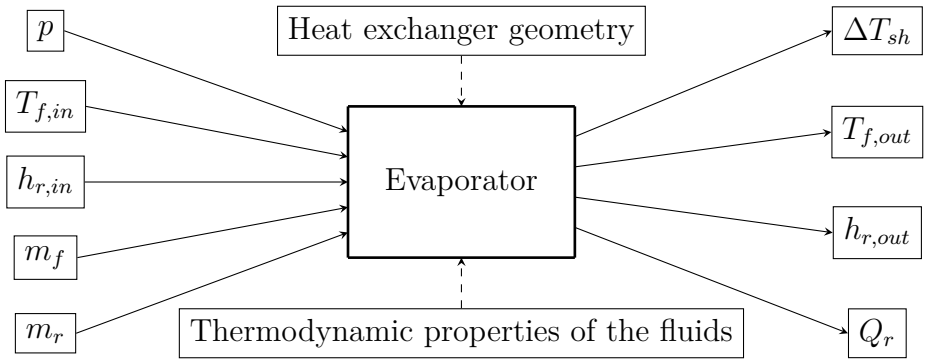

Figure 3.10
Inputs and outputs of the evaporator model.

```
eqn_efficacia_surr=epsilon_surr==(1-exp(-NTU_surr*(1-rho_c_surr)))/...
    (1-rho_c_surr*exp(-NTU_surr*(1-rho_c_surr)));
eqn_efficacia_tp=epsilon_tp==1-exp(-NTU_tp);
eqn_ntu_surr=NTU_surr==1/(1/(total_area*alpha_r_surr*zeta_surr)+...
    1/(total_area*alpha_f*zeta_surr))*1/C_min_surr;
eqn_ntu_tp=NTU_tp==1/(1/(total_area*alpha_r_tp*zeta_tp)+...
    1/(total_area*alpha_f*zeta_tp))*1/(cp_f*m_f);
eqn_somma=zeta_surr+zeta_tp==1;
```

Iterative model

The iterative method is similar to the first one presented for the condenser: this time the refrigerant temperature at the evaporator outlet has to be decreased to obey the laws of thermodynamics.

0. the variables are initialized, $T_{r,out} = T_{f,in}$;
1. the iterative cycle starts and $T_{r,out} = T_{r,out} - \Delta T$;
2. knowing $h_{r,out}$, from (2.21) and (2.19) $T_{f,v}$ and $T_{f,out}$ respectively are evaluated;
3. ε_{sh} is obtained from (2.22). If $\varepsilon_{sh} > 1 \vee \varepsilon_{sh} < 0$ the cycle restarts from point 1;
4. ε_{tp} is computed from (2.20). If $\varepsilon_{tp} > 1 \vee \varepsilon_{tp} < 0$ the cycle restarts from point 1;
5. through the inversion of (2.72) ζ_{tp} is calculated. If $\zeta_{tp} > 1 \vee \zeta_{tp} < 0$ the cycle restarts from point 1;
6. the (2.8) cannot be written isolating ζ_{sh}. In order to evaluate the value of ζ_{sh} without employing the symbolic variables an iterative cycle is necessary. WHile $\varepsilon_{sh} = \Phi(\zeta_{sc})$, determined by (2.22), falls outside a certain tolerance near the value of ε_{sh} evaluated at point 5, $\zeta_{sh} = \zeta_{sh} + \Delta\zeta$ and the (2.8) is re-evaluated. If the iteration reaches the upper limit

$\zeta_{sh} > 1$, the total cycle restart from point 1;

7. the cycle is terminated if the (2.23) is verified: when $|\zeta_{sh} + \zeta_{tp} - 1| < \varepsilon_\zeta$, the variables calculated are saved and the loop is exited. If the (2.23) is not verified the cycle restart from point 1.

The iteration step

Also in the evaporator, the computation time comparison between these two models shows that the iterative one is the faster.[3] More relevant is the problem of the step, because the evaporator model is far more sensitive to the variation of $T_{r,out}$ than that of the condenser. Besides, a small variation in $h_{r,out}$ causes a more relevant change in the inlet quality of the liquid vapor mixture x_{in}: this quantity is involved in the heat transfer and pressure drop correlations and affects the behavior of the heat exchanger as a whole. For this reason in the evaporator a smaller ΔT than in the condenser is usually required.

Pressure drop

The model that takes into account the pressure drop is based on the same iterative cycle but the thermophysical properties of the refrigerant are computed at different pressures. The pressure drop is given by the Amalfi correlation (Section 2.4) evaluated during the cycle.

To contain the computational cost a variable step is recommended (Figure 3.11).

Section 3.2

Machine algorithm

The model of the whole machine must connect correctly the inputs an the outputs of the models of the components (Figure 3.12).

The condensation p_c and the boiling p_e pressure are highlighted because they are both inputs of different models of the components. This suggests that also for the resolution of the model of the machine an iterative method is requested. In literature several methods are presented, but in this work a very similar method to the one suggested by Zsembinszki, Gracia, Moreno, Rovira, González, and Cabeza [43] is used.

Inputs of the model

The inputs of the model are the compressor frequency F and the degree of

[3] The results are not reported to make the dissertation more amenable for the reader.

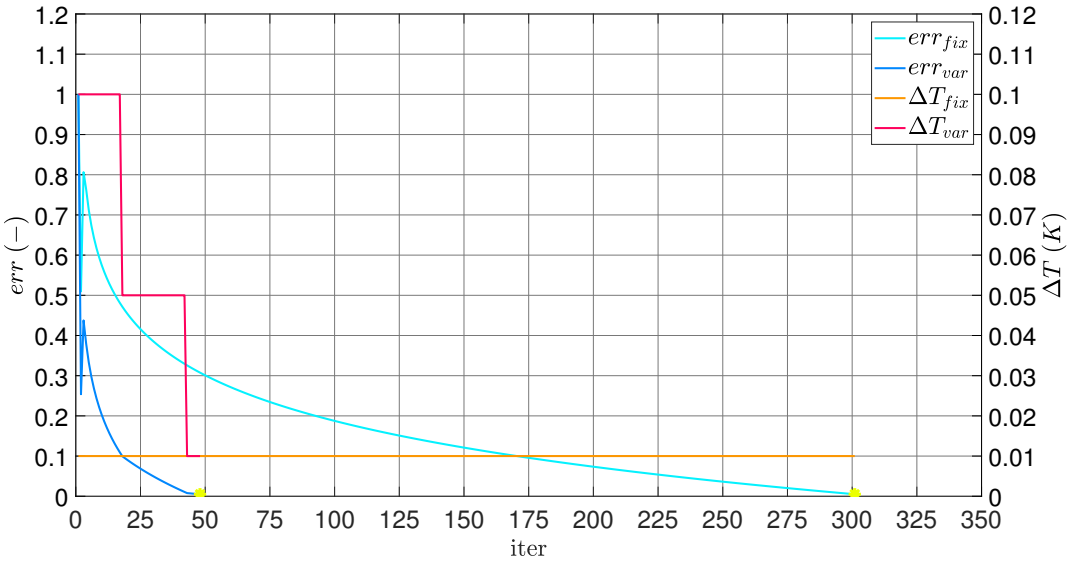

Figure 3.11

Fixed step vs variable step in the evaporator model.
Employing a variable step, the number of iterations and the computation time (fixed an equal error tolerance as termination criteria) are reduced. In the second step the error is high because only from the second step does the model take the pressure drop into account.

superheat ΔT_{sh} expected. A minimum condensation pressure and a maximum boiling pressure are given by the secondary fluid operating condition in both the heat exchangers:

- knowing the secondary fluid temperature in the condenser inlet and the subcooled degree expected, the minimum condensation pressure is fixed: it is the refrigerant pressure such that $T_{r,out}$, obtained as difference between $T_{r,l}$ at this pressure and ΔT_{sc}, equals $T_{f,in}$;

- knowing the secondary fluid temperature at the evaporator inlet and the degree of superheat expected, the maximum boiling pressure is fixed: it is the refrigerant pressure such that $T_{r,out}$, obtained as sum of $T_{r,v}$ at this pressure and ΔT_{sh}, equals $T_{f,in}$;

ΔT_{sh} is known because it is an input of the model, but ΔT_{sc} is unknown. For this reason the experimental values of ΔT_{sc} are compared with the condensation

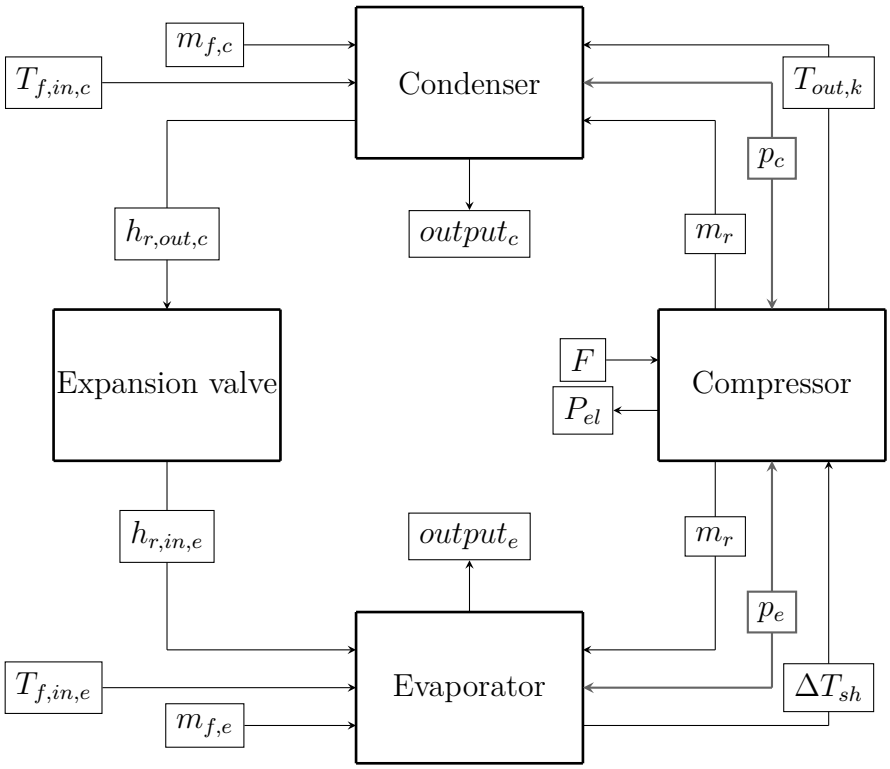

Figure 3.12
Inputs and outputs of the evaporator model.
The block of the expansion valve is reported only to respect the basilar components of a VCRS. But the function of this block is very easy: it assigns to $h_{r,in,e}$ the value of $h_{r,out,c}$.

pressure to find a function in the form:

$$\Delta T_{sc} = \Phi\left(p_c\right)$$

A simple line fits very well the experimental data and its equation is the correlation searched.

The first block

In a first block the maximum condensation pressure is found; p_e is fixed at its maximum value. The model increases p_c from its minimum value and solves only the compressor and the condenser model until the difference between $\Delta T_{sc,calc}$ and $\Delta T_{sc,exp} = \Phi\left(p_{c,calc}\right)$ is below a certain tolerance τ_{sc}. When this block is satisfied a maximum condensation pressure is fixed (Figure 3.14).

The second block

Now the second block starts. In an external iterative cycle the value of p_c is decreased. An inner iterative cycle takes into account this current value of p_c

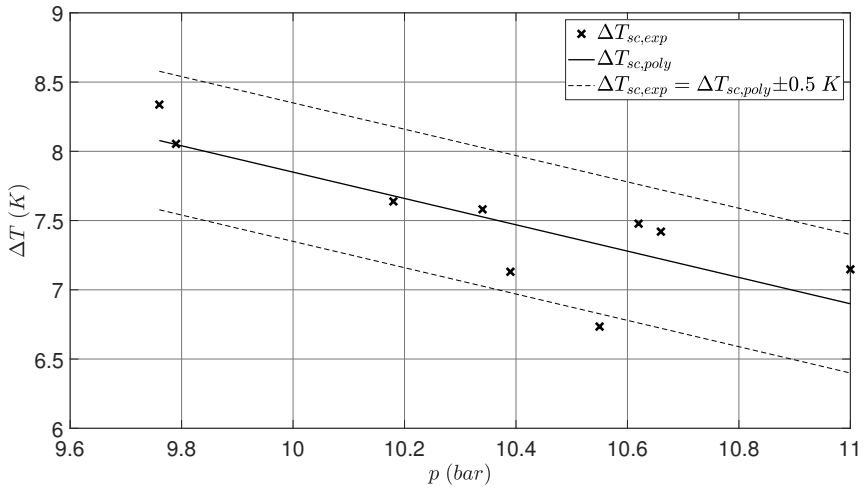

Figure 3.13
Linear polynomial fitting of the experimental data for ΔT_{sc}.
Note that the deviation between the experimental values and the fitted ones is almost always under $0.5K$.

and decreases p_e, solving the compressor and the condenser until the difference between $\Delta T_{sc,calc}$ and $\Delta T_{sc,exp} = \Phi\left(p_{c,calc}\right)$ is less than a certain tolerance τ_{sc}. When this condition is satisfied, the value of p_e is saved and the evaporator model is solved. If the difference between $\Delta T_{sh,calc}$ from the evaporator model and $\Delta T_{sh,exp}$ (the value gives in input to the model) is less than a certain tolerance τ_{sh} the external iteration cycle is stopped. Otherwise the loop on the external cycle continues, p_c is decreased and the internal cycle on p_e is restarted, initializing p_e to its maximum value (Figure 3.15).

Execution time

To decrease the computational cost for these two blocks, lighter versions of the function of the models of the components are called in the script where the model of the circuit is implemented. These versions compute only the outputs necessary for the global iteration processes. When the model converges, the output variables are used as inputs for the complete version of the function of the components' models in order to determine a significant number of interesting quantities for the VCRS cycle characterization. Also in this model, varying the values of the steps, better performances in terms of computation time are obtained.

In the model of the heat exchangers the step is variable with the error. This approach is extended to the model of the VCRS, but in this case the structure

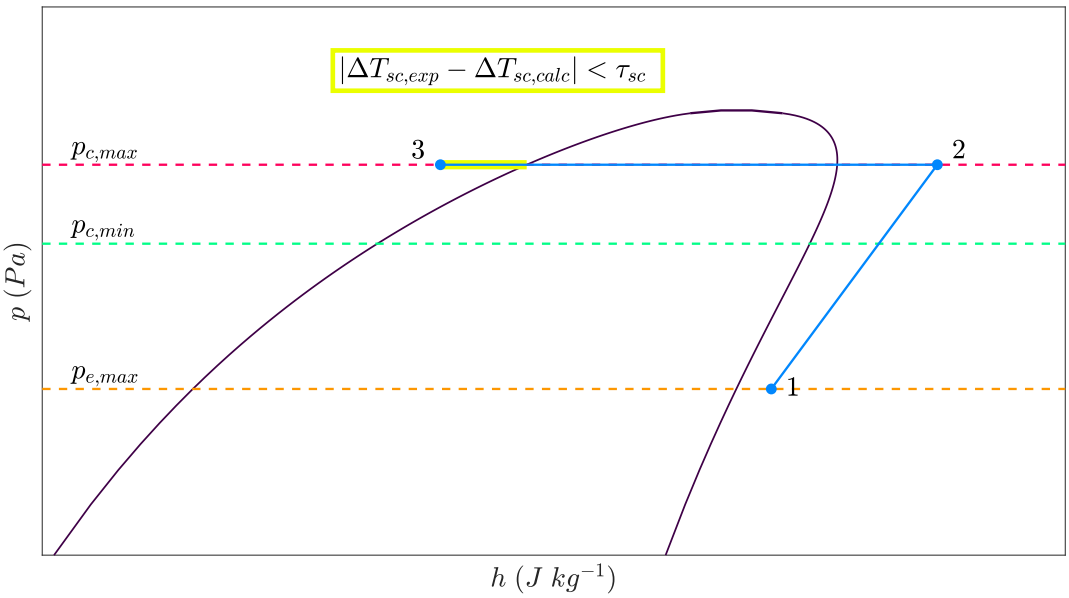

Figure 3.14
Schematic representation of the thermodynamic cycle in the first block on a $\log p - h$ *diagram.*

of the iterative cycle requires stricter control over the step. In order to increase the accuracy of this model and to decrease the number of iterations and, as a consequence, the computational cost (Figure 3.16), a step that varies as a function of the error and of its gradient is implemented.

In this way the step is reduced when the error function is small, but also when, even if its value is still high, it has been decreased with respect to its value at the previous iteration. Otherwise, when the function error given at the $n-th$ iteration is higher than the one at the $(n-1)-th$ iteration the step is progressively increased. In particular this approach is used in the external loop which decreases $T_{sat,c}$ in order to satisfy the criteria of convergence on ΔT_{sh}.

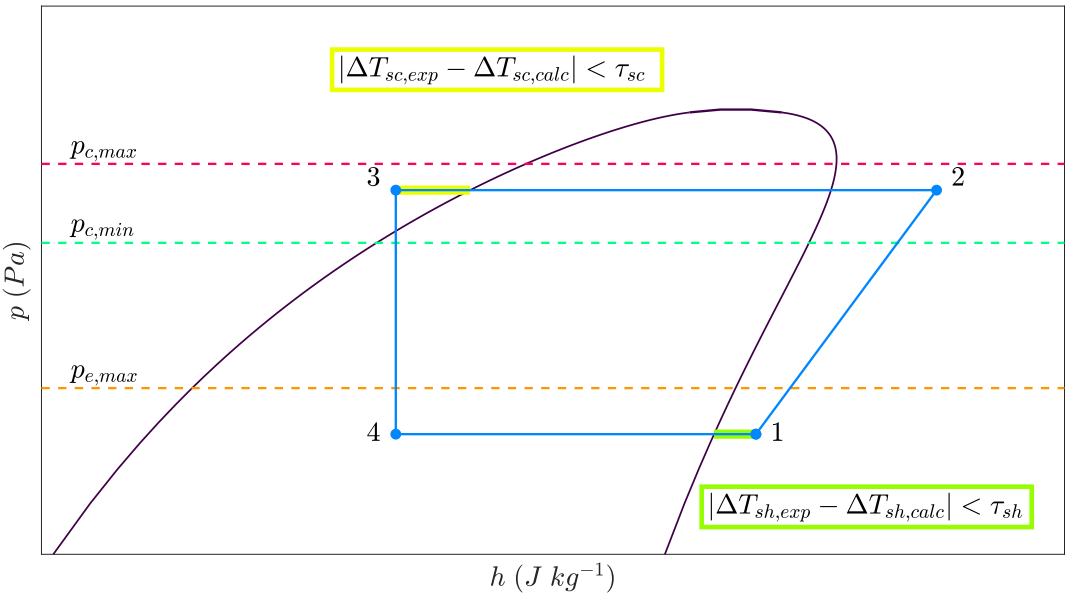

Figure 3.15
Schematic representation of the thermodynamic cycle in the second block on a $\log p - h$ *diagram.*

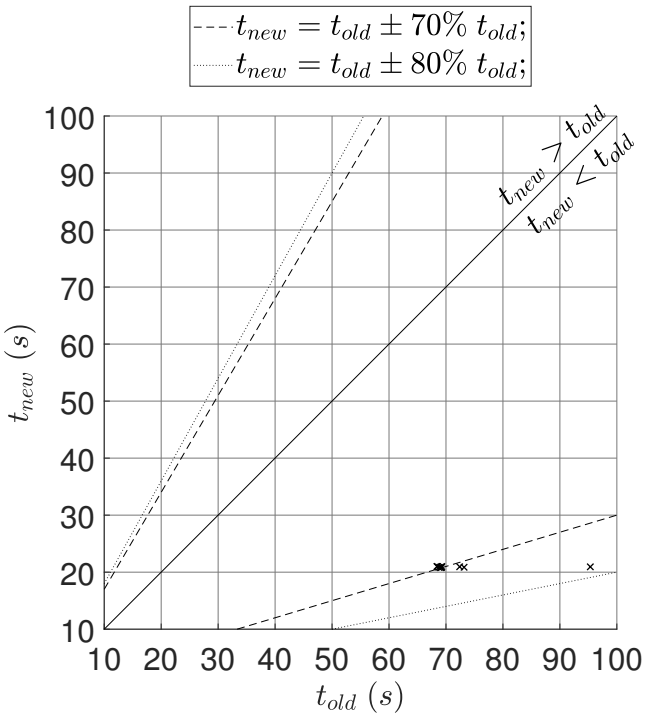

Figure 3.16
Execution time of the machine iteration cycle.
This example shows how important it is to set a correct step for the machine iteration cycle. Varying the method of control of the step the computation time can be dramatically reduced.

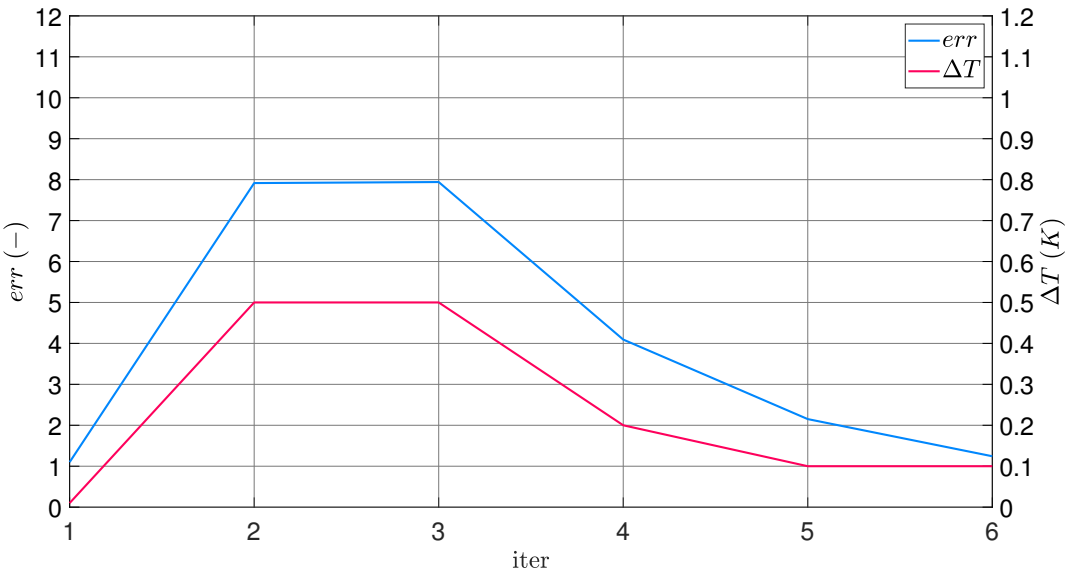

Figure 3.17
Step control based on the gradient.
The step is controlled with the gradient of the error function: in this way even if the absolute value of the error is high, the step is decreased and a possible solution of the problem can be found.

Section 3.3

Refrigerant and water properties

The refrigerant properties are evaluated trough two programs: RefProp and CoolProp.

RefProp [44], developed by the NIST (National Institute of Standards and Technology), and CoolProp [45] calculate the thermodynamic and transport properties of the most common industrial fluids and mixtures. These properties can be displayed in plots and tables through some user interfaces, they can be used in spreadsheets and they can be called in external programs [4]. Both of them are available for different operating systems (Windows, Linux, OSX, ...) and work in different programming languages (Python, Java, Matlab, C++, ...). This versatility is one of the reasons for their wide diffusion.

For this work they are configured to be used in Matlab, thanks to some extensions in .ddl format which have to be configured in the calculator (Code 3.7).

Code 3.7
Example of thermodynamics properties investigation using RefProp *and* CoolProp

```
Refrigerant='R450a.mix';
Secondary='water';

p=2345;                          %refrigerant pressure (kPa)
h=400000;                        %refrigerant enthalpy (J/kg)

p_sec=101325;                    %secondary pressure (Pa)
T_sec=300;                       %secondary temperature (K)

%% Refrigerant: REFPROP

%Temperature in function of pressure and enthalpy
T=refpropm('T','P',p,'H',h,Refrigerant);

%Viscosity in function of pressure and vapor quality
mu=refpropm('V','P',p,'Q',1,Refrigerant);

%Specific heat at constant pressure in function of pressure and vapor...
%quality
cp=refpropm('C','P',p,'Q',0,Refrigerant);
```

[4] More information is available in the technical documentation [46]

```
21
22 %% Secondary: COOLPROP
23
24 %Mass density in function of pressure and temperature
25 rho=CoolProp.PropsSI('D','P',p_sec,'T',T_sec,Secondary);
26
27 %Thermal conductivity in function of pressure and temperature
28 k=CoolProp.PropsSI('L','P',p_sec,'T',T_sec,Secondary);
```

The fluid properties are frequently evaluated in the heat exchanger models, so it is important that these calculations be made in the fastest way. From this viewpoint two methods for the evaluation of the properties are proposed:

- direct call of refpropm and CoolProp: in the script whenever it is necessary to determine a thermodynamic property the function implemented is called directly;
- use of structures: for a generic fluid or mixture a structure of data, in which the thermodynamic properties at different states as a function of the most used couples of thermodynamic variables are stored, is generated. In the script there is no direct call of the function, a generic property is evaluated thanks to the interpolation from the data stored in the structure.

Through a Matlab script the structure of properties for the R450a is generated.

Code 3.8
The data structure for the refrigerant properties and an example of its use

```
1  FluidProp =
2
3    struct with fields:
4
5              Psat: [1x500 double]
6              Tsat: [1x500 double]
7                ul: [1x500 double]
8                uv: [1x500 double]
9                hl: [1x500 double]
10               hv: [1x500 double]
11             rhol: [1x500 double]
12             rhov: [1x500 double]
13               sl: [1x500 double]
14               sv: [1x500 double]
15              cpl: [1x500 double]
16              cpv: [1x500 double]
17              mul: [1x500 double]
18              muv: [1x500 double]
19           lambdal: [1x500 double]
20           lambdav: [1x500 double]
21                P: [1x500 double]
22                H: [1x501 double]
23                T: [1x300 double]
24                S: [1x500 double]
25              rho: [1x2000 double]
26           rho_ph: [500x501 double]
27           rho_pt: [500x300 double]
28             h_pt: [500x300 double]
29             h_ps: [500x500 double]
30             T_ph: [500x501 double]
31             T_ps: [500x500 double]
32             s_ph: [500x501 double]
33          cliq_pt: [500x300 double]
34          cvap_pt: [500x300 double]
```

```
35            cliq_ph: [500x501 double]
36            cvap_ph: [500x501 double]
37      lambdaliq_pt: [500x300 double]
38      lambdavap_pt: [500x300 double]
39           muliq_pt: [500x300 double]
40           muvap_pt: [500x300 double]
41             h_prho: [500x2000 double]
42             T_prho: [500x2000 double]
43
44 %Vapor viscosity in function of
       pressure
45 mu=quick_interp1(FluidProp.P,...
46       FluidProp.muv,p);
47 %Temperature in function of
       pressure...
48 %and enthalpy
49 T=quick_interp2(FluidProp.P,...
50       FluidProp.H,FluidProp.T_ph',p,
             h_r_in);
```

Some thermodynamics properties are evaluated with both methods described above and the computation time is recorded. To take into account the effects of the variance due to the background processes on the laptop, the script determines the same properties 500 times. The results show that the fastest way to evaluate the thermodynamic properties is the direct call of the function (Figure 3.18).

Another important aspect has to be considered: RefProp is used to evaluate the properties of R450a mixture because it is not included in the CoolProp library. On the contrary, water is present in both the programs. To establish which is faster in the computation of the thermodynamic properties of water a procedure very similar to the previous case has been followed. The results underline that CoolProp is in general faster than RefProp (Figure 3.19).

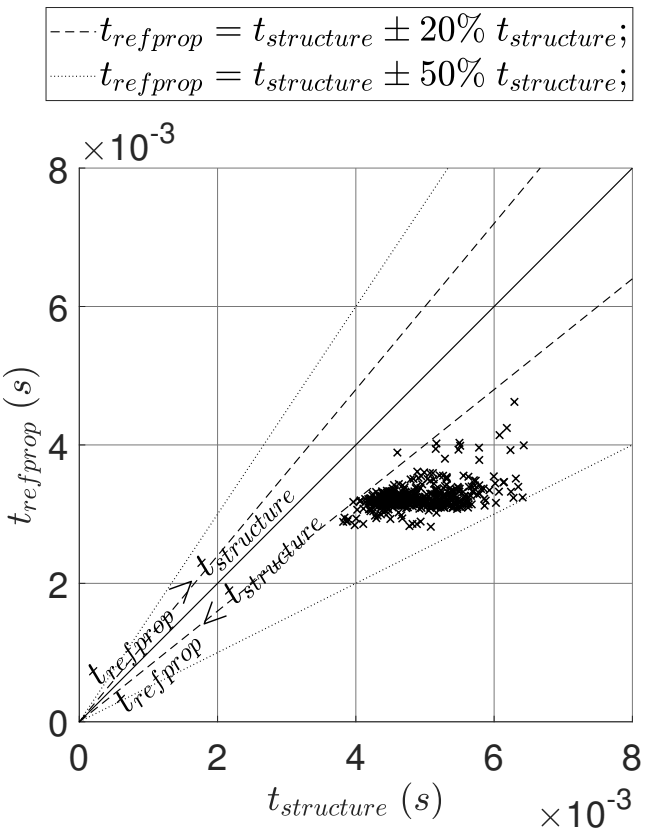

Figure 3.18
Computation time comparison: refprop vs structure.
In every instande, the direct call of the function is the faster way to evaluate the thermodynamic properties, even if the difference is of a few milliseconds only.

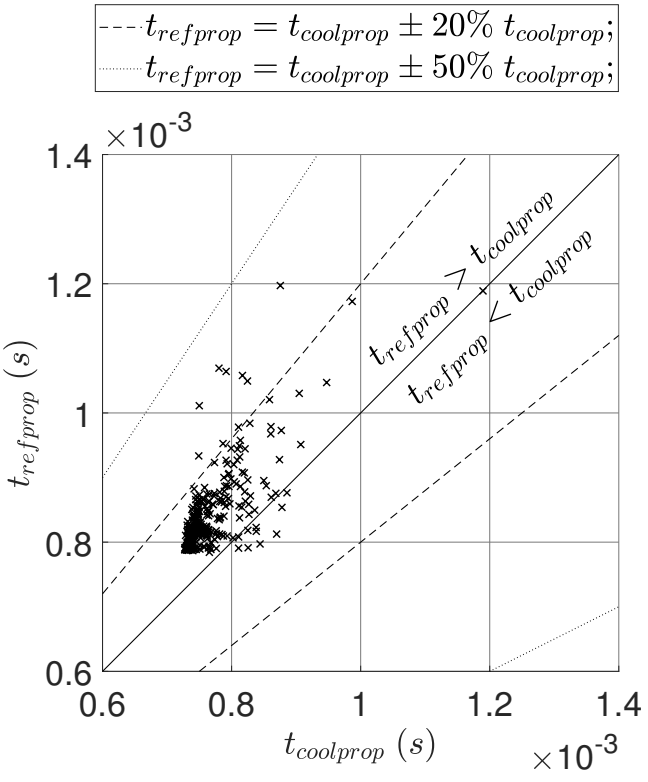

Figure 3.19
Computation time comparison: refprop vs coolprop.
Coolprop is faster than refprop. Even if the computationtime reduction in a single cycle is very small, when these functions are called in the various loops this gain increases markedly.

Chapter 4

Results and validation

Model validation is the last step required to obtain a tool able to make reliable predictions. This is possible when the model, taking into account the same inputs of the real phenomenon, gives some outputs that are similar to the real ones measured experimentally. Besides, it is necessary that the modeler know the effects of the assumptions on the solution and have a certain control on the process. When these conditions are satisfied, the model is validated and can be applied with confidence.

In this chapter the models of the components (Section 4.1) and that of the plant (Section 4.2) are validated. Then, some results and considerations about the circuit underlined by the model (Section 4.3), are presented. Lastly, some ideas for future developments (Section 4.5) are suggested.

Section 4.1

Component validation

4.1.1 | Compressor

The experimental data are compared with the calculated outputs. The results show that the model works very well for m_r (Figure 4.1) and T_{out} (Figure 4.2). Instead, P_{el} is always underestimated (Figure 4.3).

This suggest the employment of one or more corrective coefficients which can be introduced to improve the precision. Fixed F, ΔT_{sh}, $T_{c,sat}$ and $T_{e,sat}$, the model determines the outputs thanks to a polynomial function (3.1). The first

Corrective coefficient

idea is to evaluate a coefficient that multiplies the value of P_{el} estimated by the respective equation. The coefficient is determined through the fmincon solver of Matlab: it finds the set of coefficients which minimize a function. If this is dependent on the error, fmincon returns the optimal coefficient that minimize the deviation between the experimental and the calculated data. Setting correctly the problem for the compressor, fmincon finds the corrective coefficient which multiplies (3.7), as shown in (4.1)

$$P_{el} = 1.05\ \Phi\left(T_{e,sat},\ T_{c,sat},\ F\right) \tag{4.1}$$

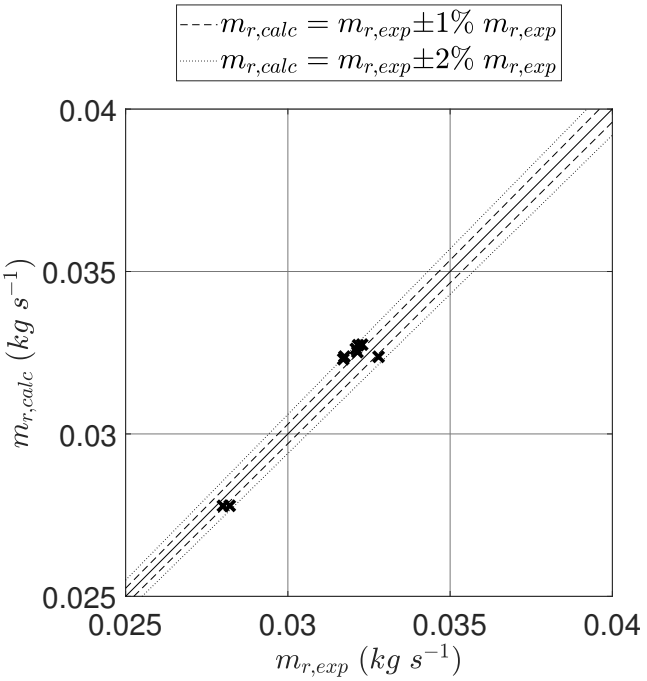

Figure 4.1
Validation of the compressor model: m_r.

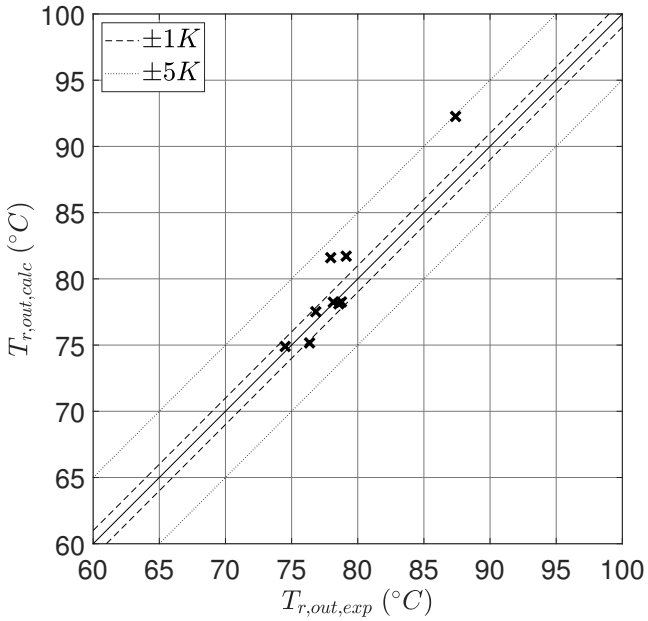

Figure 4.2
Validation of the compressor model: T_{out}.

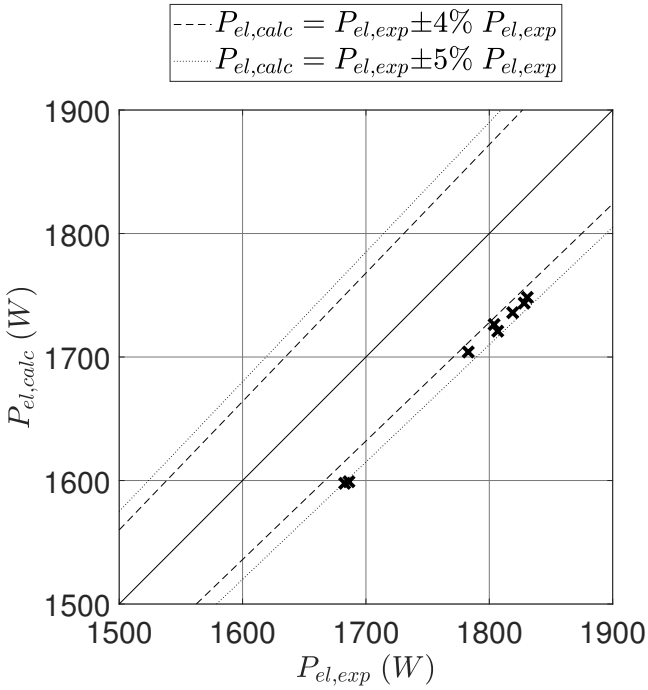

Figure 4.3
Validation of the compressor model: P_{el}.
The calculated data are smaller than experimental results at every point.

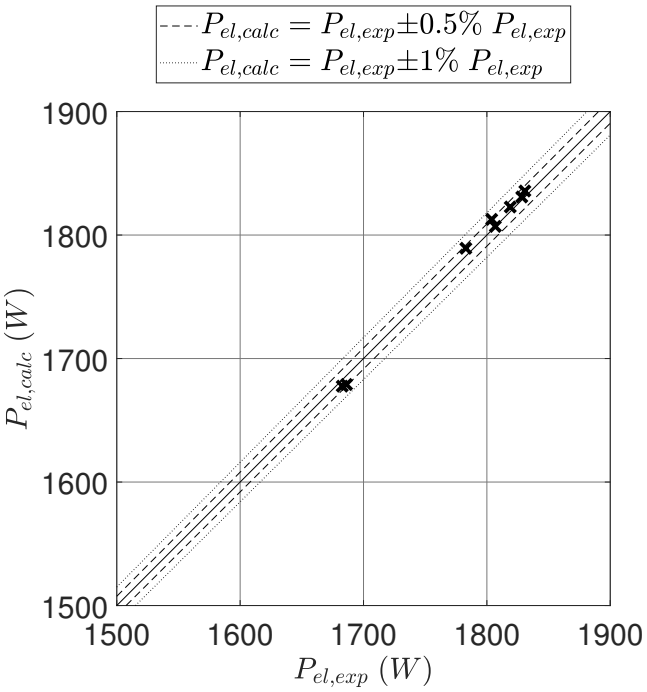

Figure 4.4
Validation of the compressor model: P_{el} with correction coefficient.
After the optimization through the coefficient the calculated P_{el} is more accurate.

4.1.2 | Condenser

The results of the symbolic and the iterative models of the condenser are compared with the experimental data (Figure 4.5, Figure 4.6, Figure 4.7). In all the models, $T_{r,v}$ is overestimated because all of them are based on the assumption that the pressure drop can be neglected: the pressure drop, in the real condenser, decreases the glide temperature and is responsible for the inconsistencies in $T_{r,v}$. $T_{r,out}$ is always overrated: this can be due to the small value of the HTCs given by the Martin correlation. This is expected from the results presented in Section 2.3, where the plots have shown that the Martin correlation is very conservative in terms of Nu.

Corrective coefficients

To increase the precision of the models some corrective coefficients are introduced as multiplier of the HTCs. So the generic $\alpha_{j,i}$ (with $i = sc,\ tp,\ sh$, $j = r,\ f$) is modified by the corrective coefficient $C_{j,i}$ (4.2).

$$\alpha_{j,i} = C_{j,i}\ \alpha_{j,i} \tag{4.2}$$

Optimization of the symbolic model

For the symbolic model these coefficients are determined thanks to the `fmincon` solver of Matlab in a process similar to what has been presented for the compressor. Operating a least-square minimization between the experimental and the calculated temperatures, following an optimization process, the correction coefficients for the symbolic model are found (Figure 4.8).

Optimization of the iterative model

This approach could be used also for the corrective coefficients of the iterative method. Unfortunately, due to the presence of the iterative cycles, the `fmincon` solver is inefficient. So, to obtain an improvement in the iterative model, as first step, the coefficients obtained for the symbolic model are employed in the iterative method (Figure 4.9).

This is not the best way to obtain the appropriate coefficients for the iterative method. For this reason, a script is written in Matlab to find iteratively the best set of coefficients which ensure the minimal deviation between the experimental and calculated temperatures. Several sets of coefficients are generated through the permutation of some scalar values (the corrective coefficients values) and these are used in the condenser model that returns the error function

(Code 4.1).

Code 4.1

The construction of the array of coefficient through the permutation of an array of values.

In this example 5^3 arrays of 3 elements are constructed through the 5 values specified in the values array. The generic i-th row is passed to the condenser model which determines the error fucntion for those coefficients.

```
values=[0.8 0.9 1 1.1 1.2];
array_coeff=permn(values,3)
array_coeff =
    0.8000    0.8000    0.8000
    0.8000    0.8000    0.9000
    0.8000    0.8000    1.0000
    0.8000    0.8000    1.1000
    0.8000    0.8000    1.2000
    0.8000    0.9000    0.8000
    0.8000    0.9000    0.9000
    0.8000    0.9000    1.0000
    0.8000    0.9000    1.1000
    0.8000    0.9000    1.2000
    0.8000    1.0000    0.8000
    0.8000    1.0000    0.9000
    0.8000    1.0000    1.0000
    0.8000    1.0000    1.1000
    0.8000    1.0000    1.2000
    0.8000    1.1000    0.8000
    0.8000    1.1000    0.9000
    0.8000    1.1000    1.0000
    0.8000    1.1000    1.1000
    0.8000    1.1000    1.2000
    0.8000    1.2000    0.8000
    0.8000    1.2000    0.9000
    0.8000    1.2000    1.0000
    0.8000    1.2000    1.1000
    0.8000    1.2000    1.2000
    0.9000    0.8000    0.8000
    0.9000    0.8000    0.9000
    0.9000    0.8000    1.0000
    0.9000    0.8000    1.1000
    0.9000    0.8000    1.2000
    0.9000    0.9000    0.8000
    0.9000    0.9000    0.9000
    0.9000    0.9000    1.0000
    0.9000    0.9000    1.1000
    0.9000    0.9000    1.2000
    0.9000    1.0000    0.8000
    0.9000    1.0000    0.9000
    0.9000    1.0000    1.0000
    0.9000    1.0000    1.1000
    0.9000    1.0000    1.2000
    0.9000    1.1000    0.8000
    0.9000    1.1000    0.9000
    0.9000    1.1000    1.0000
    0.9000    1.1000    1.1000
    0.9000    1.1000    1.2000
    0.9000    1.2000    0.8000
    0.9000    1.2000    0.9000
    0.9000    1.2000    1.0000
    0.9000    1.2000    1.1000
    0.9000    1.2000    1.2000
    1.0000    0.8000    0.8000
    1.0000    0.8000    0.9000
    1.0000    0.8000    1.0000
    1.0000    0.8000    1.1000
    1.0000    0.8000    1.2000
    1.0000    0.9000    0.8000
    1.0000    0.9000    0.9000
    1.0000    0.9000    1.0000
    1.0000    0.9000    1.1000
    1.0000    0.9000    1.2000
    1.0000    1.0000    0.8000
    1.0000    1.0000    0.9000
    1.0000    1.0000    1.0000
    1.0000    1.0000    1.1000
    1.0000    1.0000    1.2000
    1.0000    1.1000    0.8000
    1.0000    1.1000    0.9000
    1.0000    1.1000    1.0000
    1.0000    1.1000    1.1000
    1.0000    1.1000    1.2000
    1.0000    1.2000    0.8000
    1.0000    1.2000    0.9000
    1.0000    1.2000    1.0000
    1.0000    1.2000    1.1000
    1.0000    1.2000    1.2000
    1.1000    0.8000    0.8000
    1.1000    0.8000    0.9000
```

```
81   1.1000   0.8000   1.0000
82   1.1000   0.8000   1.1000
83   1.1000   0.8000   1.2000
84   1.1000   0.9000   0.8000
85   1.1000   0.9000   0.9000
86   1.1000   0.9000   1.0000
87   1.1000   0.9000   1.1000
88   1.1000   0.9000   1.2000
89   1.1000   1.0000   0.8000
90   1.1000   1.0000   0.9000
91   1.1000   1.0000   1.0000
92   1.1000   1.0000   1.1000
93   1.1000   1.0000   1.2000
94   1.1000   1.1000   0.8000
95   1.1000   1.1000   0.9000
96   1.1000   1.1000   1.0000
97   1.1000   1.1000   1.1000
98   1.1000   1.1000   1.2000
99   1.1000   1.2000   0.8000
100  1.1000   1.2000   0.9000
101  1.1000   1.2000   1.0000
102  1.1000   1.2000   1.1000
103  1.1000   1.2000   1.2000
104  1.2000   0.8000   0.8000
105  1.2000   0.8000   0.9000
106  1.2000   0.8000   1.0000
107  1.2000   0.8000   1.1000
108  1.2000   0.8000   1.2000
109  1.2000   0.9000   0.8000
110  1.2000   0.9000   0.9000
111  1.2000   0.9000   1.0000
112  1.2000   0.9000   1.1000
113  1.2000   0.9000   1.2000
114  1.2000   1.0000   0.8000
115  1.2000   1.0000   0.9000
116  1.2000   1.0000   1.0000
117  1.2000   1.0000   1.1000
118  1.2000   1.0000   1.2000
119  1.2000   1.1000   0.8000
120  1.2000   1.1000   0.9000
121  1.2000   1.1000   1.0000
122  1.2000   1.1000   1.1000
123  1.2000   1.1000   1.2000
124  1.2000   1.2000   0.8000
125  1.2000   1.2000   0.9000
126  1.2000   1.2000   1.0000
127  1.2000   1.2000   1.1000
128  1.2000   1.2000   1.2000
```

The script finds then the minimum values of the function error and saves the corresponding array of coefficients. Toggling the range of the scalar values and decreasing it progressively, the coefficients are refined. Through this procedure, the best array of coefficients is chosen considering also what the correlation analysis shows, in order to have some values of the coefficients that can be justified by the trend of the correlation used. The iterative model is now tested with the values obtained (Figure 4.10).

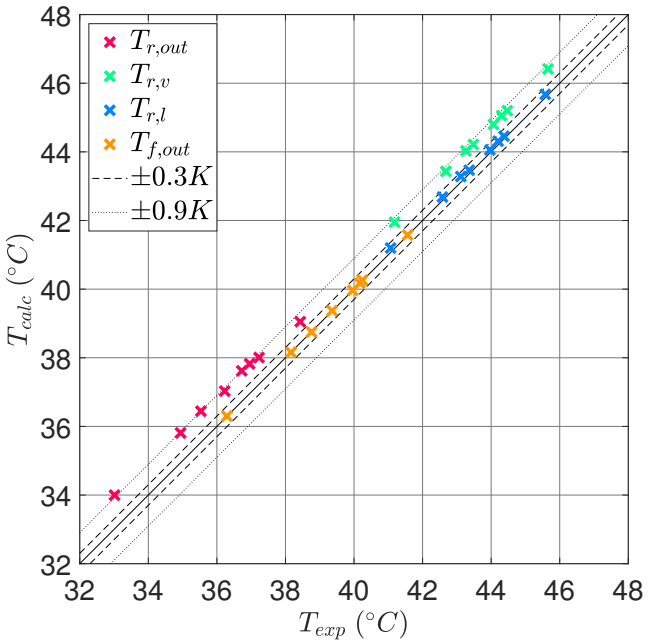

Figure 4.5
Validation of the symbolic condenser model.
The results are very accurate. $T_{r,out}$ is overestimated by about 0.9 K.

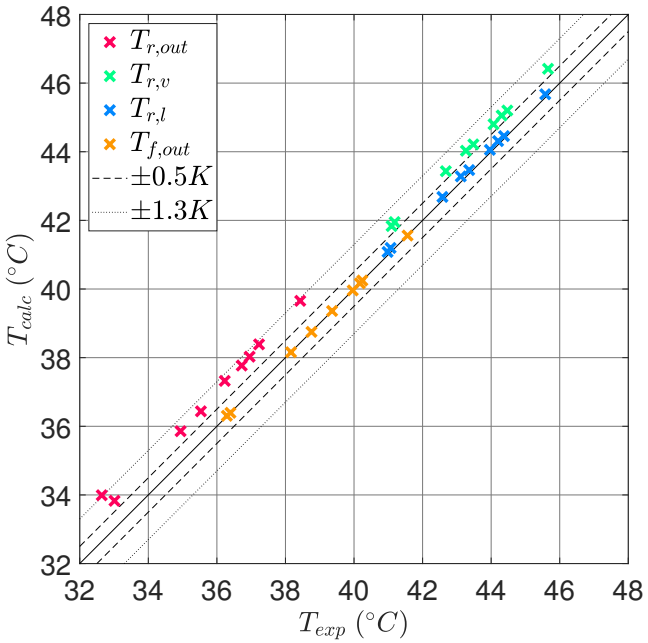

Figure 4.6
Validation of the first iterative condenser model.
The deviation for $T_{r,out}$ is larger than for the symbolic model, but, it is still acceptable.

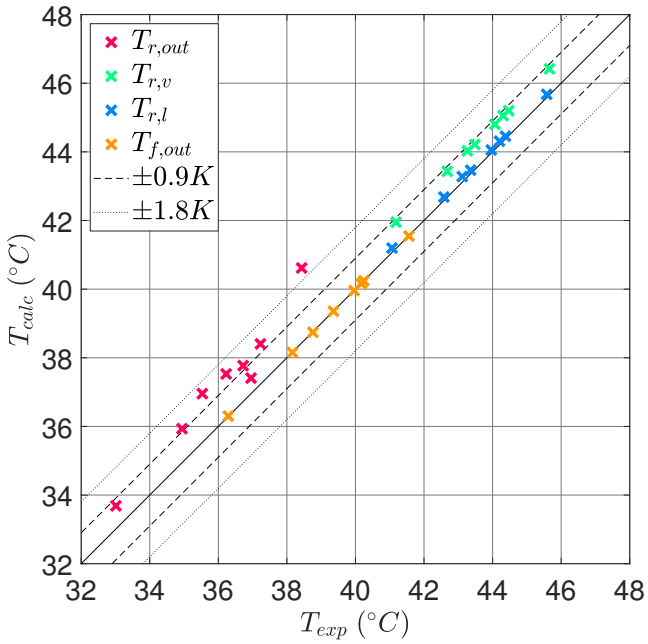

Figure 4.7
Validation of the second iterative condenser model.
In this case, the deviation is more significant, especially for $T_{r,out}$.

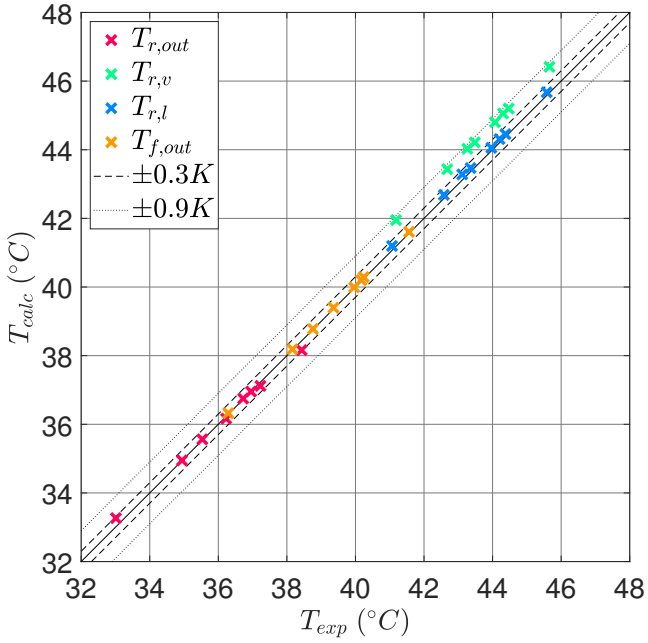

Figure 4.8
Validation of the symbolic optimized condenser model.
There is an important improvement in $T_{r,out}$ determination: the deviation is contained in a range of about $\pm 0.3\ K$.

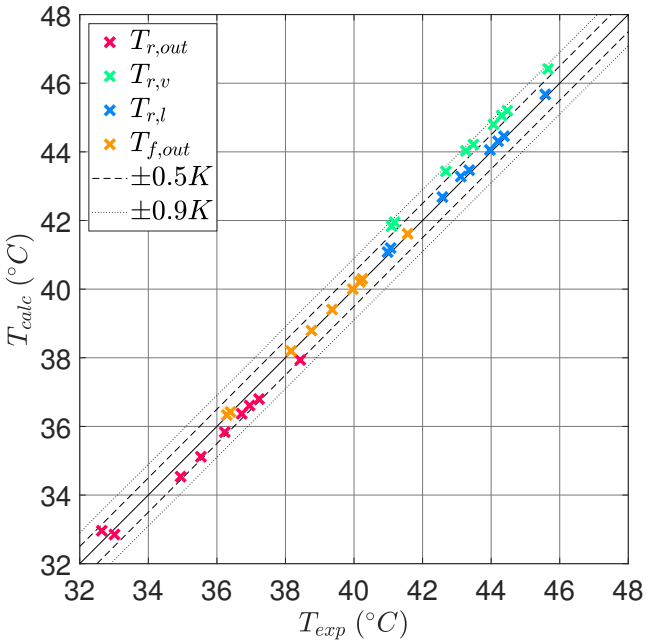

Figure 4.9
Validation of the first iterative condenser model optimized through the symbolic one.
The results given by the model are fairly more accurate than those of the same model without coefficients, but could be improved.

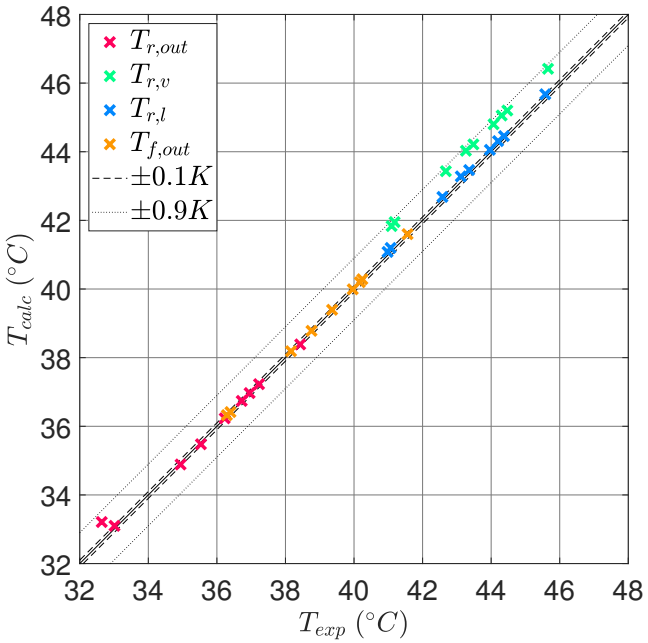

Figure 4.10
Validation of the first iterative condenser model.
The optimization process invented for the iterative model gives some interesting results. The deviation for $T_{r,out}$ is now often under $\pm 0.1\ K$.

4.1.3 | Evaporator

The results of the symbolic and iterative methods of the evaporator are compared with the experimental data (Figure 4.11, Figure 4.12).

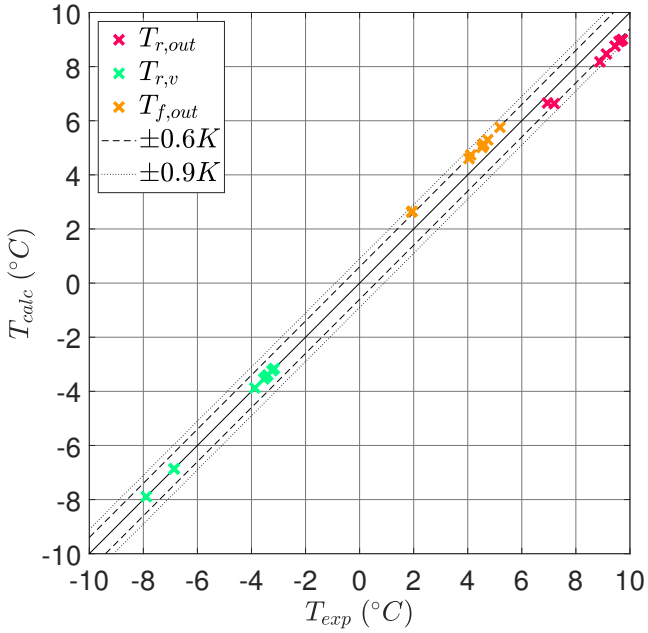

Figure 4.11
Validation of the symbolic evaporator model.
The calculated temperatures are very similar to the experimental ones.

Optimized models

As done for the condenser, also for the evaporator the symbolic (Figure 4.13) and the iterative model can be optimized.

Pressure drop model

The model which takes into account the pressure drop is the less accurate one (Figure 4.14). But after the optimization procedure, it assures very interesting performances (Figure 4.15). Also in this case the coefficients given by this procedure are justified by the analysis on the correlations previously presented.

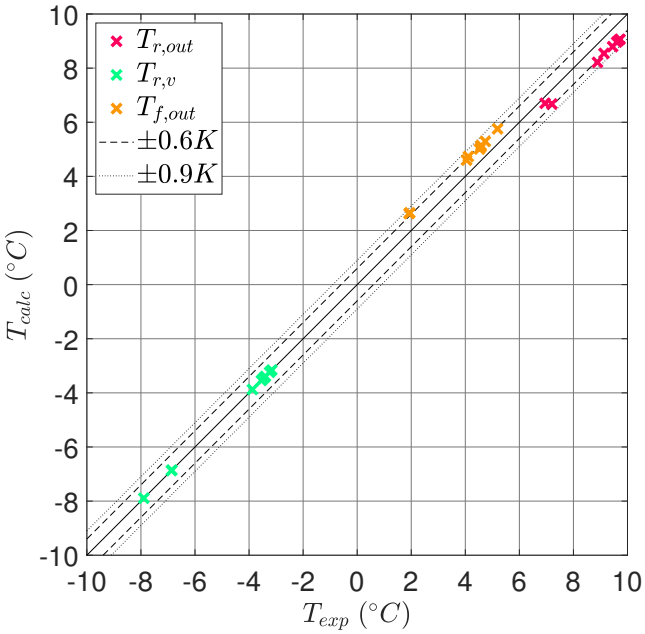

Figure 4.12
Validation of the iterative evaporator model.
Even if the results for the $T_{r,out}$ are very interesting, this temperature is always underestimated because the influence of the pressure drop is not considered.

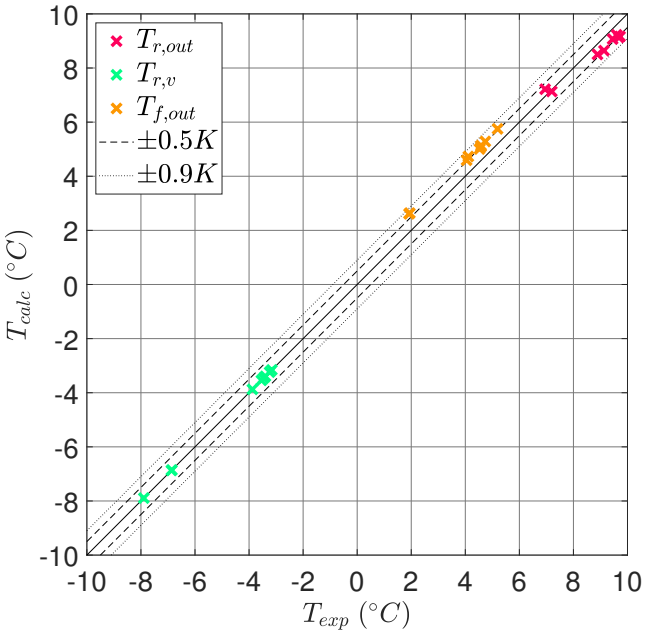

Figure 4.13
Validation of the optimized symbolic evaporator model.
There is an improvement in the calculated temperatures with respect to the model without coefficients.

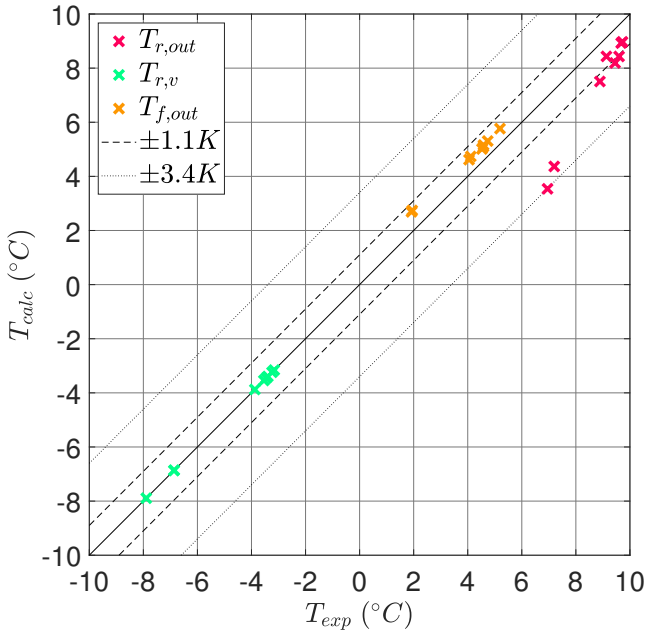

Figure 4.14
Validation of the iterative evaporator model with pressure drop.
For some points of work, the deviation between the calculated and the experimental $T_{r,out}$ is higher than 3 K.

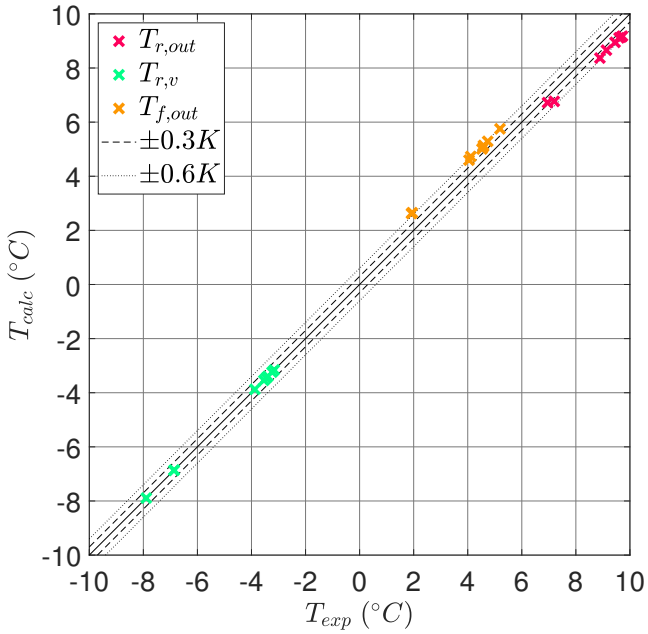

Figure 4.15
Validation of the optimized iterative evaporator model with pressure drop.
With the corrective coefficients the deviation is under 0.3 K.

Section 4.2

Machine validation

The model of the machine is made of two blocks: the first estimates the maximum condensation pressure, the second finds the solution. The former block is validated first (Figure 4.16): in this case it is important that the calculated condensation pressure be always larger than the experimental one, because the second block decreases this maximum value in order to solve the model of the VCRS.

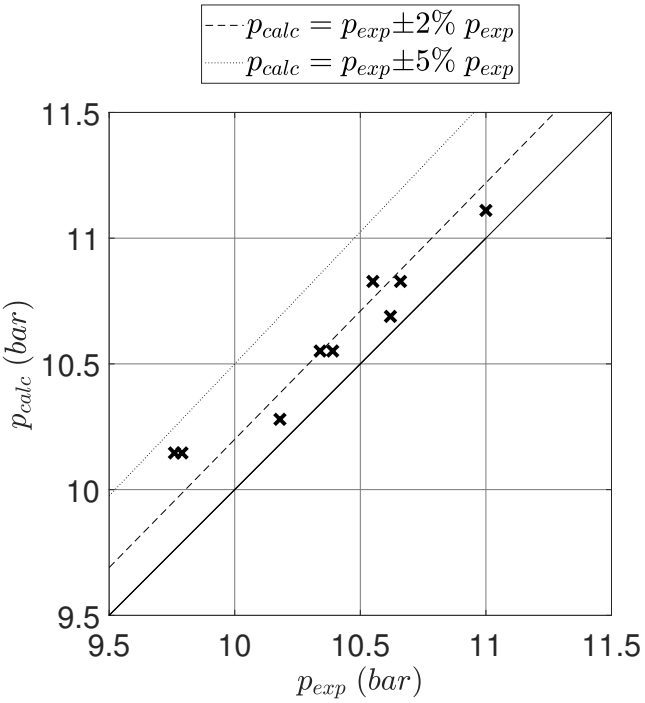

Figure 4.16
Validation of the first iterative block of the global model of the machine: p.

Now themodel of the whole machine can be validated. Temperatures (Figure 4.17), pressures (Figure 4.18), degrees of superheat subcooling (Figure 4.19) and mass flow rates (Figure 4.20) given by the model are compared with the experimental data.

Some correction coefficients could be used to reach higher precision, but the accuracy of the results found does not justify this approach. Besides, in this way, a global model depending on the models of the components which have been optimized individually is developed.

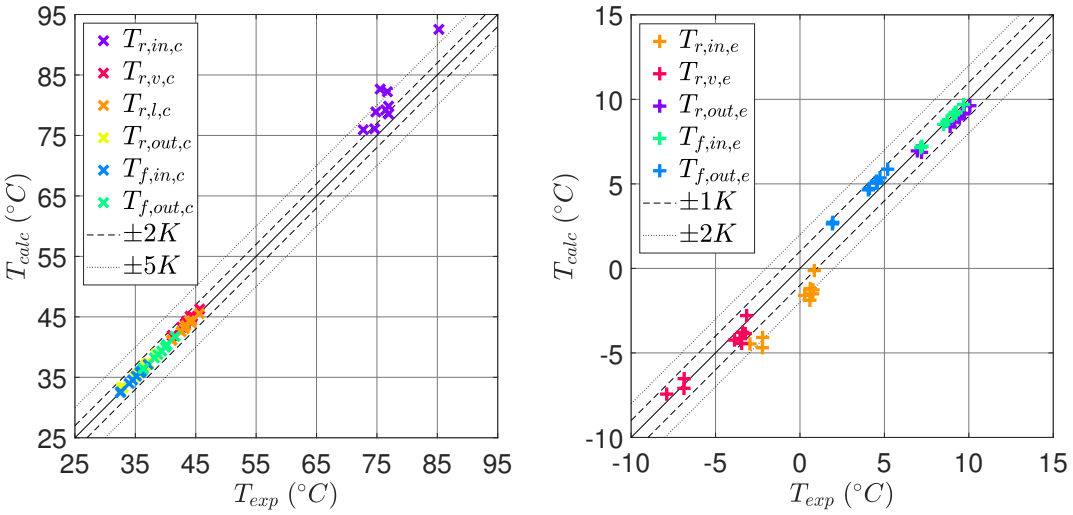

Figure 4.17

Validation of global model of the machine: T.
Only $T_{r,in,c}$ differs slightly from the experimental data, but in all the other cases, the deviation between the experimental and the calculated data is moslty under $1K$, i.e. within measurement uncertainty.

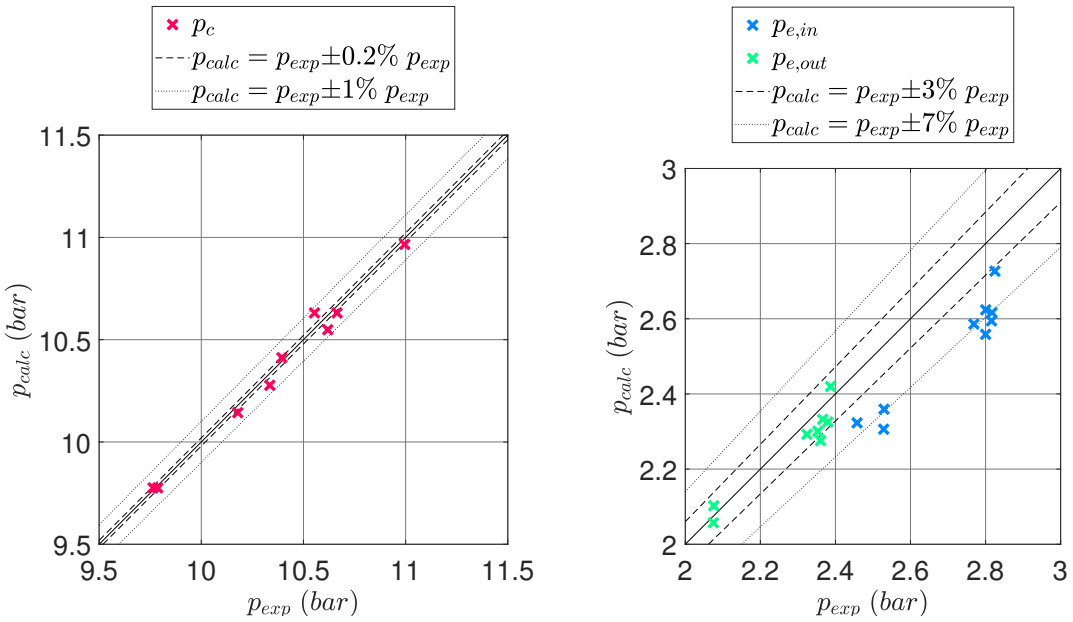

Figure 4.18

Validation of global model of the machine: p.
The pressure at the evaporator inlet is always underrated but this deviation from the experimental data is below 10%. p_c and $p_{e,out}$ are very accurate and this is important in order to compute the correct quantities in the model of the compressor.

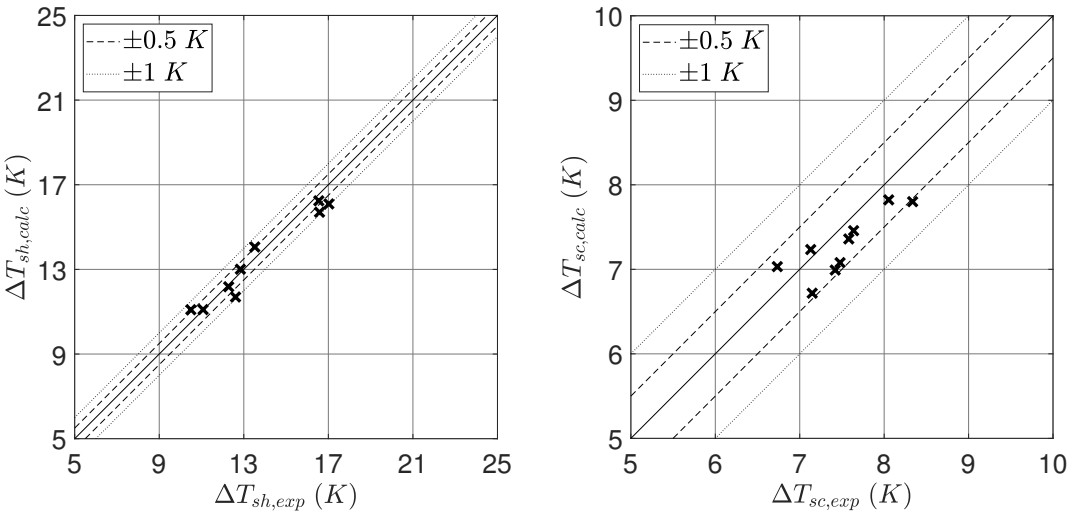

Figure 4.19
Validation of global model of the machine: ΔT.
This values depends on the tolerances set before the execution of the script. In this example $\tau_{sc} = 1$ and $\tau_{sh} = 1$.

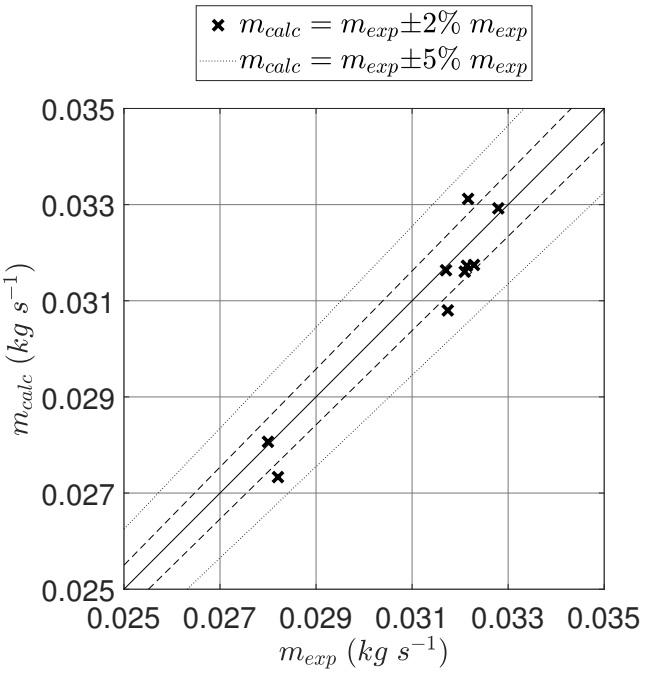

Figure 4.20
Validation of global model of the machine: m.
Comparing this plot with the same results from the model of the compressor it is evident that implementation in the whole model is responsible for an increase in the deviation between the predicted and the experimental data, yet the accuracy is still acceptable.

Section 4.3

Application of the models

The models could now be employed to investigate the characteristics of a plant. For example, fixing the operation conditions, it is possible to plot and analyse the $T-Q$ diagrams of the condenser (Figure 4.21) and the evaporator (Figure 4.22), the $\log p - h$ diagram of the cycle (Figure 4.23), the energy transfer rate in the machine (Figure 4.24), the coefficients of performances (Figure 4.25), the exergetic efficiency in the components (Figure 4.26) and in the machine (Figure 4.27).

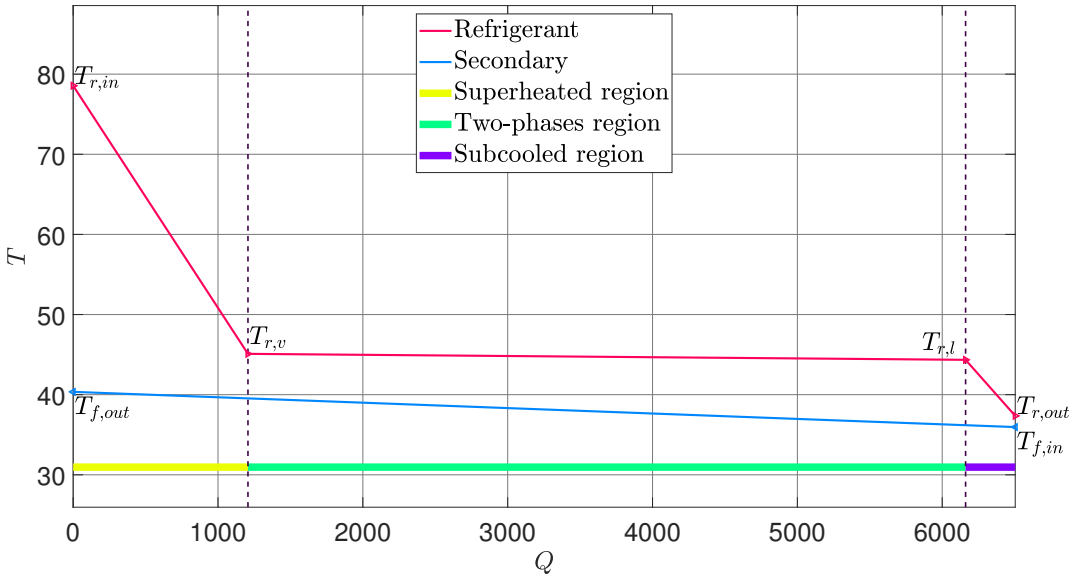

Figure 4.21

Global model of the machine: condenser $T-Q$ diagram.
A significant part of heat is transferred in the two-phase zone, where conditions are most favourable. It is reasonable to expect high exergetic efficiency for this component, also because the temperature drop at the outlet is really small.

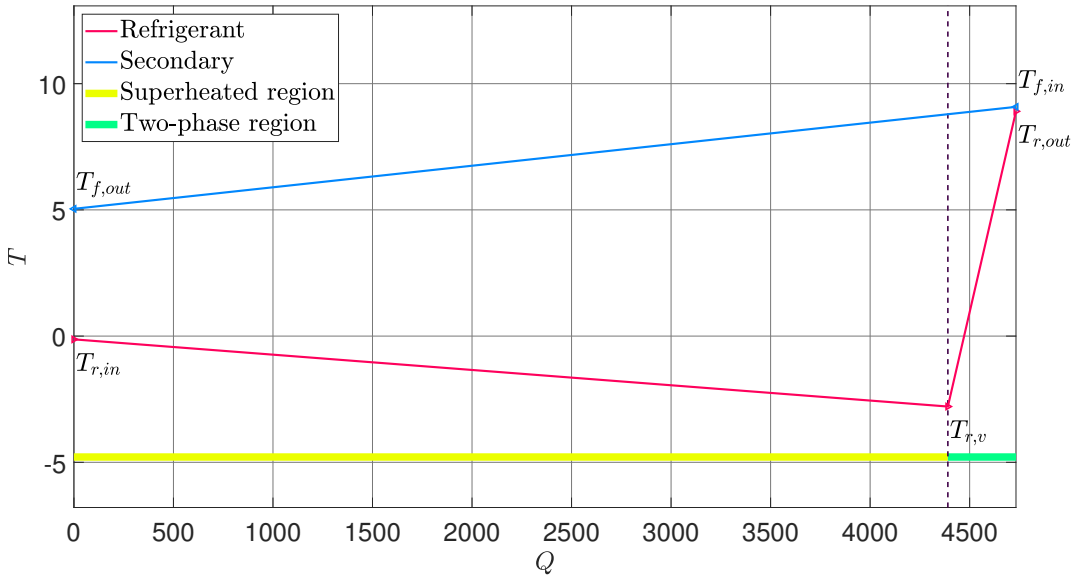

Figure 4.22

Global model of the machine: evaporator $T - Q$ diagram.

In the two-phase zone of the evaporator, the refrigerant temperature decreases because of the effect of the pressure drop. The same consideration about the condenser can be extended to the evaporator.

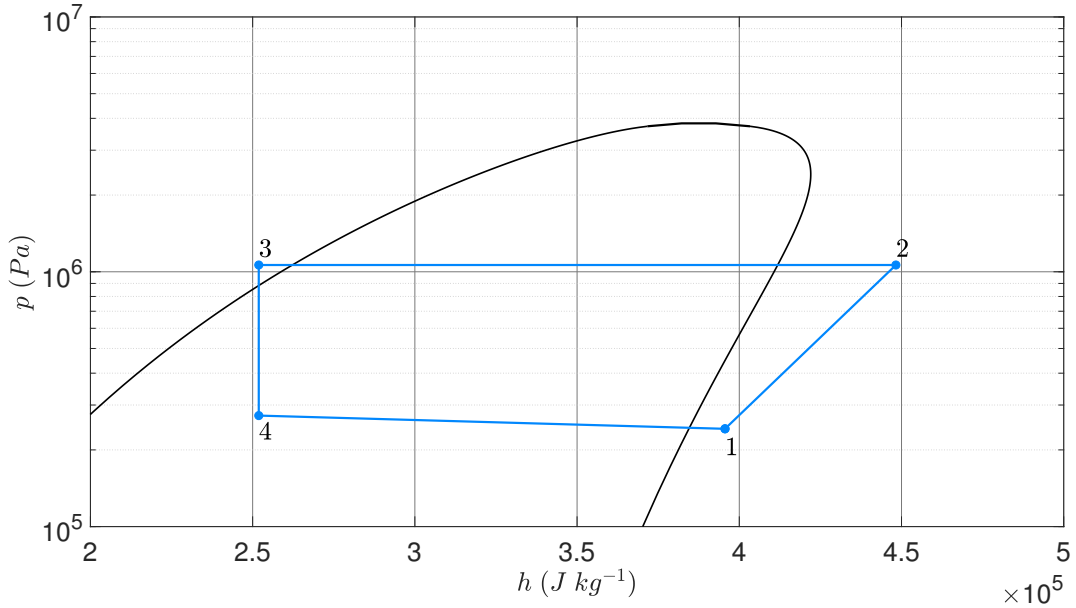

Figure 4.23

Global model of the machine: $\log p - h$ diagram.

The thermodynamic transformations are crystal-clear: with respect to an ideal cycle, the compression is not isoentropic and the pressure in the evaporator is not constant.

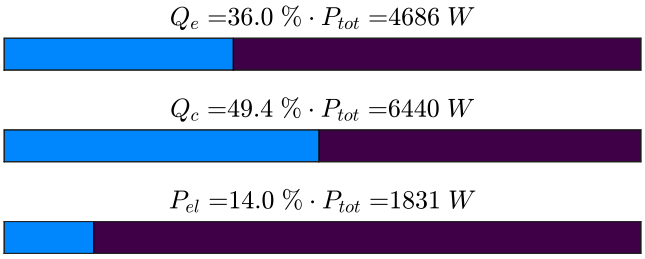

Figure 4.24
Global model of the machine: Q balance.
Due to the tolerances used in the various models, the first law of the thermodynamics is not exactly respected.

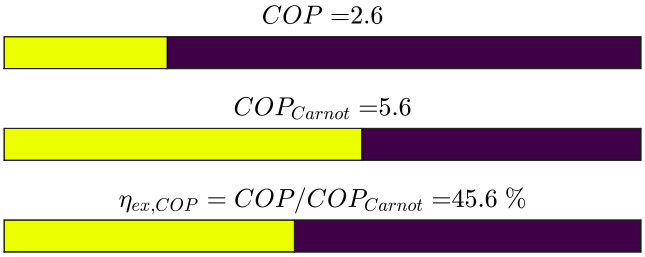

Figure 4.25
Global model of the machine: COP.
COP_{Carnot} is the COP of a Carnot cycle operating between the saturation temperatures of this point of work.

Figure 4.26
Global model of the machine: η_{ex} in the components.
The most critical component in terms of exergy destruction is the compressor.

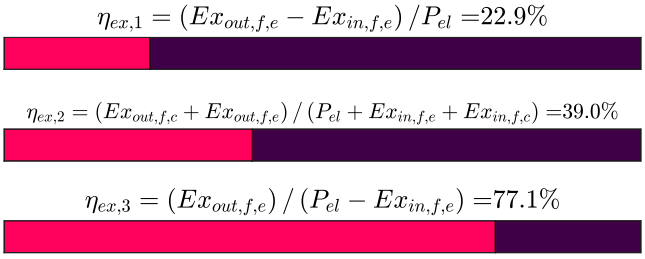

Figure 4.27
Global model of the machine: η_{ex} in the machine.
η_{ex} for the machine can be defined in several ways, but through the model its estimation is really simple.

Through the models of the heat exchangers is possible to plot some $T - \zeta_i$ diagrams (Figure 4.28), that express the connection between the extension of the $i - th$ region of the heat exchanger as a function of the working pressure. In the examples proposed (Figure 4.29) (Figure 4.30), the plots are evaluated in the experimental working points, but other tests can be carried out varying of a constant step the saturation pressure of condensation and boiling.

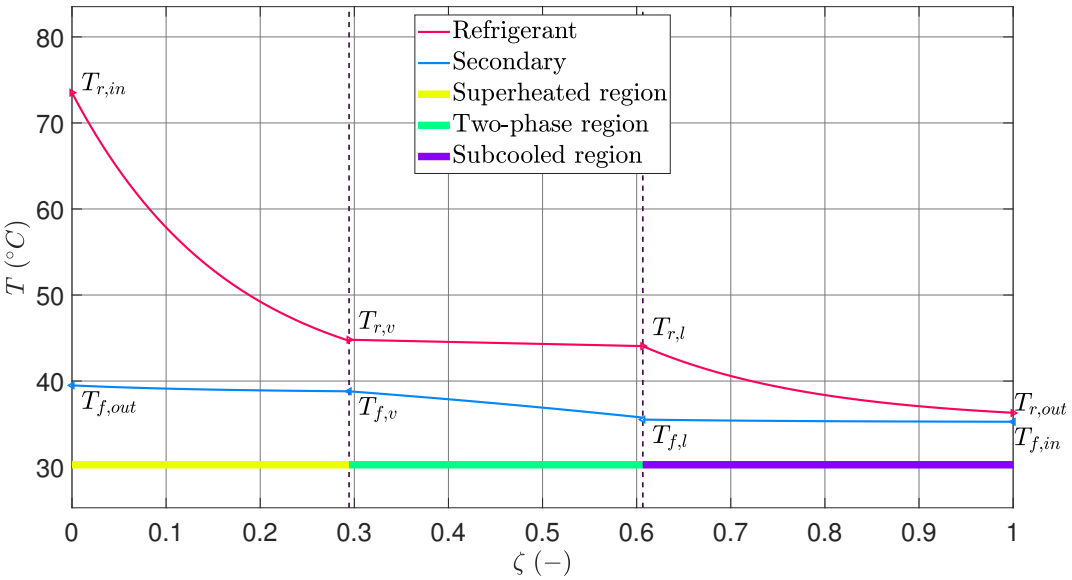

Figure 4.28
$T - \zeta_i$ diagram for the condenser.
Fixed a point of work is possible to scope the evolution of the fluid temperatures flowing in the condenser.

The model can be also employed to find the best operating condition of the plant: for example, when the secondary circuit of the evaporator is setted to ensure a small mass flow rate of water[1] the model shows that the plant works more efficiently if the heat transfer rate that has to be removed from the cold sink is high (Figure 4.31).

[1]The experimental data show that for low values of p_c, $m_{f,e}$ is about 0.24 $kg\ s^{-1}$, while for high values of p_c, $m_{f,e}$ is about $0.28; kg\ s^{-1}$.

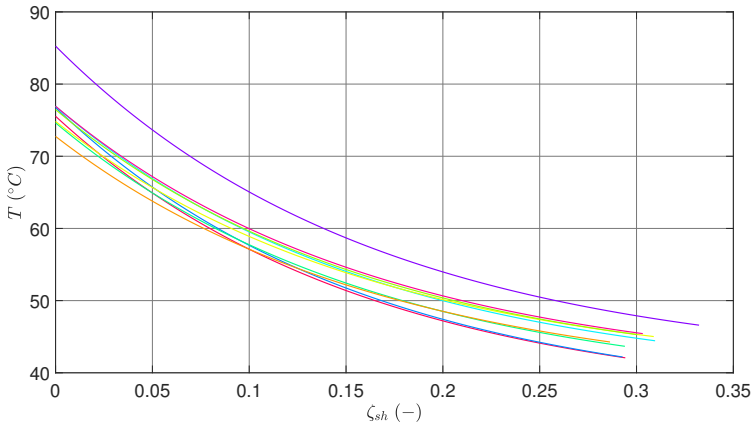

(a) $T - \zeta_{sh}$ *diagram*

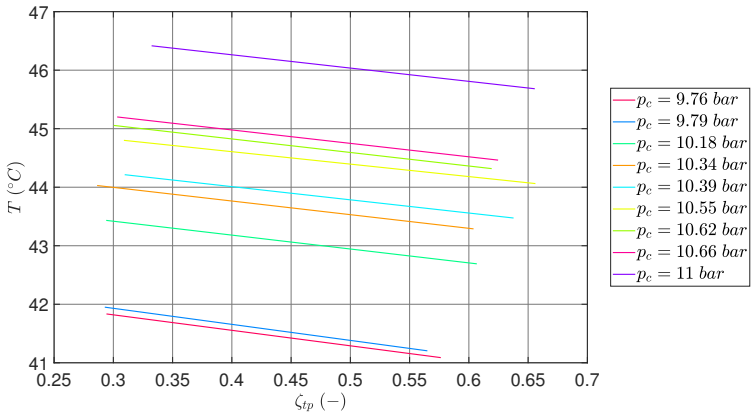

(b) $T - \zeta_{tp}$ *diagram*

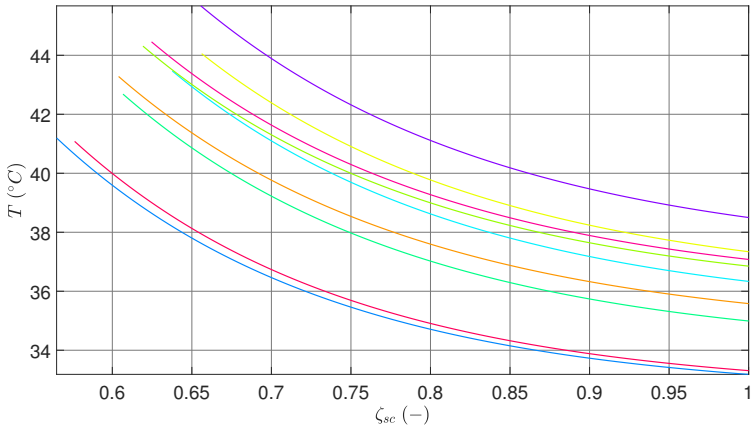

(c) $T - \zeta_{sc}$ *diagram*

Figure 4.29

$T - \zeta_i$ diagram for the condenser.

The plots underline a certain correlation between the condensation pressure and the extension of the superheated and the subcooled zones: when p_c increases, ζ_{sh} increases too while ζ_{sc} decreases and vice versa. The extension of the two-phase zone is quite constant.

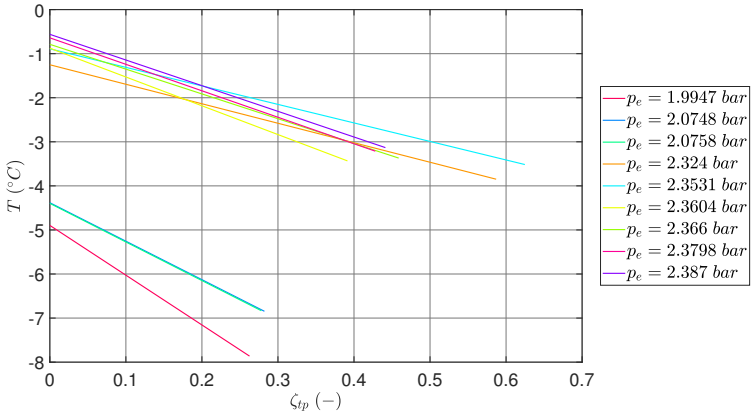

(a) $T - \zeta_{tp}$ *diagram*

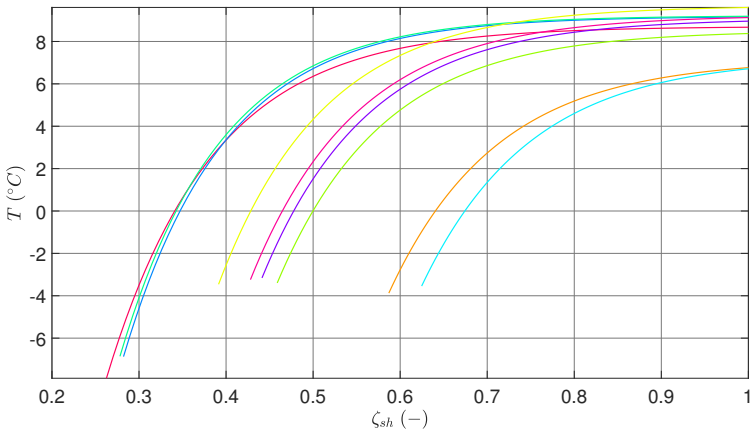

(b) $T - \zeta_{sh}$ *diagram*

Figure 4.30
$T - \zeta_i$ diagram for the evaporator.
In this case there is no clear relation between the boiling pressure and the extension of the two zones.

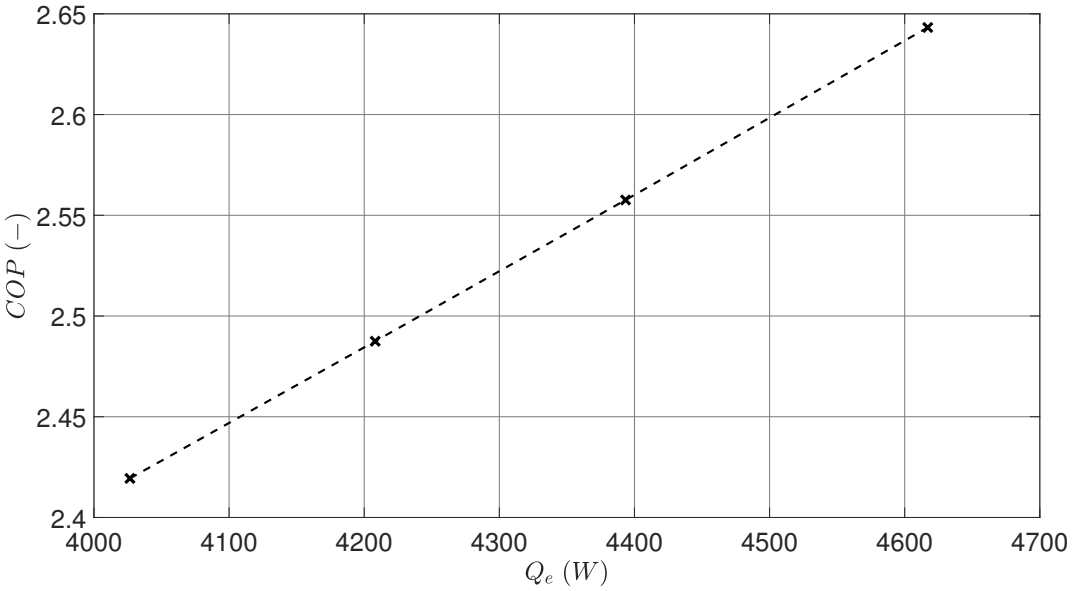

(a) *COP* trend

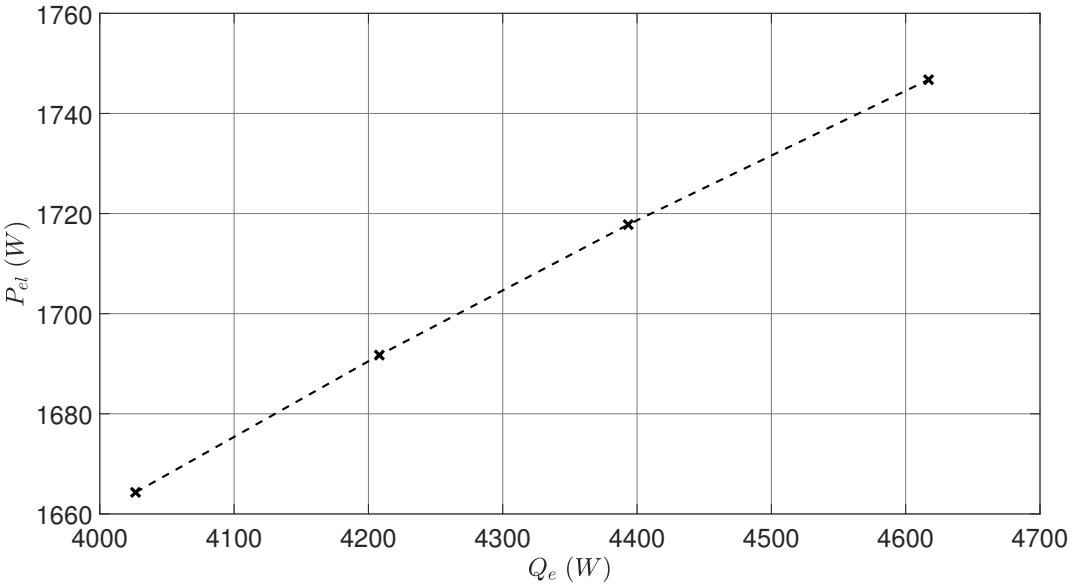

(b) P_{el} trend

Figure 4.31
Efficiency analysis: part one.
Even if the electrical consumption is higher, the machine works more efficiently if Q_e is higher.

Section 4.4

Conclusions

All the models of the components and that of the VCRS have been validated. In the compressor model the error between the predicted and the experimental data is below 2% for the mass flow rate, $5K$ for the discharge temperature and 1% for the electric consumption. The deviation on the temperatures is below $1K$ and $0.6K$ in the condenser and in the evaporator model respectively. In the model of the machine, except for the temperature at the condenser inlet, all the other temperatures deviate a maximum of $2K$. The offset on the condensation pressure is below 1%, whilst for boiling the error varies from 3% for the suction to 7% for the discharge pressure. The accuracy on the degree of superheat and subcooling depends on the tolerance set on the algorithm and in the present case is equal to $1K$. The estimation on the mass flow rate of the refrigerant is accurate to below 5%. The computational cost depends on the operating point selected. The condenser model runs in a few tenths of a second, while the evaporator is a little slower. The model of the machine requires a few seconds instead. The computation time and the accuracy of the results depend on the tolerances set in the criteria of convergence, especially in the model of the machine. An analysis on the performances of the plant shows the best operating conditions in terms of efficiency.

Section 4.5

Future developments

First of all the operative range of the heat exchanger models can be extended. In this work, the condenser processes a refrigerant from superheated vapor, to subcooled liquid and the evaporator takes a two-phase mixture and discharges a superheated vapor. In some particular conditions, at the condenser outlet the refrigerant could be two-phase or the evaporator could discharge a two-phase refrigerant. To model such situations, some heat exchanger model which has different operating zones could be developed. Inserting some toggling criteria for the transition from a model to the other, the machine could be more

complete.

The machine algorithm has been developed in order to be independent of the type of the model of the components: obviously, this suggests that models of different types of compressors and heat exchangers can be developed and replaced in the model of the machine.

This steady-state model could also be used in parallel with a dynamic model in order to verify the accuracy of its results after the development of the transient phenomena. Low computation times are in this case fundamental to satisfy the requirement.

Appendix A

Zeotropic mixtures

Zeotropic mixtures are usually used in combination with a counter-flow PHE in order to increase efficiency. These mixtures are penalized in terms of heat transfer coefficients due to the mass transport phenomenon caused by the difference of concentration between the liquid and the vapor phase.

Refrigerants and environmental impact

The reason for the use of these mixtures is not connected with an improvement of the performance, rather it is related to their small environmental impact. Some detailed studies show that the refrigeration sector is responsible for the 7.8% of greenhouse gas emissions [47]. For this reason, during the last years, international politics, pressed by the scientific data, are encouraging the employment of refrigerant mixtures more environmentally friendly. For example, according to the Montreal protocol, in the next century, the increase of the mean temperature of the atmosphere will be of only 1.5 degrees, instead of 2 degrees, only reducing the use of hydrofluorocarbon like the R134a [48]. For this reason, the R134a, the main refrigerant in terms of global warming [49], which was one of the most common mixtures in recent years is nowadays replaced by new mixtures. The R450a is one of the most interesting contestants as alternative to R134a. Prevention is useful in order to reduce refrigerant emissions. For this reason, there are projects and classes like the Real-Skills Europe, which can help the mechanical engineers and technicians employed in the conditioning and refrigeration sector to learn the specialistic skills for a correct management of the refrigerants in the plants [50].

Some important properties of R134a and R450a are listed in the Table A.1. The $\mathrm{GWP}_{100_{yr}}$ index shows how many times a kilogram of gas is more relevant in the atmosphere warming respect to an equivalent weight of a CO_2 in an interval of one hundred years. The $\mathrm{GWP}_{100_{yr}}$ of the R450a is quite three times smaller than that of the R134a. However, the lower vapor density of R450a

Table A.1
R134a vs R450a: properties comparison [51].

	UoM	*R134a*	*R450a*
Composition		pure R134a	R134a/R1234ze (E)
wt	%	100	42/58
ANSI/ASHRAE safety classification		A1	A1
$GWP_{100_{yr}}$		1300	547
Average molar mass	$kg\ mol^{-1}$	102.03	108.69
Critical temperature	$C°$	101.06	104.47
Critical pressure	Mpa	4.06	3.82
Boiling point at 0.1 MPa	$C°$	-26.36	-23.35
Glide at 0.1 MPa	$C°$	0	0.61
Latent heat of vaporization	$kJ\ kg^{-1}$	198.6	188.8
Liquid density	$kg\ m^{-3}$	1294.8	1259.6
Vapor density	$kg\ m^{-3}$	14.43	13.18
Liquid c_p	$kJ\ kg^{-1}\ K^{-1}$	1.34	1.33
Vapor c_p	$kJ\ kg^{-1}\ K^{-1}$	0.9	0.89
Liquid thermal conductivity	$mW\ m^{-1}\ K^{-1}$	92.01	86.23
Vapor thermal conductivity	$mW\ m^{-1}\ K^{-1}$	11.51	11.70
Liquid viscosity	$\mu Pa\ s$	266.53	264.23
Vapor viscosity	$\mu Pa\ s$	10.73	11.16

implies a decrease of the refrigeration capacity with the same compressor. The Figure A.1 underline in a $\log p - h$ diagram some differences between the two mixtures.

A series of studies investigated the performance of the R450a in the VCRS. Makhnatch, Mota-Babiloni, and Khodabandeh [52] showed that the compression ratio and the discharge temperature of the compressor remain equal using either R450a and R134a; instead, there is a decrease into the mass flow rate and the refrigeration capacity (due to the smaller density). There is also a reduction in electric consumption, but this is not high enough to balance the lower refrigeration load and the COP is slightly penalized. Mota-Babiloni, Navarro-Esbrí, Barragán-Cervera, Molés, and Peris [53] completed some experimental studies on a medium-capacity refrigeration machine with these two refrigerants. They noticed that the COP varies about 1%, while the reduction in the refrigeration capacity is around 6%. Other researchers focussed on more complex plants: for example, Mendoza-Miranda, Mota-Babiloni, Ramírez-Minguela, Muñoz-Carpio, Carrera-Rodríguez, Navarro-Esbrí, and Salazar-Hernández [54] considered a variable speed open reciprocating compressor.

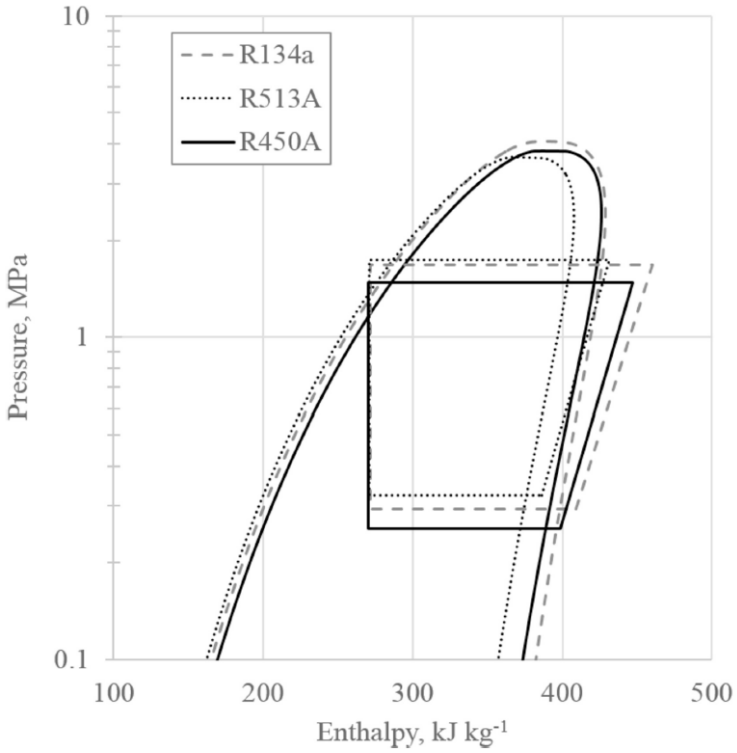

FIGURE A.1
R134a vs R450a: $\log p - h$ *diagram* [51].

Appendix B

The effectiveness NTU method

The effectiveness of a heat exchanger can be defined from knoledge of the maximum possible heat transfer rate. In a counterflow heat exchanger of infinite length, one of the fluids would experience the maximum possible temperature difference: according to the method, this happens to the fluid with the minimum heat capacity rate. If $C_{cold} < C_{hot}$, the coldest fluid would be heated to the inlet temperature of the hot fluid. Similarly, if $C_{hot} < C_{cold}$, the hottest fluid would be cooled to the inlet temperature of the cold fluid. In every case, the maximum possible heat transfer rate can be expressed as a function of the inlet temperatures of the two fluids (B.1).

$$Q_{max} = C_{min} \left(T_{hot,in} - T_{cold,in} \right) \tag{B.1}$$

The effectiveness ε can be now defined as the ratio of the actual heat transfer rate for a heat exchanger to the maximum possible heat transfer rate (B.2).

$$\varepsilon = \frac{Q}{Q_{max}} \tag{B.2}$$

By definition, the effectiveness is non-dimensional and its value is in the range $0 \leq \varepsilon \leq 1$. This method is very useful when the outlet temperatures of the fluids are unknown. Developing the (B.2), the outlet temperature of the cold or hot fluid can be expressed as a function of the effectiveness.

$$\varepsilon = \frac{C_{hot} \left(T_{hot,in} - T_{hot,out} \right)}{C_{min} \left(T_{hot,in} - T_{cold,in} \right)} = \frac{C_{cold} \left(T_{cold,out} - T_{cold,in} \right)}{C_{min} \left(T_{hot,in} - T_{cold,in} \right)} \tag{B.3}$$

This method can be used only if there is another function which gives the value of the effectiveness: for any heat exchanger it can be shown that this function

depends on NTU and γ (B.4).

$$\varepsilon = f\ (NTU,\ \gamma) \tag{B.4}$$

$$NTU = \frac{U\ A}{C_{min}} \tag{B.5}$$

$$\gamma = \frac{C_{min}}{C_{max}} \tag{B.6}$$

The number of transfer units NTU (B.5) and the heat capacity ratio γ (B.6) are non-dimensional parameters that are widely used for heat exchangers' analysis. Several expressions in the form (B.4) have been developed for a variety of heat exchangers [55]. In general for a counterflow heat exchanger ε can be determined by the following equation (B.7).

$$\varepsilon = \frac{1 - e^{-NTU(1-\gamma)}}{1 - \gamma\ e^{-NTU(1-\gamma)}} \tag{B.7}$$

Only when $\gamma = 0$ does the effectiveness have the same value for all the heat exchangers type and configurations (B.8).

$$\varepsilon = 1 - e^{-NTU} \tag{B.8}$$

Note that $\gamma = 0$ when at least one fluid is two-phase [27].

Appendix C

Condensation and boiling: an overview

In this appendix some basic concepts on condensation and boiling are introduced. Thanks to their high HTCs, they are present in many thermal energy conversion processes.

Condensation

According to Theodore [56], the condensation can be classified in:

- surface condensation: vapor is in contact with a cool surface;
- homogeneous condensation: vapor condenses as droplets in the gas phase under the effect of a cooler gas;
- direct contact condensation: vapor is in contact with a cool liquid.

In the most important industrial processes surface condensation is usually employed and can be divided into:

- film condensation: when the heat exchanger surface is clean and uncontaminated, the fluid condensing forms a layer of liquid, called film, which covers the surface and prevents vapor droplets from interacting with it;
- dropwise condensation: when the heat exchanger surface is coated with a substance which inhibits wetting, during condensation, the fluid forms some drops of liquid that can coalesce but cannot stick to the surface, encouraging the contact between them and the vapor particles.

In film condensation, the thermal resistance between the surface and the vapor is related to conduction through the film of liquid condensate on the wall. Approximately, the HTC is inversely proportional to the film thickness [57]. For this reason, to evaluate correctly the convective HTC, it is necessary to

establish in which way the film moves in the heat exchangers. There are mainly two types of film dynamics which are connected with the fundamental force that operates on the fluid:

- gravity controlled condensation: the fluid flows at low velocity and its film is dragged down by gravitational acceleration;
- shear controlled condensation: the fluid high flow rate makes the shear stress of the vapor on the liquid film preponderant over gravity. The fluid dynamic is more complex and usually increase the heat transfer rate.

In real cases, these two phenomena occur together, yet the distinction is necessary to justify the existence of two different types of correlation for the two-phase zone of the condenser, as shown by Longo, Righetti, and Zilio [33].

Boiling

To increase the heat transfer rate in the boiling process, over the years a series of studies aimed at describing the phenomenon have been carried out. The first significant contribution was given by Nukiyama [58]. He found a relation between the heat transfer rate and a quantity called excess temperature T_{ecc}, defined as the difference between the heat exchanger surface temperature and the saturation temperature of the boiling fluid. In the following years some experimental campaigns were conducted, confirming and generalizing what was observed by Nukiyama [58]: independently of the working fluid, the pressure and (within certain bounds) the heat exchanger geometry, the relation between the heat transfer rate and the T_{ecc} has the characteristic shown in Figure C.1.

$\rightarrow A$ Free convection regime: the heat transfer process is dominated by convection.

$A \rightarrow B$ Nucleate regime: some drops of vapor start to form. Due to their lower density they move upward, shaking the liquid particles. In this way the HTC is increased.

$B \rightarrow C$ Nucleate regime: the dimension of the drops is more relevant and the coalescence starts. Their movement is more difficult and this determines an increase in the thermal resistance.

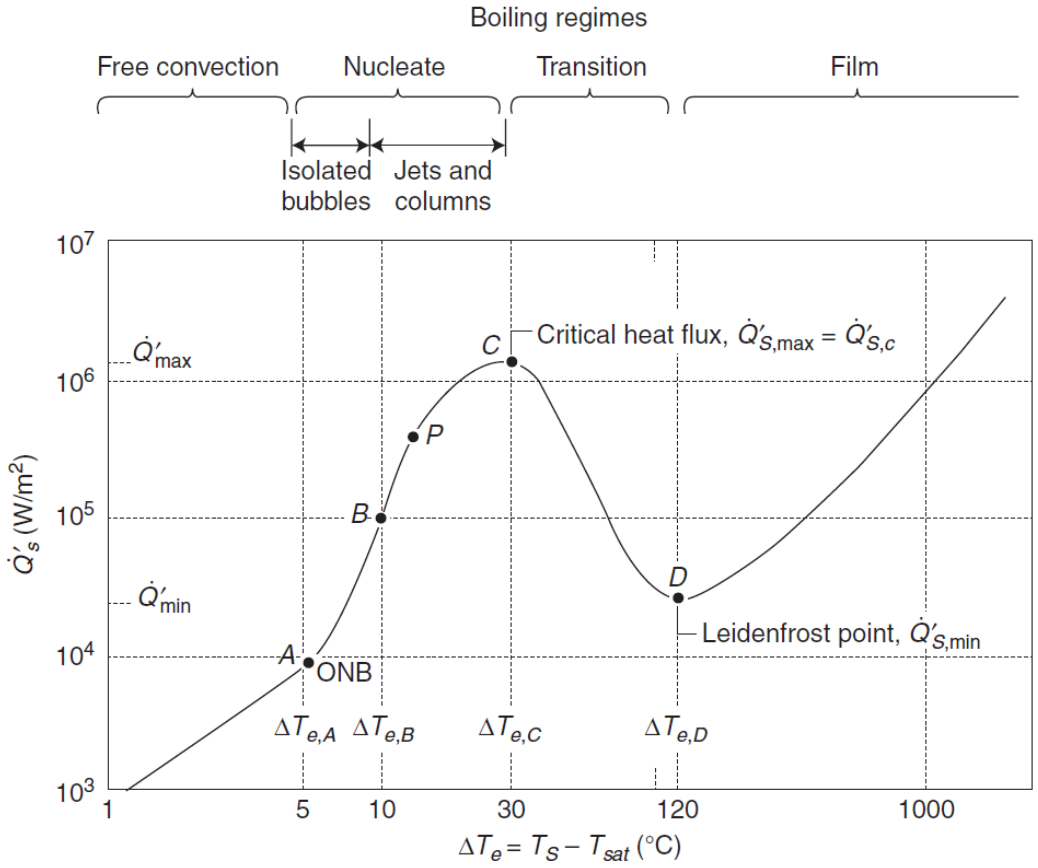

FIGURE C.1
Evolution of the heat transfer rate as a function of T_{ecc} for the water at ambient pressure [56].

C	Point of critical heat flux: the heat transfer rate has a maximum value due to the compensation between the improvement of turbulence caused by the movement of the drops and the adverse effect of coalescence.
$C \rightarrow D$	Transition regime: the coalescence has a preponderant position causing a decrease in the heat transfer rate. When T_{ecc} is more relevant, the heat exchanger surface temperature is higher and with it also the radiative heat transfer process is more important. This effect slows the decrease in the global heat transfer rate.
D	Leidenfrost point: the radiative contribute compensates the effect of the coalescence. The heat transfer rate has a minimum value.

$D \rightarrow$ Film regime: the radiative heat transfer process is dominant with respect to the other processes and the heat transfer rate rapidly increases.

The point of critical heat flux is also called burnout point: exceeding this point is often referred to as the boiling crisis because the heat transfer rate given to the fluid tends do damage or melt most materials. For this reason, the devices usually work with a heat flux that is kept below the burnout point so that the boiling crisis is avoided and the device operates safely [57].

According to the T_{ecc} expected in the evaporator, only the convection and nucleate boiling are possible in the plant studied.

Bibliography

[1] Robert T. Balmer. *Modern Engineering Thermodynamics*. Elsevier, 2011.

[2] a Blue Ribbon Panel of the NSC. *Revolutionizing Engineering Science through Simulation*. report. National Science Foundation, 2006.

[3] M. Willatzen, N.B.O.L Pettit, and L. Ploug-Sørensen. "A general dynamic simulation model for evaporators and condensers in refrigeration. Part I: moving-boundary formulation of two-phase flows with heat exchange". In: *International Journal of Refrigeration* 5 (1998), pp. 398–403.

[4] N.B.O.L Pettit, M. Willatzen, and L. Ploug-Sørensen. "A general dynamic simulation model for evaporators and condensers in refrigeration. Part II: simulation and control of an evaporator". In: *International Journal of Refrigeration* 5 (1998), pp. 404–414.

[5] Thomas L. McKinley and Andrew G. Alleyne. "An advanced nonlinear switched heat exchanger model for vapor compression cycles using the moving-boundary method". In: *International Journal of Refrigeration* 31 (2008), pp. 1253–1264.

[6] S. Yang and J.C. Ordonez. "Integrative thermodynamic optimization of a vapor compression refrigeration system based on dynamic system responses". In: *Applied Thermal Engineering* 135 (2018), pp. 493–503.

[7] Guillermo Bejarano, David Rodríguez, José A. Alfaya, Manuel G. Ortega, and Fernando Castaño. "On identifying steady-state parameters of an experimental mechanical-compression refrigeration plant". In: *Applied Thermal Engineering* 109 (2016), pp. 318–333.

[8] S. Yang, J.C. Ordonez, and J.V.C. Vargas. "Constructal vapor compression refrigeration (VCR) systems design". In: *International Journal of Heat and Mass Transfer* 115 (2017), pp. 754–768.

[9] J.A. Demko. *Superconductors in the Power Grid*. Ed. by Christopher Rey. Woodhead publishing series in energy, 2015. Chap. 8.

[10] Ibrahim Dinçer and Mehmet Kanoğlu. *Refrigeration Systems and Applications*. 2nd ed. Wiley, 2010.

[11] Ken Arnold and Maurice Stewart. *Design of Gas-Handling Systems and Facilities*. 2nd ed. Elsevier Science, 1999.

[12] Kuppan Thulukkanam. *Heat Exchanger Design Handbook*. 2nd ed. Taylor & Francis Group, 2013.

[13] A.R. Trott and T. Welch. *Refrigeration and Air-Conditioning*. 3rd ed. Butterworth-Heinemann, 2000.

[14] G.F. Hundy, A.R. Trott, and T. Welch. *Refrigeration and Air - Conditioning*. 4th ed. Butterworth-Heinemann, 2008.

[15] Wilbert F. Stoecker. *Industrial Refrigeration Handbook*. McGraw-Hill Education, 1998.

[16] Ibrahim Dincer and Marc A. Rosen. *Optimization of Energy Systems*. 1st ed. John Wiley & Sons Ltd, 2017.

[17] John Tomczyk. *Electronic Expansion Valves: The Basics*. 2004. URL: `https://www.achrnews.com/articles/95056-electronic-expansion-valves-the-basics`.

[18] Adrián Mota-Babiloni, Joaquín Navarro-Esbrí, Ángel Barragán-Cervera, Francisco Molés, Bernardo Peris, and Gumersindo Verdú. "Commercial refrigeration - An overview of current status". In: *International Journal of Refrigeration* 57 (2015), pp. 186–196.

[19] Jahar Sarkar. "Ejector enhanced vapor compression refrigeration and heatpumpsystems - A review". In: *Renewable and Sustainable Energy Reviews* 16 (2012), pp. 6647–6659.

[20] H. Kursad Ersoy and Nagihan Bilir Sag. "Preliminary experimental results on the R134a refrigeration system using a two-phase ejector as an expander". In: *International Journal of Refrigeration* 43 (2014), pp. 97–110.

[21] Holger Martin. "A theoretical approach to predict the performance of chevron type plate heat exchangers". In: *Chemical Engineering and Processing* 35 (1996), pp. 301–310.

[22] O. Arsenyeva, P. Kapustenko, L. Tovazhnyanskyy, and Khavin G. "The influence of plate corrugations geometry on plate heat exchanger performance in specified process conditions". In: *Energy* 57 (2013), pp. 201–207.

[23] SWEP, ed. *B10T*. 2019. URL: `https://www.swep.net/products/b10t/`.

[24] SWEP, ed. *B16*. 2019. URL: `https://www.swep.net/products/b16/`.

[25] Frascold, ed. *D3-13.1Y*. 2019. URL: `https://www.frascold.it/en/products/d3_13_1y-2873`.

[26] CAREL, ed. *E2V Proportional electronic expansion valve*. 2019. URL: https://www.carel.com/documents/10191/0/+302235241/880d0dd4-6f56-4454-ae16-fcfd6e49eb2c?version=1.0.

[27] Theodore L. Bergman, Adrienne S. Lavine, Frank P. Incropera, and David P. Dewitt. *Fundamentals of Heat and Mass Transfer*. 7th ed. John Wiley & Sons, 2012.

[28] J.R. García - Cascales, F. Vera - García, J.M. Corberán - Salvador, and J. Gonzálvez - Maciá. "Assessment of boiling and condensation heat transfer correlations in the modelling of plate heat exchangers". In: *International Journal of Refrigeration* 30 (2007), pp. 1029–1041.

[29] A.S. Wanniarachchi, U. Ratnam, B.E. Tilton, and K. Dutta-Roy, eds. *Approximate correlations for chevron-type plate heat exchangers*. Vol. 12. ASME-HTD 314. New York, 1995, pp. 145–152.

[30] B. Bogaert and A. Böles. "Global performance of a prototype brazed plate heat exchanger in a large Reynolds number range". In: *Experimental Heat Transfer* 8 (1995), pp. 293–311.

[31] A. Muley and R. M. Manglik. "Experimental Study of Turbulent Flow Heat Transfer and Pressure Drop in a Plate Heat Exchanger With Chevron Plates". In: *Journal of Heat Transfer* 121 (1999), pp. 110–117.

[32] Radia Eldeeb, Vikrant Aute, and Reinhard Radermacher. "A survey of correlations for heat transfer and pressure drop for evaporation and condensation in plate heat exchangers". In: *International Journal of Refrigeration* 65 (2016), pp. 12–26.

[33] Giovanni A. Longo, Giulia Righetti, and Claudio Zilio. "A new computational procedure for refrigerant condensation inside herringbone-type Brazed Plate Heat Exchangers". In: *International Journal of Heat and Mass Transfer* 82 (2015), pp. 530–536.

[34] W. Nusselt. *Die Oberflächenkondensation des Wasserdampfes*. VDI Zeitschriften, 1916.

[35] Giovanni A. Longo, Simone Mancin, Giulia Righetti, and Claudio Zilio. "A new model for refrigerant boiling inside Brazed Plate Heat Exchangers (BPHEs)". In: *International Journal of Heat and Mass Transfer* 91 (2015), pp. 144–149.

[36] Jianchang Huang, Thomas J. Sheer, and Michael Bailey-McEwan. "Heat transfer and pressure drop in plate heat exchangernrefrigerant evaporators". In: *International Journal of Refrigeration* 35 (2012), pp. 325–335.

[37] Raffaele L. Amalfi, Farzad Vakili-Farahani, and John R. Thome. "Flow boiling and frictional pressure gradients in plate heat exchangers. Part 2: Comparison of literature methods to database and new prediction methods". In: *International Journal of Refrigeration* 61 (2016), pp. 185–203.

[38] Kexin Xu, Robin Smith, and Nam Zhang. "Design and optimization of plate heat exchanger networks". In: *Computer Aided Chemical Engineering* 40 (2017). Proceedings of the 27th European Symposium, pp. 1819–1824.

[39] S.G. Kandlikar and R.K. Shah. "Multipass Plate Heat Exchangers Effectiveness NTU Results and Guidelines for Selecting Pass Arrangements". In: *Journal of Heat Transfer* 111 (1989), pp. 300–313.

[40] S.G. Kandlikar and R.K. Shah. "Asymptotic Effectiveness-NTU Formulas for Multipass Plate Heat Exchangers". In: *Journal of Heat Transfer* 111 (1989), pp. 314–321.

[41] M. Fernández-Torrijos, J.A. Almendros-Ibáñez, C. Sobrino, and D. Santana. "$\varepsilon - NTU$ relationships in parallel-series arrangements: Application to plate and tubular heat exchangers". In: *Applied Thermal Engineering* 99 (2016), pp. 1119–1132.

[42] Jonathan Winkler, Vikrant Aute, and Reinhard Radermacher. "Comprehensive investigation of numerical methods in simulating a steady-state vapor compression system". In: *International Journal of Refrigeration* 31 (2008), pp. 930–942.

[43] Gabriel Zsembinszki, Alvaro de Gracia, Pere Moreno, Ricard Rovira, Miguel Ángel González, and Luisa F. Cabeza. "A novel numerical methodology for modelling simple vapour compression refrigeration system". In: *Applied Thermal engineering* 115 (2017), pp. 188–200.

[44] Eric W. Lemmon, Ian H. Bell, Marcia L. Huber, and Mark O. McLinden. *NIST Standard Reference Database 23: Reference Fluid Thermodynamic and Transport Properties-REFPROP, Version 10.0, National Institute of Standards and Technology*. 2018. DOI: https://dx.doi.org/10.18434/T4JS3C. URL: https://www.nist.gov/srd/refprop.

[45] Ian H. Bell, Jorrit Wronski, Sylvain Quoilin, and Vincent Lemort. "Pure and Pseudo-pure Fluid Thermophysical Property Evaluation and the Open-Source Thermophysical Property Library CoolProp". In: *Industrial & Engineering Chemistry Research* 53.6 (2014), pp. 2498–2508. DOI: 10.1021/ie4033999. eprint: http://pubs.acs.org/doi/pdf/10.1021/ie4033999. URL: http://pubs.acs.org/doi/abs/10.1021/ie4033999.

[46] NIST, ed. *REFPROP Documentation*. Version Release 10.0. 2018.

[47] International Institute of Refrigeration, ed. *The impact of the refrigeration sector on climate change*. 35th Informatory Note on Refrigeration Technologies. 2017.

[48] European Commission, ed. *Proposal for a Council Decision on the Conclusion of the Agreement to Amend the Montreal Protocol on Substances that Deplete the Ozone Layer Adopted in Kigali*. 2017. URL: https://eur-lex.europa.eu/legal-content/EN/TXT/?uri=CELEX%3A52017PC0051.

[49] Gunnar Myhre, Drew Shindell, François-Marie Bréon, William Collins, Jan Fuglestvedt, Jianping Huang, Dorothy Koch, Jean-François Lamarque, David Lee, Blanca Mendoza, Teruyuki Nakajima, Alan Robock, Graeme Stephens, Toshihiko Takemura, and Hua Zhang. "Anthropogenic and Natural Radiative Forcing". In: Climate Change 2013: The Physical Science Basis (2013). Contribution of Working Group I to the Fifth Assessment Report of the Intergovernmental Panel on Climate Change.

[50] I.P. Koronaki, D. Cowan, G. Maidment, K. Beerman, M. Schreurs, K. Kaar, I. Chaer, G. Gontarz, R.I. Christodoulaki, and X. Cazauran. "Refrigerant emissions and leakage prevention across Europe - Results from the RealSkillsEurope project". In: *Energy* 45 (2012), pp. 71–80.

[51] Pavel Makhnatch, Adrián Mota-Babiloni, Alejandro López-Belchí, and Rahmatollah Khodabandeh. "R450A and R513A as lower GWP mixtures for high ambient temperature countries: Experimental comparison with R134a". In: *Energy* 166 (2019), pp. 223–235.

[52] Pavel Makhnatch, Adrián Mota-Babiloni, and Rahmatollah Khodabandeh. "Experimental study of R450A drop-in performance in an R134a small capacity refrigeration unit". In: *International Journal of Refrigeration* 84 (2017), pp. 26–35.

[53] Adrián Mota-Babiloni, Joaquín Navarro-Esbrí, Ángel Barragán-Cervera, Francisco Molés, and Bernardo Peris. "Experimental study of an R1234ze (E) / R134a mixture (R450A) as R134a replacement". In: *International Journal of Refrigeration* 51 (2015), pp. 52–58.

[54] J.M. Mendoza-Miranda, A. Mota-Babiloni, J.J. Ramírez-Minguela, V.D. Muñoz-Carpio, M. Carrera-Rodríguez, J. Navarro-Esbrí, and C. Salazar-Hernández. "Comparative evaluation of R1234yf, R1234ze (E) and R450A asalternatives to R134a in a variable speed reciprocating compressor". In: *Energy* 114 (2016), pp. 753–766.

[55] W.M. Kays and A.L. London. *Compact Heat Exchangers*. 3rd ed. McGraw-Hill, 1984.

[56] Louis Theodore. *Heat Transfer Applications for the Practicing Engineer*. John Wiley & Sons Ltd, 2011.

[57] Gregory Nellis and Sanford Klein. *Heat Transfer*. Cambridge University Press, 2009.

[58] Shiro Nukiyama. "The maximum and minimum values of the heat Q transmitted from metal to boiling water under atmospheric pressure". In: *International Journal of Heat and Mass Transfer* 9 (1934), pp. 1419–1433.

Acknowledgements

This work is the conclusion of my academic career as student, a career that I have chosen to take.

For this reason, first of all, I wish to thank my family that with a lot of sacrifices has given me the possibility to pursue my objectives. A thanks to my mum, Lucrezia, that has been always next to me in the difficult moments with the affection and the behavior that only a mum could give you; every day that passes I realize how lucky I am. A thanks to my father, Walter, who has always put the interest of his sons before his passions and desires: I hope one day I will be a man, first of all, and a father, next, like you, other words are very unnecessary. A thanks to my younger brother, Emanuele: maybe the distance keeps some moments to share from us, but I'm sure that has strengthened our connection and helps you to find your way, I'm very proud of you.

I'm grateful to Prof. Marco Lorenzini and Dr. Michael Lucchi for their disponibility and attention that they have always had regarding my thesis. I will treasure the advices I have received from you in the following chapters of my life.

A particular thanks to Luca: I believe that I've found a friend and not only a person that helps me to write my first important work in English.

Last but not least, thanks to all those who were there for me, with their friendship, their presence even despite the physical distance.